NASA TECHNICAL MEMORANDUM

NASA TM X-71963

COPY NO.

NASA TM X-71963

AN EXPERIMENTAL INVESTIGATION OF JET PLUME SIMULATION WITH SOLID CIRCULAR CYLINDERS

BY DAVID E. REUBUSH

MAY 1974

NATIONAL AERONAUTICS AND SPACE ADMINISTRATION

LANGLEY RESEARCH CENTER, HAMPTON, VIRGINIA 23665

1. Report No.	2. Government Accession No.	3. Recipient's Catalog No.
NASA TM X-71963		

4. Title and Subtitle	5. Report Date
An Experimental Investigation of Jet Plume Simulation With Solid Circular Cylinders	May 1974
	6. Performing Organization Code

7. Author(s)	8. Performing Organization Report No.
David E. Reubush	

9. Performing Organization Name and Address	10. Work Unit No
NASA Langley Research Center Hampton, Va. 23665	501-24-06-01
	11. Contract or Grant No.

12. Sponsoring Agency Name and Address	13. Type of Report and Period Covered
	Technical Memorandum
	14. Sponsoring Agency Code

15. Supplementary Notes
National Aeronautics and Space Administration
Washington, D.C. 20546

16. Abstract An investigation has been conducted in the Langley 16-foot transonic tunnel to determine the effectiveness of utilizing solid circular cylinders to simulate the jet exhaust plume for a series of four isolated circular arc afterbodies with little or no flow separation. This investigation was conducted at Mach numbers from 0.40 to 1.30 at 0° angle of attack. Plume simulators with simulator diameter to nozzle exit diameter ratios of 0.82, 0.88, 0.98, and 1.00 were investigated with one of the four configurations while the 0.82 and 1.00 simulators were investigated with the other three. Reynolds number based on maximum model diameter varied from approximately 1.50×10^6 to 2.14×10^6.

Results of this investigation indicate that, for jet total-pressure ratios near 2, jet-on boattail pressure coefficient distributions and pressure drag coefficients for any of the configurations are closely approximated at the low subsonic Mach numbers (eg. M = 0.40 and 0.60) by one of the smaller diameter simulators (diameter ratios of 0.82 or 0.88), while at the higher subsonic and transonic Mach numbers (eg. M = 0.80 to 1.30) use of one of the larger diameter simulators (diameter ratios of 0.98 or 1.00) resulted in good approximations of the jet-on pressure coefficient distributions and drag coefficients. However, use of one of the larger diameter simulators at all Mach numbers would generally result in pressure coefficient distributions and drag coefficients useful for preliminary design work. The two theoretical methods of boattail pressure coefficient distribution prediction evaluated as a part of this investigation generally gave reasonably good approximations to the jet-on (again, jet total-pressure ratios near 2) boattail pressure coefficient distributions but the resultant pressure drag coefficients were not satisfactory.

17. Key Words (Suggested by Author(s)) (STAR category underlined)	18. Distribution Statement
Boattail Drag Jet Plume Simulation Jet Effects Boattail Pressure Distributions	Unclassified - Unlimited

19. Security Classif. (of this report)	20. Security Classif. (of this page)	21. No. of Pages	22. Price*
Unclassified	Unclassified	96	$4.00

*Available from { The National Technical Information Service, Springfield, Virginia 22151
STIF/NASA Scientific and Technical Information Facility, P.O. Box 33, College Park, MD 20740

ABSTRACT

An investigation has been conducted in the Langley 16-foot transonic tunnel to determine the effectiveness of utilizing solid circular cylinders to simulate the jet exhaust plume for a series of four isolated circular arc afterbodies with little or no flow separation. This investigation was conducted at Mach numbers from 0.40 to 1.30 at 0° angle of attack. Plume simulators with simulator diameter to nozzle exit diameter ratios of 0.82, 0.88, 0.98, and 1.00 were investigated with one of the four configurations while the 0.82 and 1.00 simulators were investigated with the other three. Reynolds number based on maximum model diameter varied from approximately 1.50×10^6 to 2.14×10^6.

Results of this investigation indicate that, for jet total-pressure ratios near 2, jet-on boattail pressure coefficient distributions and pressure drag coefficients for any of the configurations are closely approximated at the low subsonic Mach numbers (eg. M = 0.40 and 0.60) by one of the smaller diameter simulators (diameter ratios of 0.82 or 0.88), while at the higher subsonic and transonic Mach numbers (eg. M = 0.80 to 1.30) use of one of the larger diameter simulators (diameter ratios of 0.98 or 1.00) resulted in good approximations of the jet-on pressure coefficient distributions and drag coefficients. However, use of one of the larger diameter simulators at all Mach numbers would generally result in pressure coefficient distributions and drag coefficients useful for

preliminary design work. The two theoretical methods of boattail pressure coefficient distribution prediction evaluated as a part of this investigation generally gave reasonably good approximations to the jet-on (again, jet total-pressure ratios near 2) boattail pressure coefficient distributions but the resultant pressure drag coefficients were not satisfactory.

TABLE OF CONTENTS

LIST OF SYMBOLS

A	cross-sectional area, m^2
A_b	nozzle base area, m^2
A_e	nozzle exit area, m^2
A_m	maximum cross-sectional area, m^2
A_t	nozzle throat area, m^2
A_β	incremental area assigned to a boattail static-pressure orifice for drag integration, m^2
$C_{D,\beta}$	boattail pressure drag coefficient, $\frac{D_\beta}{q_\infty A_m}$
$C_{p,\beta}$	boattail pressure coefficient, $\frac{p_\beta - p_\infty}{q_\infty}$
D_β	pressure drag on boattail, N
d_b	base diameter of afterbody, m
d_e	exit diameter of nozzle, m
d_m	maximum diameter of model, m
d_s	diameter of plume simulator, m
ℓ	length of boattail, m
M	free-stream Mach number
$p_{t,j}$	jet total pressure, N/m^2
$p_{t,\infty}$	free-stream total pressure, N/m^2
p_∞	free-stream static pressure, N/m^2
p_β	boattail static pressure, N/m^2

q_∞	free-stream dynamic pressure, N/m^2
R	boattail circular-arc radius, m
RN	Reynolds number
r	radial distance from center line of model, m
S	nozzle convergence length, m
s	axial coordinate in nozzle convergence section, m
$T_{DP,\infty}$	free-stream dewpoint, K
$T_{t,j}$	jet stagnation temperature, K
$T_{t,\infty}$	free-stream stagnation temperature, K
t	nozzle throat length, m
X	axial distance aft from model nose, m
x	axial distance aft from start of boattail, m
β	terminal boattail angle, deg
β_c	boattail chord angle, deg
ϕ	meridianal angle about model axis, positive clockwise when viewed from rear, 0° at top of model, deg

LIST OF TABLES

LIST OF FIGURES

Figure Page

Figure | Page

CHAPTER I

INTRODUCTION

One of the most critical areas in the design of an aircraft as far as the requirement for a low drag configuration is concerned is in the area of the afterbody and nozzles. The flow in this region is extremely complex with upstream disturbances interacting with the expansion and succeeding recompression on the boattail surface and both interacting with the jet exhaust plume. It is therefore important to obtain knowledge of the afterbody and nozzle flowfield and resultant drag as early as possible in the design procedure to insure that the afterbody-nozzle design is the best possible. Unfortunately, wind tunnel models for afterbody-nozzle investigations which include means to simulate the jet exhaust are extremely complex and costly; both of which work to the disadvantage of the designer in his attempt to obtain data early in the design procedure. The complexity associated with the internal plumbing required for the jet simulation medium whether it be air, H_2O_2, H_2, or propane, etc. means that there is a long lead time between the initial requirement for a model and its design and completion. The cost of this type of model also helps to deter the construction of the model until the configuration lines are frozen to be sure that the model will correctly represent the final selected configuration.

It would therefore be extremely advantageous to devise a method whereby the afterbody-nozzle pressure distributions and hence drag

of a configuration could be reasonably well predicted early in the design process either analytically or by use of a relatively cheap wind-tunnel model. An attempt at a cheap, simple substitute for jet simulation has been used by Lewis Research Center and others (refs. 1 to 13 - These references are all which could be found by the author at this writing which utilize this technique for simulating the jet effects of a jet engine exhaust plume at subsonic and transonic speeds.). This method involves the use of a sting mounted model with a "jet boundary," "sting," or "plume" simulator (hereafter referred to as a simulator) which is normally a circular cylinder mounted on the model support sting whose diameter is equal to that of the nozzle exit, thus simulating the on-design jet plume shape when external flow effects on the plume are neglected (refs. 13 to 17). On-design means that the exit static pressure of the jet equals the free-stream static pressure. For convergent nozzles, like those of this investigation, this occurs at a jet total-pressure ratio, $p_{t,j}/p_{\infty}$, of about 1.9. At jet total-pressure ratios below this point the nozzle flow is not choked and thus the exhaust remains subsonic while at pressure ratios above this the exhaust flow is underexpanded and the exhaust plume will billow out trying to equalize static pressure with the free stream.

Note: References 1 to 13 and this investigation are limited solely to the simulation of the effects of the exhaust from a jet engine at subsonic and transonic speeds and thus the references exclude all work on the simulation of jet engine exhaust effects at supersonic speeds and the simulation of rocket engine exhaust effects at all speeds. A typical example of the former is reference 13 while references 19 and 20 are typical examples of the latter.

The decision to eliminate work on simulation of both jet engine and rocket plume effects at supersonic speeds was made because the plume blockage effect predominates at those speeds and can be reasonably well predicted with techniques such as the method of characteristics (ref. 18). Work on rockets at subsonic and transonic speeds was excluded because rocket engines generally operate at very high jet total-pressure ratios and thus operate underexpanded due to nozzle weight considerations and at those conditions the plume is definitely not a circular cylinder (refs. 21 to 23).

Although this method has been used a number of times there has been little work done to determine its validity. Most previous comparisons between models with simulators and models with blowing jets have been between models of two different scales, or even between model scale and full scale. As a result, any agreement between models could be fortuitous or any disagreement could be due to other factors such as Reynolds number differences, model support system differences, or variations in instrumentation location and accuracy between tests.

In order to assess the validity of using simulators an investigation utilizing simulators of various diameters was conducted in the Langley 16-foot transonic tunnel in conjunction with the air powered model investigation of several circular arc afterbodies (refs. 24 and 25).

The investigation was conducted at Mach numbers from 0.40 to 1.30 at 0° angle of attack (The investigation of references 24 and 25 covered the same Mach number range with jet total-pressure ratios varying from jet-off to about 6 depending on Mach number.). Of those afterbodies reported in references 24 and 25 only those with little

or no boundary layer separation will be reported in this paper. In addition to evaluating the usefulness of the simulators two theoretical techniques for the prediction of afterbody pressure distributions for nonseparated afterbodies (refs. 26 and 27) will be evaluated. There are numerous other theoretical techniques for afterbody pressure distribution prediction. Some are strictly inviscid (eg. refs. 28 to 32) while others add a boundary layer solution (eg. refs. 13, and 33 to 35) but it was felt that the two methods examined herein would be representative of the current "state of the art."

CHAPTER II

EXPERIMENTAL APPARATUS AND PROCEDURE

Wind Tunnel

This investigation was conducted in the Langley 16-foot transonic tunnel, which is a single-return, continuous, atmospheric tunnel. The test section is a regular octagon in cross section with slots at the corners of the octagon. The tunnel speed is continuously variable from Mach 0.20 to 1.30. Further description of the Langley 16-foot transonic tunnel can be found in references 36 to 38.

Model and Support System

A sketch of the single-engine nacelle model used in the air powered portion of this investigation (refs. 24 and 25) is shown in figure 1 with a typical circular-arc boattail configuration attached. Figure 2 is a photograph of the nacelle model installed in the Langley 16-foot transonic tunnel. The cone-cylinder nacelle had a rounded shoulder at the junction of the conical nose and cylindrical section. In this nacelle, dry, high-pressure air at a stagnation temperature of about 274K is introduced from the high pressure plenum perpendicularly to the model axis into the low pressure plenum through eight multi-holed sonic nozzles spaced at equal angles around the axis of the high pressure plenum and thence accelerated rearward. The flow smoothing screens in the model tailpipe were constructed of 0.635-cm-mesh, 0.0635 cm-diameter-wire screen supported by four vanes.

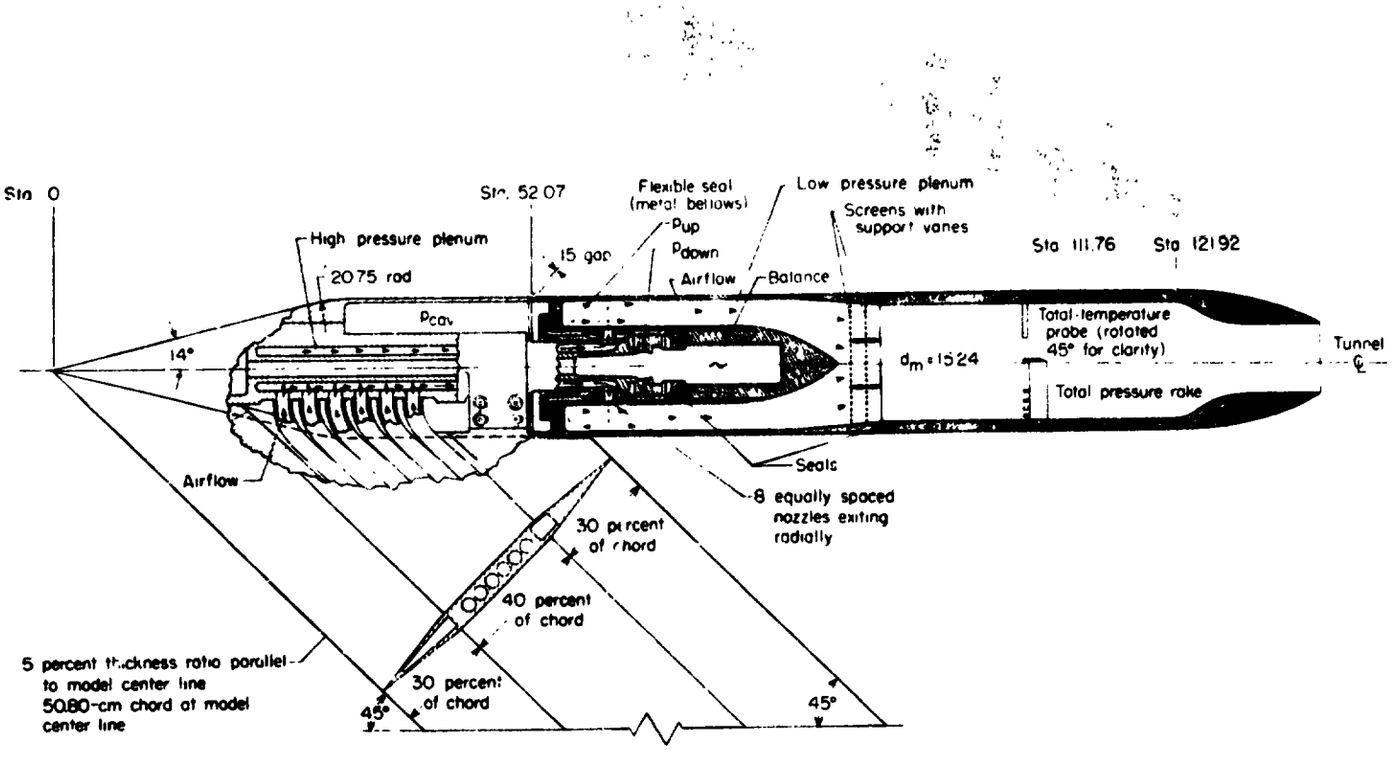

Figure 1.- Sketch of air-powered cone-cylinder model with a typical circular arc convergent nozzle installed. All dimensions are in centimeters unless otherwise noted.

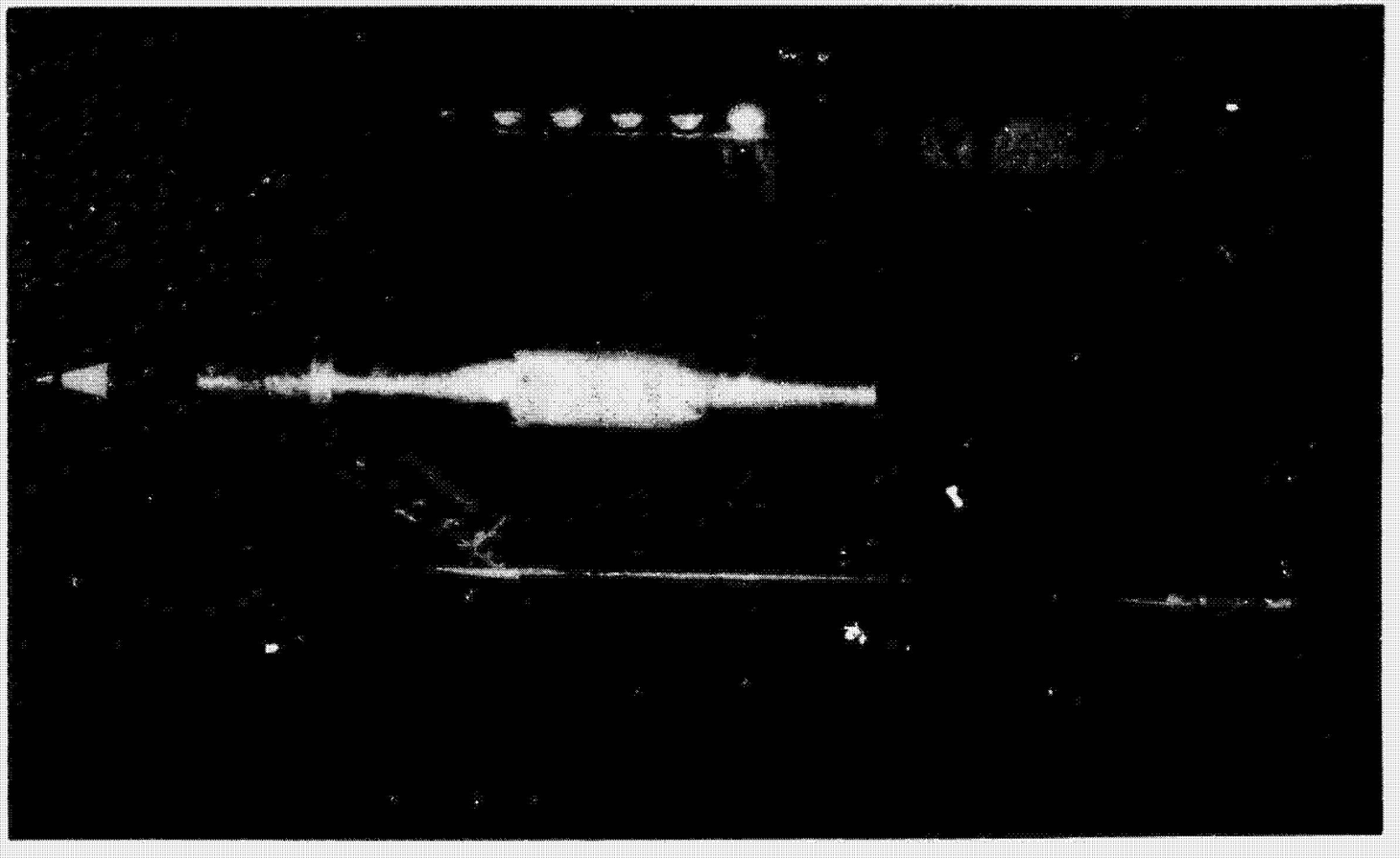

Figure 2.- Air powered model with configuration 4 attached installed in the Langley 16-foot transonic tunnel.

For the simulator investigation the cone-cylinder single engine nacelle model was modified by the addition of an internal sting arrangement to provide a support for the various simulators. A sketch of the modified model is shown in figure 3 with a typical circular-arc boattail configuration attached. Figure 4 is a photograph of the nacelle model installed in the Langley 16-foot transonic tunnel with a typical configuration and $d_s/d_e = 1.0$ simulator attached.

The model was supported in the tunnel by a sting-strut support system, the swept strut being attached to the nose of the model as shown in figures 1 to 5. The center line of the model was located on the wind-tunnel center line, with the center line of the sting 55.88 cm below that level. The sting was 5.08 cm by 10.16 cm in cross section with the top and bottom capped by half-cylinders of 2.54 cm radius. The strut blade was 5 percent thick with a 50.8 cm chord in the streamwise direction and with the leading and trailing edges swept 45°.

A sketch of the model and support system is shown in figure 5 along with corresponding cross-sectional area distributions. The model blockage was 0.099 percent of the test-section cross section, and the maximum blockage cross section of the model and support system was 0.148 percent. The sting-strut positioned the nose of the model at tunnel station 39.93 meters.

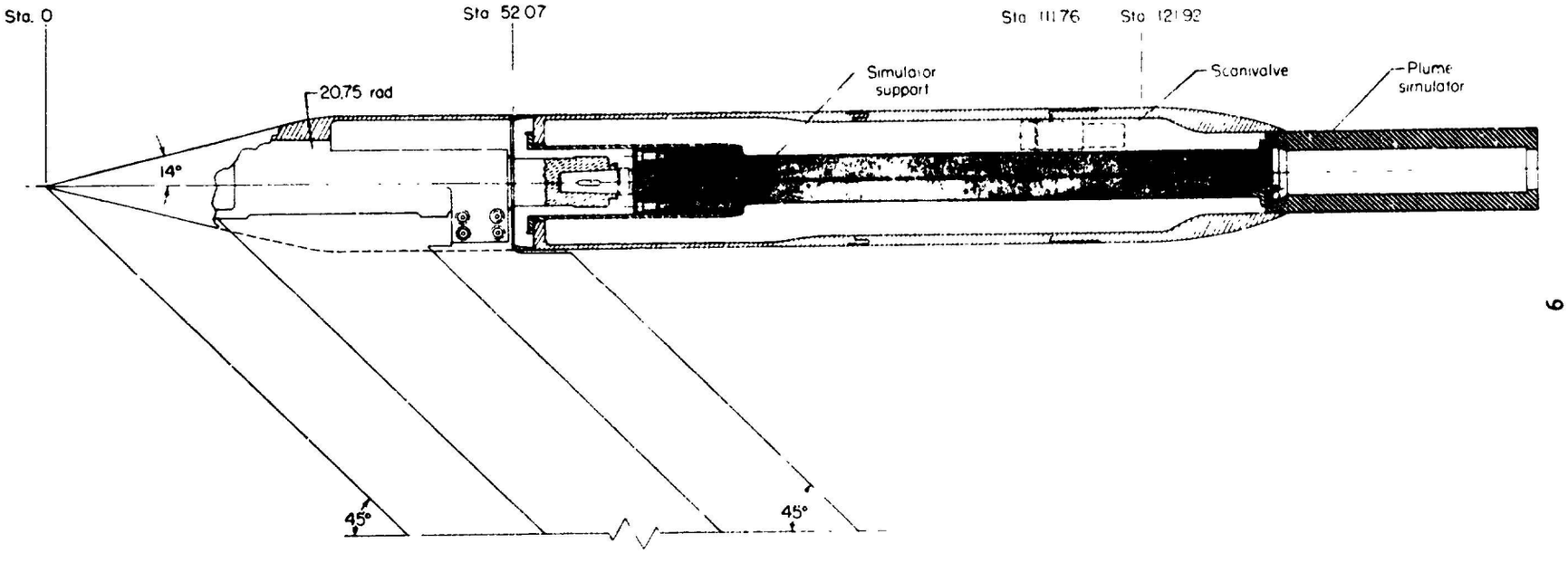

Figure 3.- Sketch of cone-cylinder nacelle model showing internal sting arrangement for support of simulators.

Figure 4.- Nacelle model installed in the Langley 16-foot transonic tunnel with typical circular-arc afterbody and $d_s/d_e = 1.00$ simulator attached.

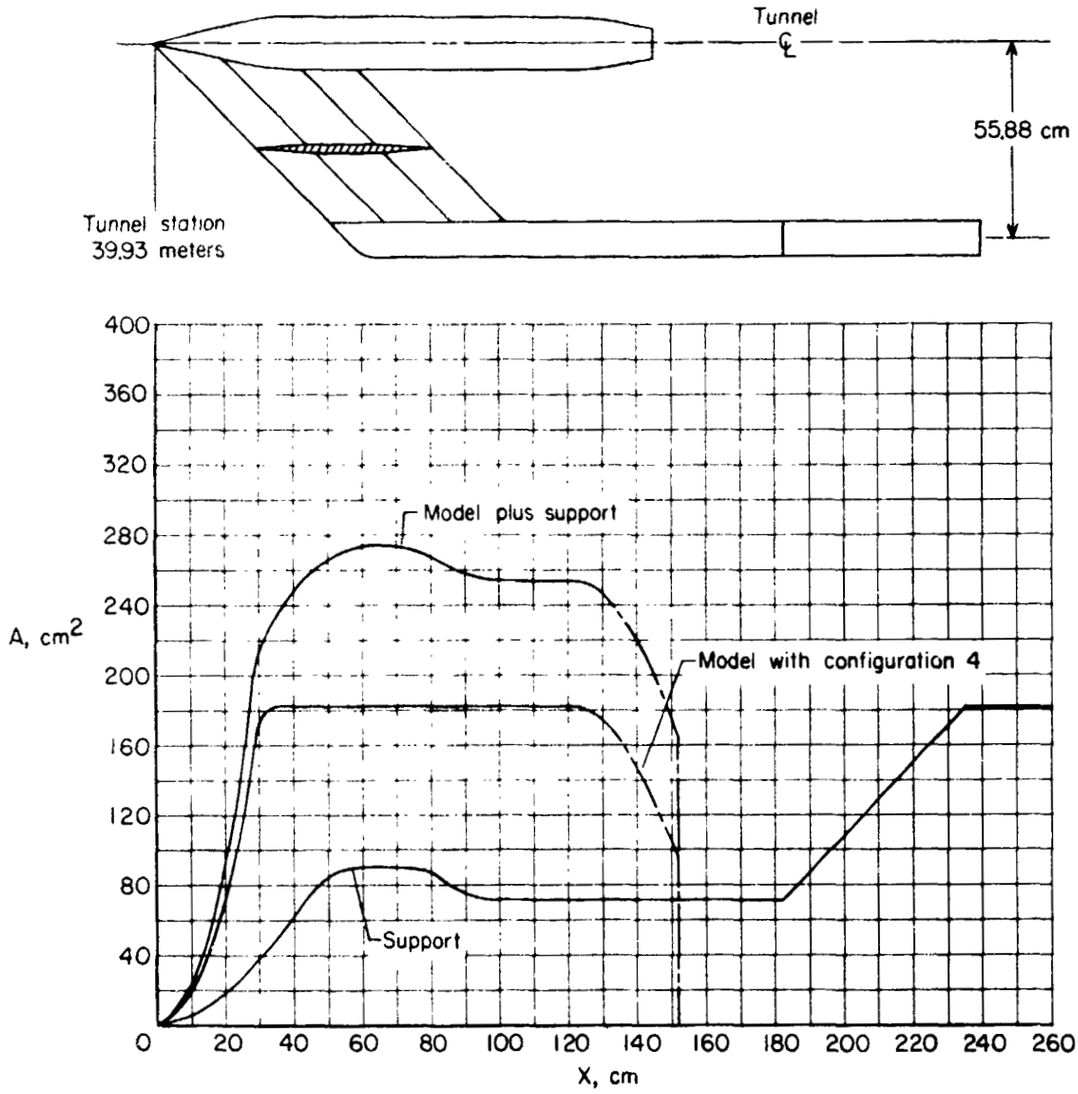

Figure 5.- Sketch of model and support system with corresponding cross-sectional area distributions.

Afterbody Models

A detailed sketch of a typical afterbody model and a table of dimensions for the four configurations are presented in figure 6. For the air powered portion of the investigation (refs. 24 and 25) the internal contour of each of the nozzles was essentially an ASME long-throat nozzle (ref. 39) modified to fit within dimensional constraints imposed by the external contour of each afterbody (length S and r as a function of s - fig. 6 - changed from the ASME contours as necessary to go from a fixed internal diameter to the required exit diameter within the bounds set by the external contour of the boattail and the required space for tube routing and the length of the boattail). The throat (length t in fig. 6) was circular in cross section.

Instrumentation and Tests

The four afterbody models were equipped with static-pressure orifices distributed longitudinally on an equal-annular area basis at the locations given in table 1. The models had from 48 to 72 orifices (depending on configuration) which were connected to individual, remotely located, electrical strain gage pressure transducers. The simulators were each instrumented with 16 static-pressure orifices at the locations given in table 2. These orifices were connected to a pressure scanning valve installed in the model. All pressure transducers were calibrated to an accuracy of ± 0.5 percent of the capacity of the gage (static-pressure gages 1.72×10^4 N/m^2 and 3.45×10^4 N/m^2; jet total-pressure gages 6.89×10^5 N/m^2).

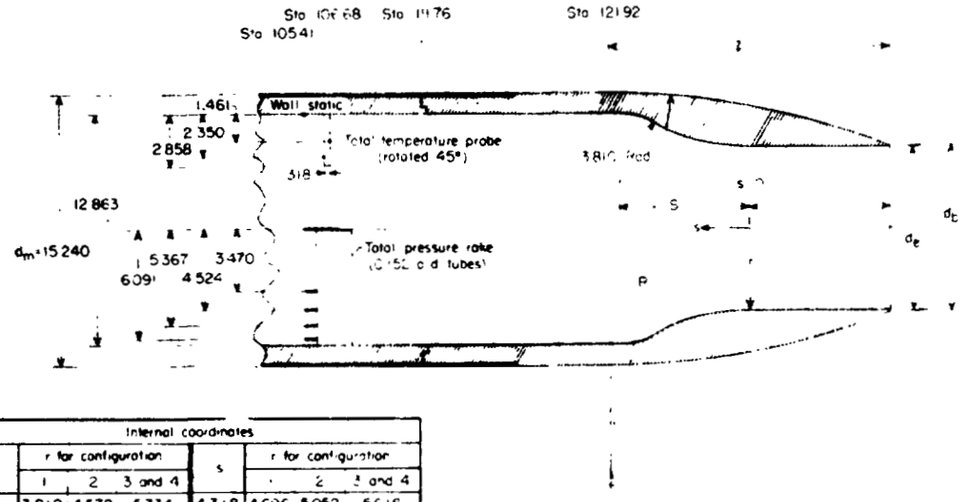

Internal coordinates							
s	r for configuration			s	r for configuration		
	1	2	3 and 4		1	2	3 and 4
0	3.810	4.572	5.334	4.318	4.696	5.052	5.618
.254	3.813	4.575	5.337	4.445	4.755	——	——
.508	3.820	4.577	5.339	4.572	4.816	5.123	5.659
.762	3.835	4.585	5.342	4.699	4.882	——	——
1.016	3.856	4.595	5.349	4.826	4.948	5.209	5.705
1.270	3.881	4.608	5.357	4.953	5.019	5.245	——
1.524	3.912	4.625	5.364	5.080	5.090	5.29	5.758
1.778	3.950	4.646	5.377	5.207	5.169	5.339	5.786
2.032	3.993	4.669	5.390	5.334	5.248	5.392	5.819
2.286	4.041	4.694	5.405	5.461	5.334	5.448	5.852
2.540	4.097	4.722	5.423	5.588	5.420	5.512	5.888
2.794	4.161	4.757	5.443	5.715	5.514	5.578	5.928
3.048	4.229	4.793	5.466	5.842	5.611	5.654	5.972
3.302	4.308	4.836	5.489	5.969	5.715	5.738	6.022
3.556	4.392	4.882	5.517	6.096	5.822	5.839	6.081
3.810	4.483	4.933	5.547	6.223	——	5.961	6.154
3.937	4.534	——	——	6.350	——	6.137	6.259
4.064	4.585	4.991	5.580	6.431	——	6.431	6.431
4.191	4.641	——	——				

Geometric parameters									
Configuration	ℓ/d_m	d_e/d_m	d_t/d_m	R_1/d_m	r_1/d_m	S_1/d_m	β, deg	β_c, deg
1	1.768	.650	.251	6.500	.0500	.0458	15.781	7.891
2	1.500	.66	.61	5.867	.592	.536	14.814	7.407
3	1.500	.70	.71	7.831	.667	.507	11.043	5.521
4	2.000	.70	.71	13.866	.833	.507	8.293	4.147

Figure 6.- Detailed sketch of typical nozzle model with tables of geometric parameters and internal coordinates. All dimensions are in centimeters unless otherwise noted.

Table 1

AFTERBODY-SURFACE ORIFICE LOCATIONS

x/l	x/dm	ø, deg 0	30	60	90	120	135	150	180	225	315
					CONFIGURATION 1						
0	0	x		x	x			x	x	x	x
.209	.370	x	x		x	x			x		
.366	.647	x		x	x			x	x		
.478	.845	x	x	x	x	x		x	x	x	x
.572	1.012	x	x	x	x	x		--	x		
.657	1.162	x	x	x	x	x			x		
.737	1.303	x	x	x	x	x			x	x	x
.815	1.440	x	x	x	x	x			x		
.891	1.576	x	x	x	x	x		x	x		
.969	1.714	x	x	x	x	x		x	x	x	x
					CONFIGURATION 2						
0	0	x	x	x	x		x		x	x	x
.234	.351	x	x	x	x		x		x		
.410	.615	x	x	x	x		x		x		
.535	.802	x	x	x	x		x		x	x	x
.640	.961	x	x	x	x		x		x		
.736	1.104	x	x	x	x		x		x		
.825	1.238	x	x	x	x		x		x	x	x
.911	1.367	x	x	x	x		x		x		
.972	1.458	x	x	x	x		x		x		
					CONFIGURATION 3						
0	0	x	x	x	x		x		x	x	x
.271	.406	x	x	x	x		x		x		
.474	.711	x	x	x	x		x		x		
.618	.928	x	x	x	x		x		x	x	x
.741	1.111	x	x	x	x		x		x		
.851	1.276	x	x	x	x		x		x		
.955	1.432	x	x	x	x		x		x	x	x
					CONFIGURATION 4						
0	0	x	x	x	x		x		x	x	x
.270	.540	x	x	x	x		x		x		
.473	.946	x	x	x	x		x		x		
.618	1.235	x	x	x	x		x		x	x	x
.740	1.480	x	x	x	x		x		x		
.850	1.701	x	x	x	x		x		x		
.954	1.909	x	x	x	x		x		x	x	x

Table 2

SIMULATOR-SURFACE ORIFICE LOCATIONS

CONFIGURATION 1		CONFIGURATIONS 2 AND 3		CONFIGURATION 4	
x/ℓ	x/d_m	x/ℓ	x/d_m	x/ℓ	x/d_m
1.047	1.851	1.056	1.583	1.042	2.083
1.094	1.935	1.111	1.667	1.083	2.167
1.141	2.018	1.167	1.750	1.125	2.250
1.189	2.101	1.222	1.833	1.167	2.333
1.236	2.185	1.278	1.917	1.208	2.417
1.283	2.268	1.333	2.000	1.250	2.500
1.330	2.351	1.389	2.083	1.292	2.583
1.377	2.435	1.444	2.167	1.333	2.667
1.424	2.518	1.500	2.250	1.375	2.750
1.471	2.601	1.556	2.333	1.417	2.833
1.519	2.685	1.611	2.417	1.458	2.917
1.566	2.768	1.667	2.500	1.500	3.000
1.660	2.935	1.778	2.667	1.583	3.167
1.754	3.101	1.889	2.833	1.667	3.333
1.848	3.268	2.000	3.000	1.750	3.500
1.943	3.435	2.111	3.167	1.833	3.667

All tests were conducted in the Langley 16-foot transonic tunnel at Mach numbers from 0.40 to 1.30 at an angle of attack of 0°. Model attitude was set so as to account for tunnel upflow, but no account was taken of possible sting deflection which was found to be extremely small. Boundary layer transition on the model was fixed by a 0.254-cm strip of No. 100 grit, 2.54 cm from the nose, in accordance with the techniques described in references 40 and 41.

Since the Langley 16-foot transonic tunnel is an atmospheric

tunnel the tunnel free-stream conditions will vary according to the ambient conditions. The range of free-stream conditions versus Mach number is shown in figure 7. To keep the variation in tunnel total temperature as small as possible data were taken at the highest Mach number first and then at progressively lower Mach numbers. For each Mach number at which data were required the tunnel conditions were set and allowed to stabilize at which time a number of frames of data were taken, the average of which was used to compute the desired coefficients. An average of a number of frames of data was used because the 16-foot tunnel has a small cyclic variation in the flow with a period of about 10 seconds and it was felt that an average of a number of frames would give the best answer.

Data Reduction

Pressure drag coefficients were computed from the measured pressures on each boattail. These coefficients are based on maximum cross-sectional area of the model and were obtained from the pressure data by assigning an equal annular area to each orifice in the top row and computing them from the equation:

$$C_{D,\beta} = \frac{1}{q_\infty A_m} \sum_{i=1}^{n} (p_\infty - p_{\beta,i}) A_{\beta,i}$$

The top row of orifices was used exclusively because of the possibility of support-strut interference. In references 24 and 25 it was reported that the data from the $\phi = 0°$ row of orifices could be assumed to be interference free, and unpublished data from the present

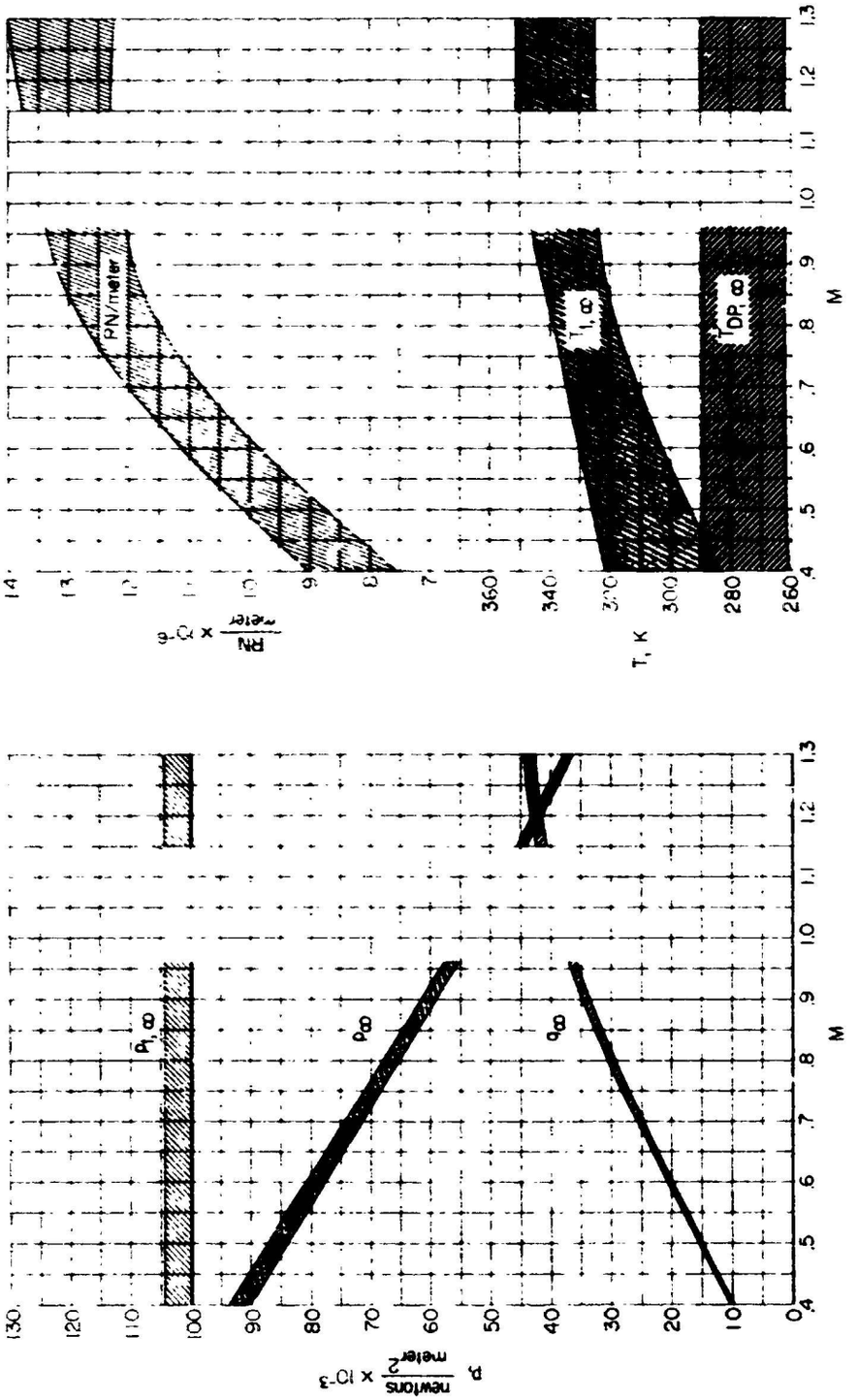

Figure 7.- Band of the free stream parameters encountered during the investigation.

investigation which compared pressures on these boattails mounted on the sting-strut with pressures on the same boattails mounted on a sting support this belief. No attempt was made to include the forces on the small rim at the nozzle exit between d_b and d_e (see fig. 6).

CHAPTER III

RESULTS AND DISCUSSION

Pressure distributions.- The jet exhaust plume affects the afterbody boattail pressures in two ways: by the entrainment of external air flowing over the boattail and by the solid blockage or shape effect of a body downstream of the boattail. These two phenomena result in opposite effects on the boattail pressure distributions. The entrainment of the external flow causes a reduction in the afterbody pressure coefficients while the solid blockage effect causes a rise in the afterbody pressure coefficients. In trying to model the effects of the jet exhaust on the afterbody both of these phenomena should be taken into account. However, at the present time it is impossible to predict the entrainment of any given jet. Therefore, the use of circular cylinder simulators is, at best, a compromise in that the jet entrainment effects will not be simulated and only the plume shape of a nozzle operating at its design point will be matched (strictly true only at static conditions due to the effect of the body induced flow angle of the external flow on the plume shape, that is, the flow over the boattail is parallel to the boattail surface and thus has a finite momentum directed toward the center of the jet when it leaves the end of the boattail). Fortunately this compromise is not too bad, especially for the higher subsonic Mach numbers. Most subsonic transport aircraft and fighters

at subsonic cruise utilize convergent nozzles and turbofan engines which operate in a range of jet total-pressure ratios near the convergent nozzle design point of about 2 (see fig. 20). Also the data of references 24 and 25 show that there are no significant variations in afterbody boattail drag levels with jet total-pressure ratio until well past a jet total-pressure ratio of about 3. As a result, simulating the design point jet total-pressure ratio ($p_{t,j}/p_\infty \approx 2$) with the solid cylinder simulator should result in an error in drag due only to the missing entrainment effect and the effect of the body induced flow angle on the jet plume.

Shown in figures 8 to 11 are comparisons of the afterbody pressure coefficient distributions for the four configurations of this paper obtained through the use of simulators of varying diameters (d_s/d_e of 1.00, 0.98, 0.88, and 0.82 for configuration 1 and d_s/d_e of 1.00 and 0.82 for configurations 2, 3, and 4) with pressure distributions from references 24 and 25 which were obtained with high pressure air (at $p_{t,j}/p_\infty = 2$) as the exhaust medium. Simulators of smaller than exit diameter were utilized in an attempt to lessen the blockage effects and as a result simulate the combination of blockage and entrainment effects. The pressure coefficient distributions on the simulators themselves are shown for information.

Figure 8 presents the simulator-jet-on comparisons for configuration 1 ($\ell/d_m = 1.77$, $d_e/d_m = 0.50$). At the lower Mach numbers (eg. M = 0.40 and 0.60) entrainment has a larger effect on the afterbody

pressure coefficient distribution than it does at the higher subsonic Mach numbers where the exhaust and free stream have close to the same velocity (eg. M = 0.85 to 0.96). As a result, the jet-on pressure coefficient distributions at the low Mach numbers are more closely represented by one of the smaller diameter simulators than by the $d_s/d_e = 1.00$ simulator while those at the higher subsonic Mach numbers are most closely represented by the $d_s/d_e = 0.98$ simulator. At the supersonic Mach numbers investigated, the boattail pressure coefficients upstream of the shock (shock located at approximately $x/d_m = 1.45$ for this configuration) are about the same for all the simulators and for jet-on while downstream of the shock in the separated region (shock induced separation) the jet-on pressure coefficients generally fall between the pressure coefficients for the $d_s/d_e = 0.98$ and $d_s/d_e = 0.88$ simulators. However, use of one of the larger diameter simulators at all Mach numbers would generally result in pressure coefficient distributions with the correct shape and minimum pressure coefficient satisfactory for preliminary design work.

The same general comments are valid for the other three configurations ($\ell/d_m = 1.50$, $d_e/d_m = 0.60$; $\ell/d_m = 1.50$, $d_e/d_m = 0.70$; and $\ell/d_m = 2.00$, $d_e/d_m = 0.70$) in figures 9, 10, and 11. Also, by examining the various pressure coefficient distributions at any given subsonic Mach number it becomes apparent that as the boattail angle and the resultant inflow into the plume are reduced so is the effect of the entrainment and as a result the pressure coefficient distributions obtained with the larger diameter simulators (eg. $d_s/d_e = 0.98$ and 1.00)

more closely match the jet-on ($p_{t,j}/p_\infty = 2$) data since they more closely match the plume blockage effect.

Comparison with theory.- There are several theoretical techniques available with which to predict afterbody pressure distributions (refs. 26 to 35). One of the most widely used and one of the most recent are given in references 26 and 27 respectively. These methods are both inviscid solutions but utilize different solution techniques. Reference 26, which is a relatively inexpensive method in terms of computer time and cost, utilizes distributed sources and sinks on the body surface to calculate the flow-field and resulting body pressure distribution. In order to simulate jet effects with this method the jet plume shape must be specified and input like a solid body downstream of the nozzle exit. Reference 27 utilizes a stream tube curvature analysis in which an initial grid of streamlines and orthogonals is set up and then refined in an iterative solution (relatively expensive in computer time and cost). This method has the capability of calculating its own plume shape for low jet total-pressure ratio exhaust flows so that only jet total-pressure, total-temperature, and exit Mach number need be specified in order to simulate a jet exhaust (plumes resulting from this calculation are very close to cylindrical). Since these methods are inviscid solutions they do not take into account the boundary layer development on the afterbody. This can often result in neglecting a significant contribution to the resultant pressure distribution. In an attempt

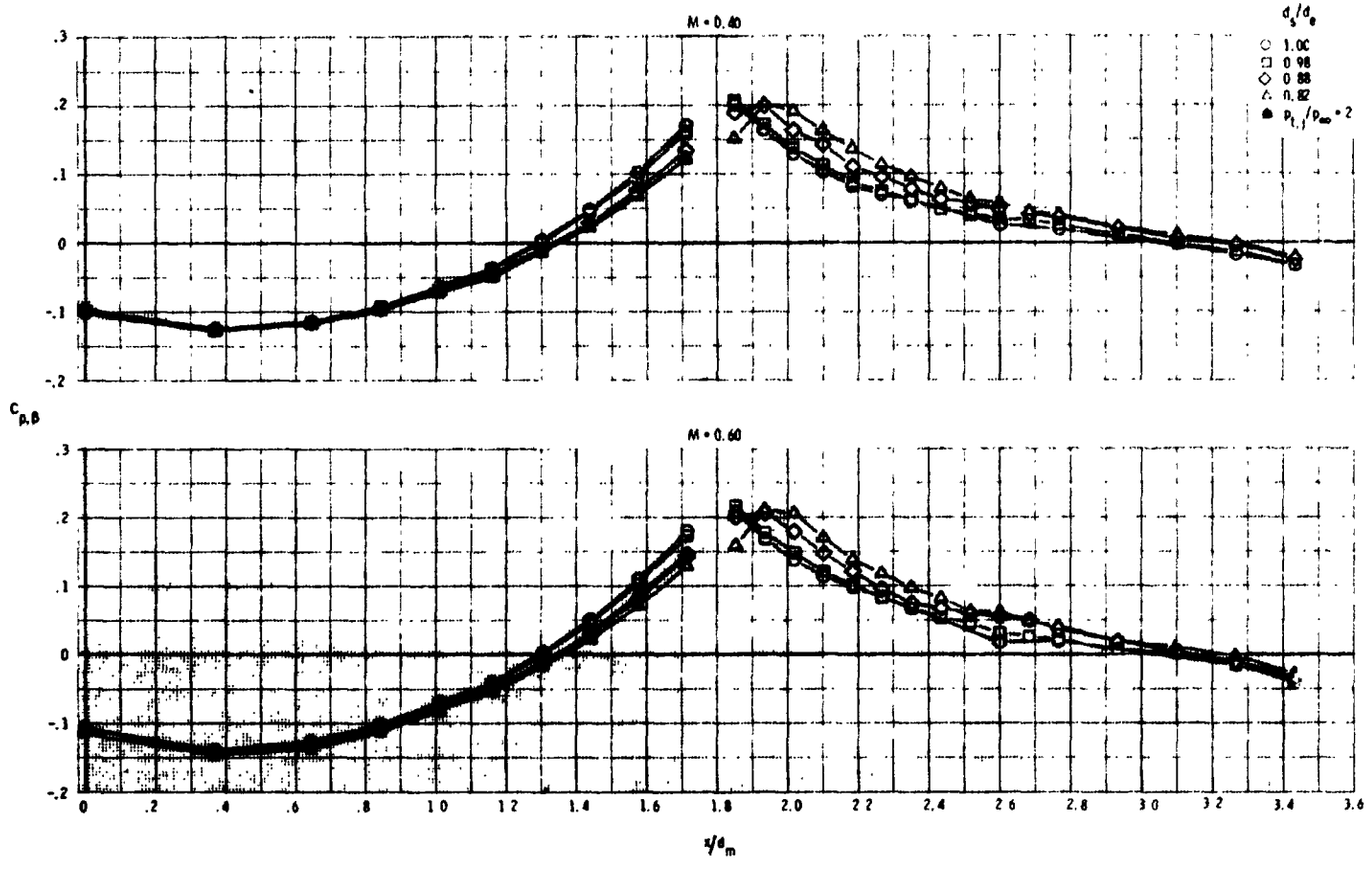

(a) M = 0.40 and 0.60

Figure 8.- Comparison of pressure coefficient distributions obtained through the use of plume simulators with those obtained from jet operation at $p_{t,j}/p_\infty = 2$ for configuration 1 ($\ell/d_m = 1.77$, $d_e/d_m = 0.50$).

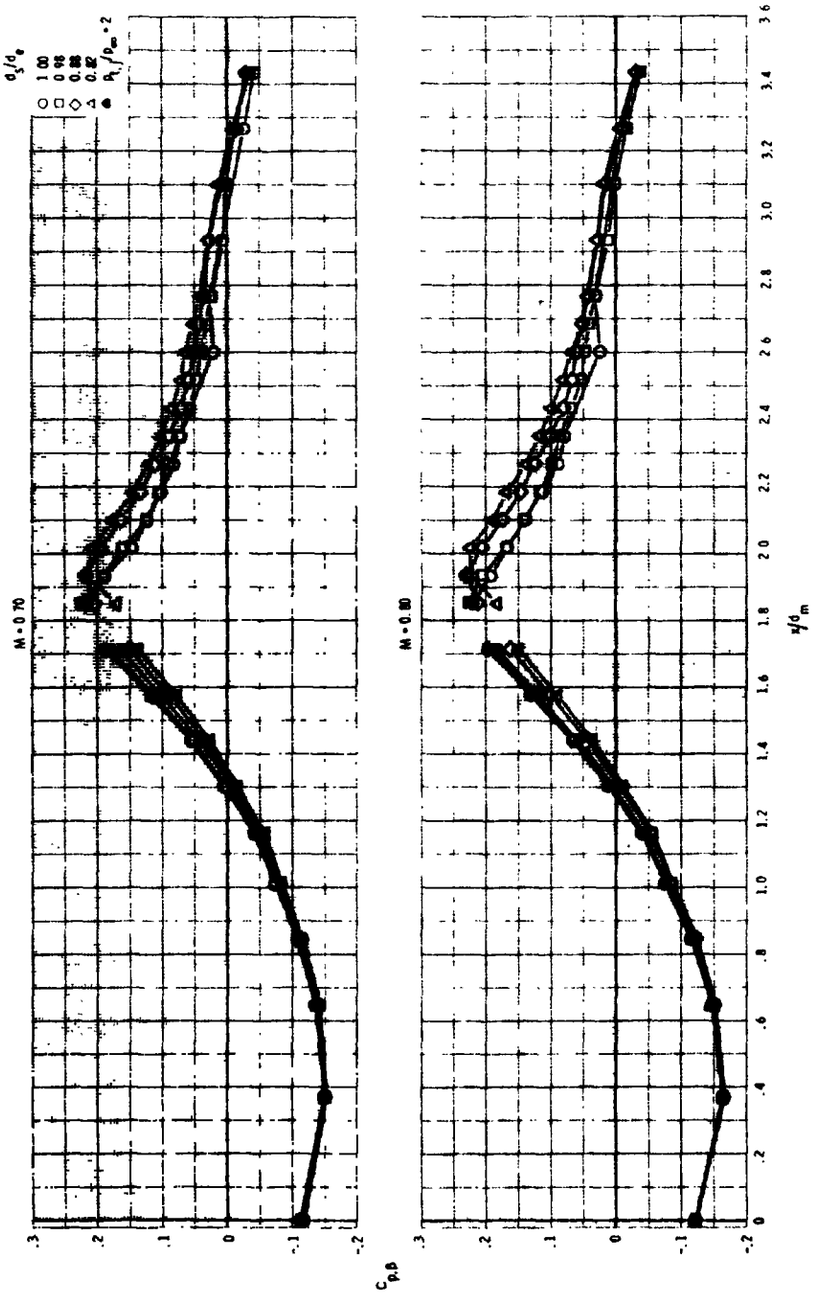

(b) M = 0.70 and 0.80

Figure 8.- Continued.

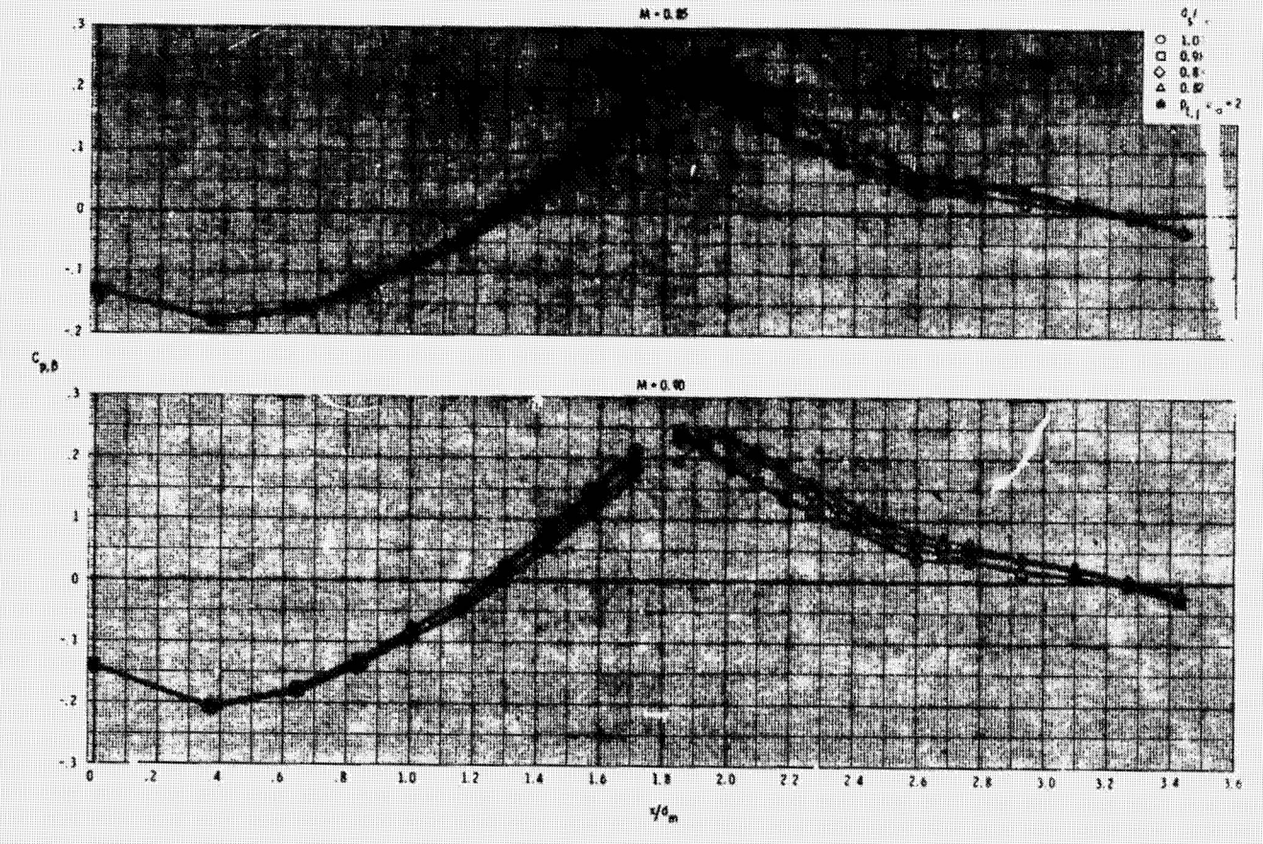

(c) M = 0.85 and 0.90

Figure 8.- Continued.

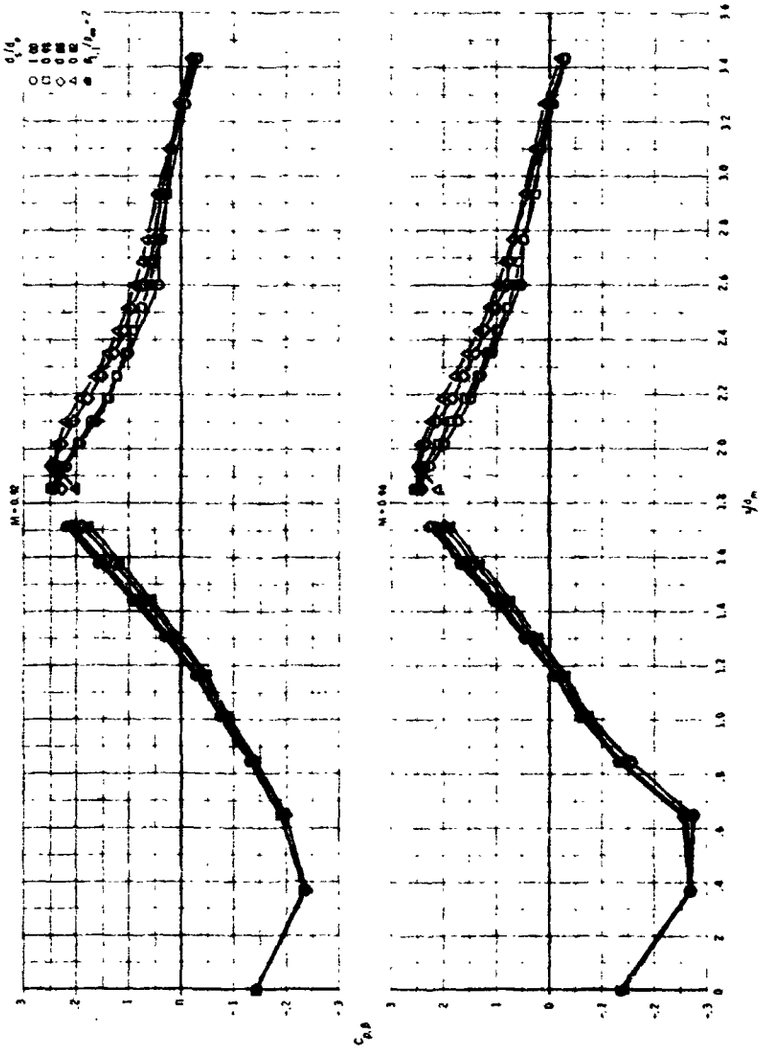

(d) M = 0,92 and 0,94

Figure 8.- Continued.

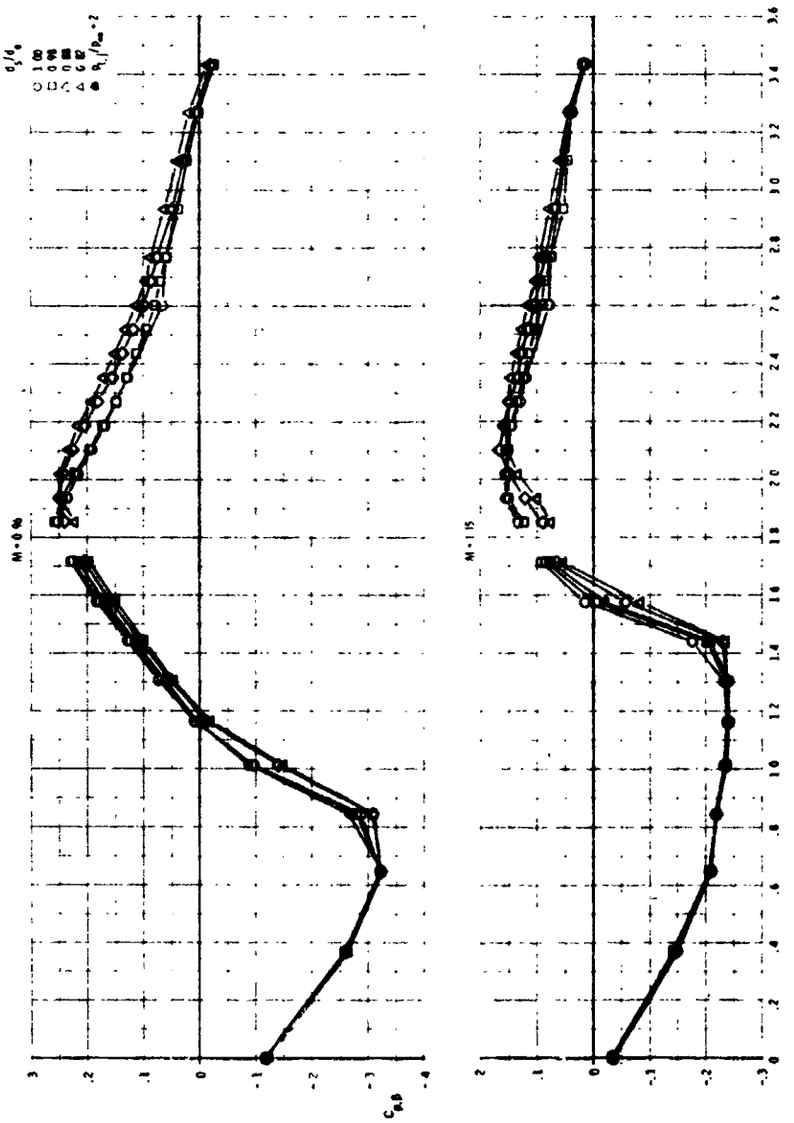

(e) M = 0.96 and 1.15

Figure 8.- Continued.

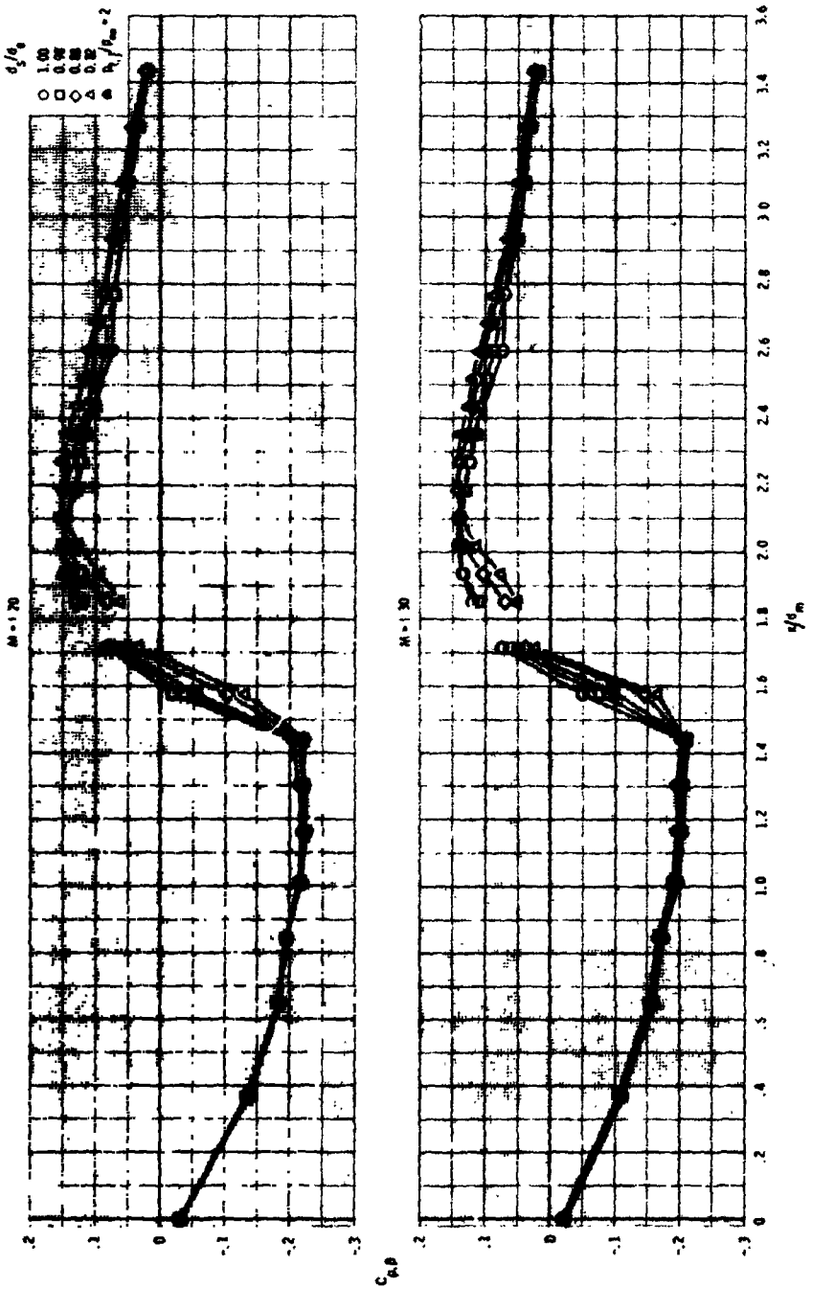

(f) M = 1.20 and 1.30

Figure 8.- Concluded.

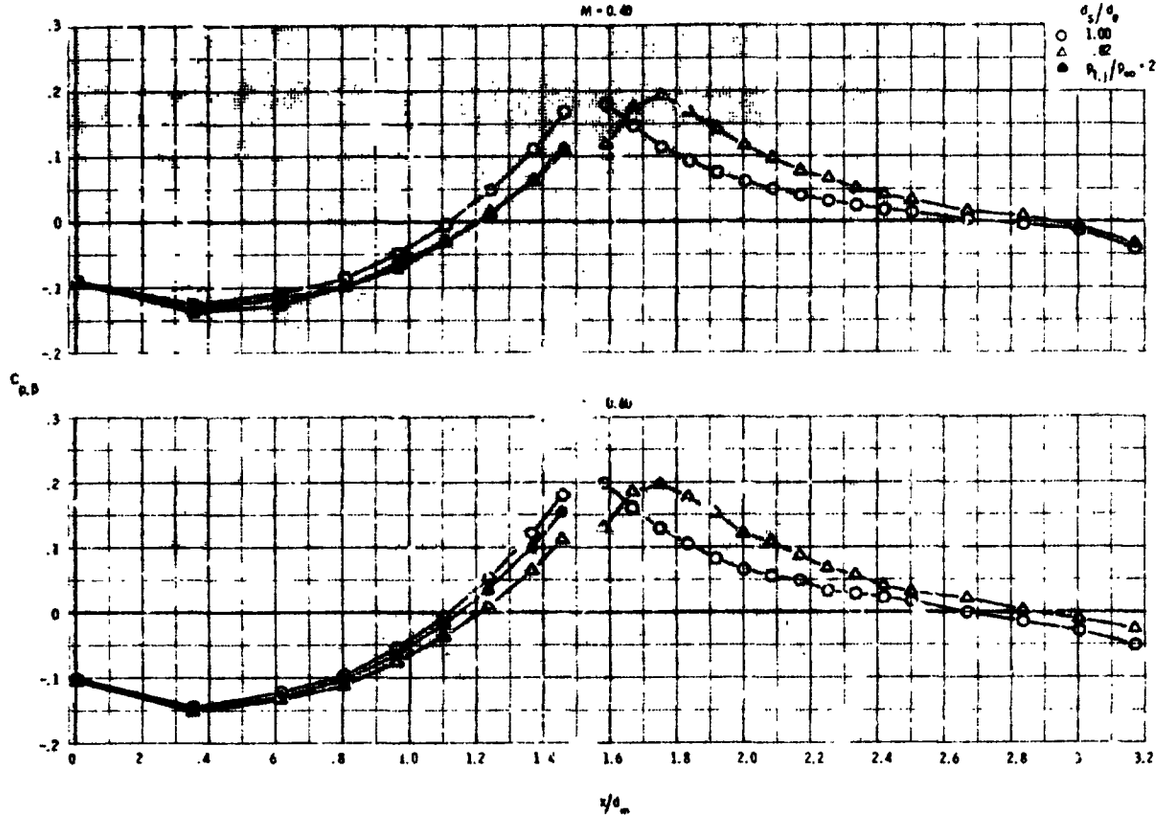

(a) M = ^,40 and 0.60

Figure 9.- Comparison of pressure coefficient distributions obtained through the use of plume simulators with those obtained from jet operation at $p_{t,j}/p_\infty = 2$ for configuration 2 ($\ell/d_m = 1.50$, $d_e/d_m = 0.60$).

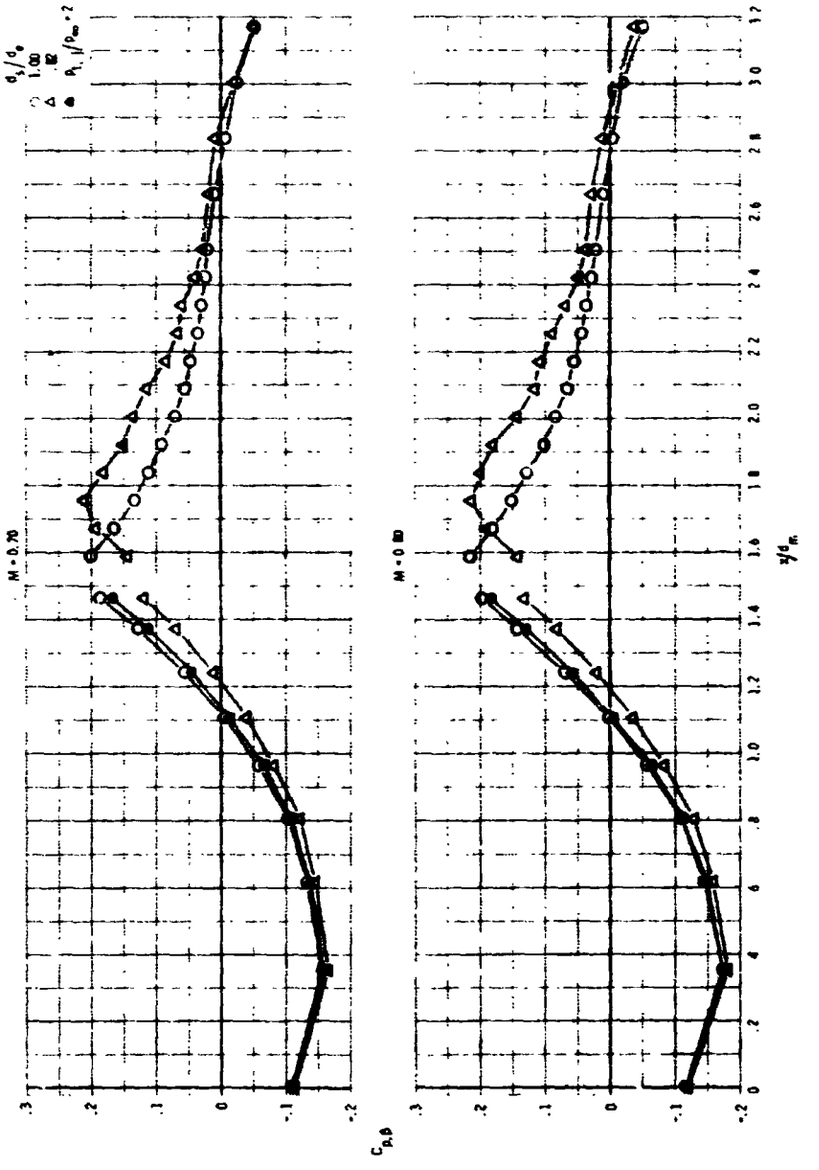

(b) M = 0.70 and 0.80

Figure 9.- Continued.

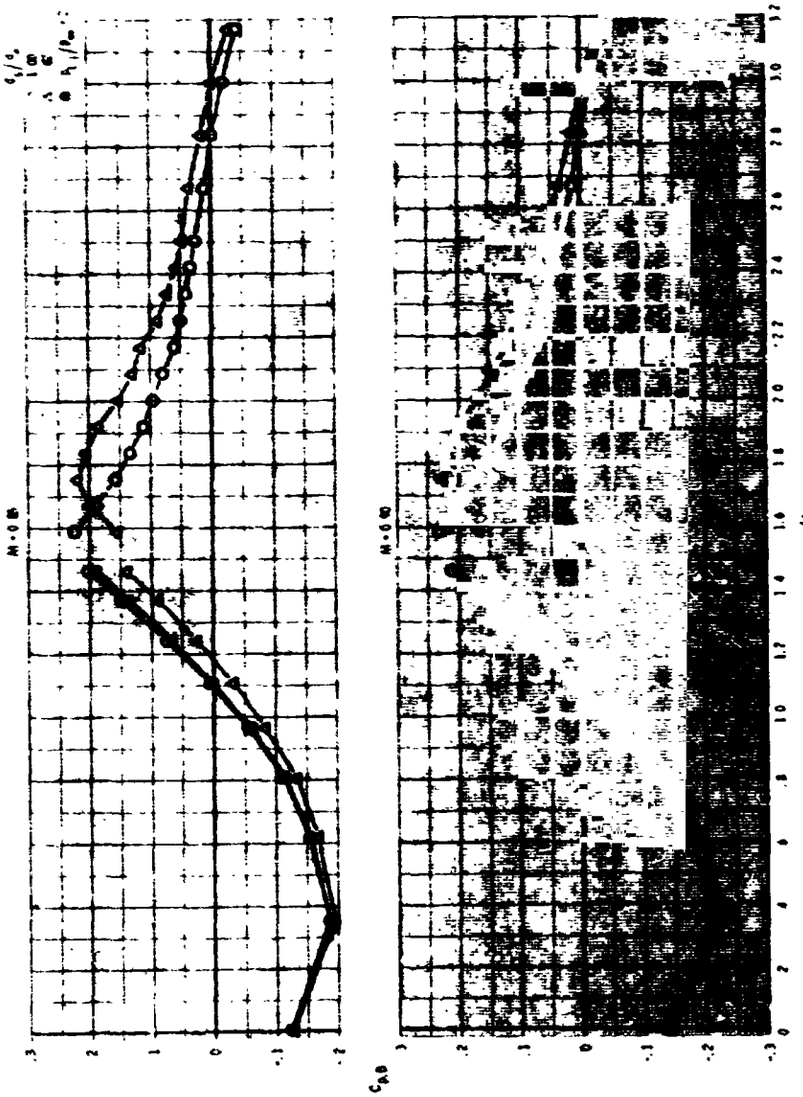

(c) M = 0,85 and 0,90

Figure 9.- Continued.

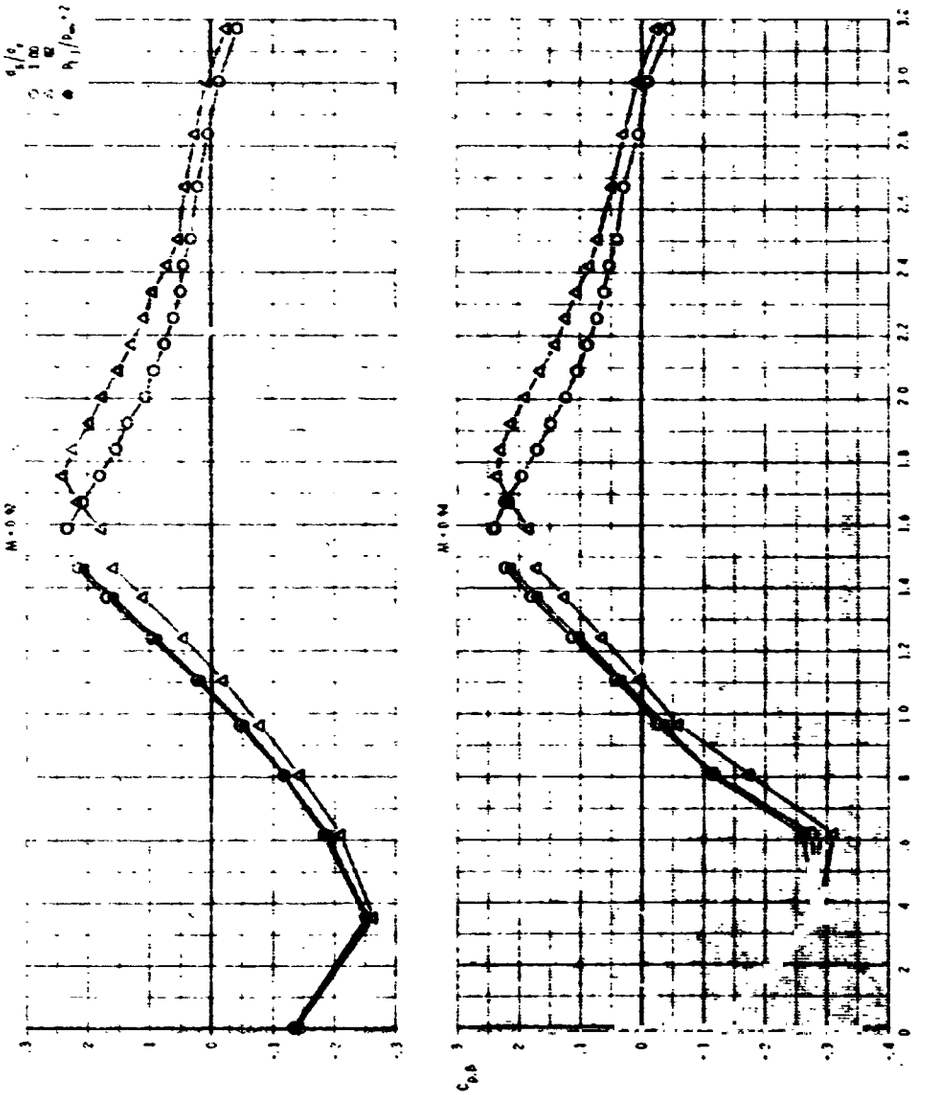

(d) M = 0.92 and 0.94

Figure 9.- Continued.

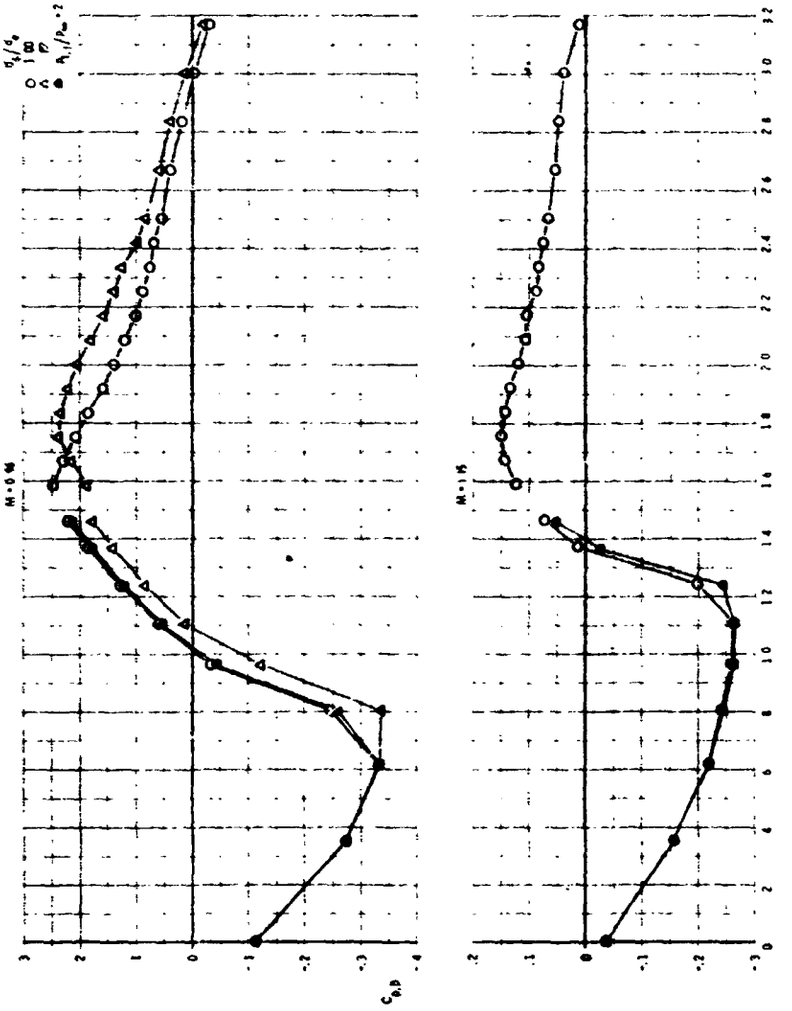

(e) M = 0.96 and 1.15

Figure 9.- Continued.

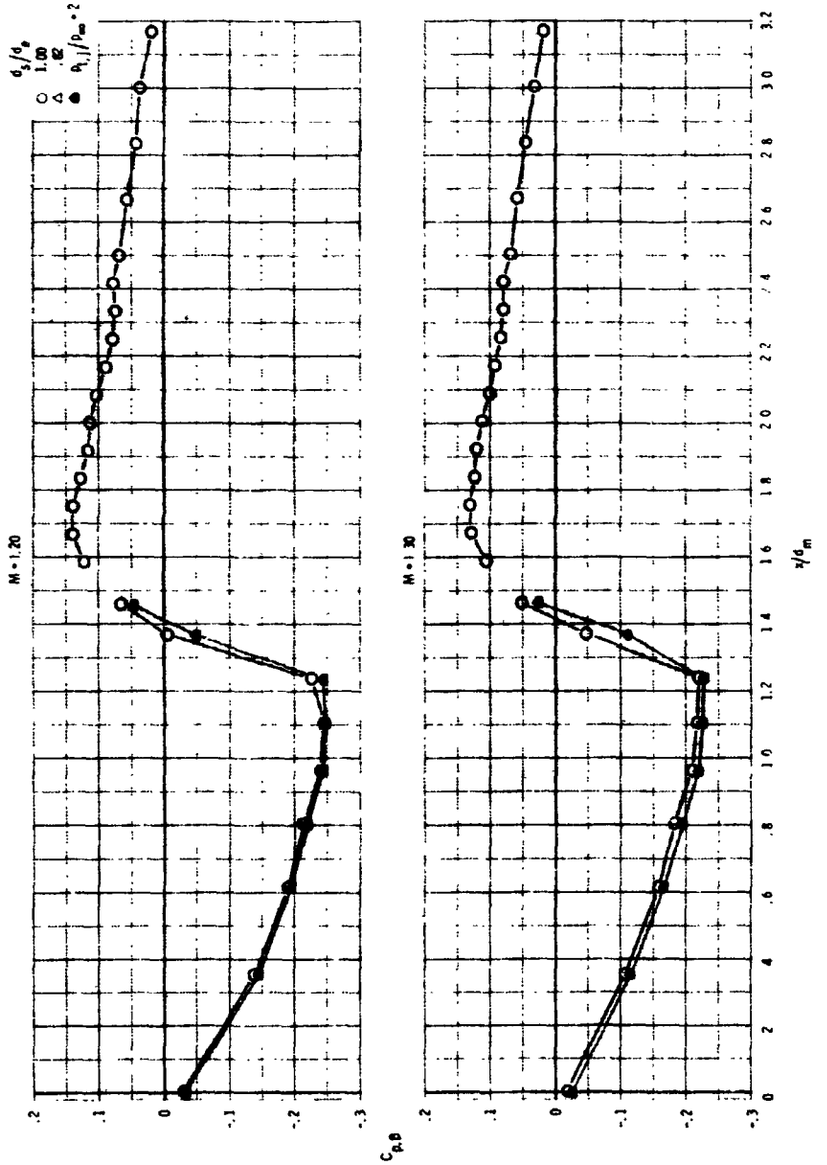

(f) M = 1.20 and 1.30

Figure 9.- Concluded.

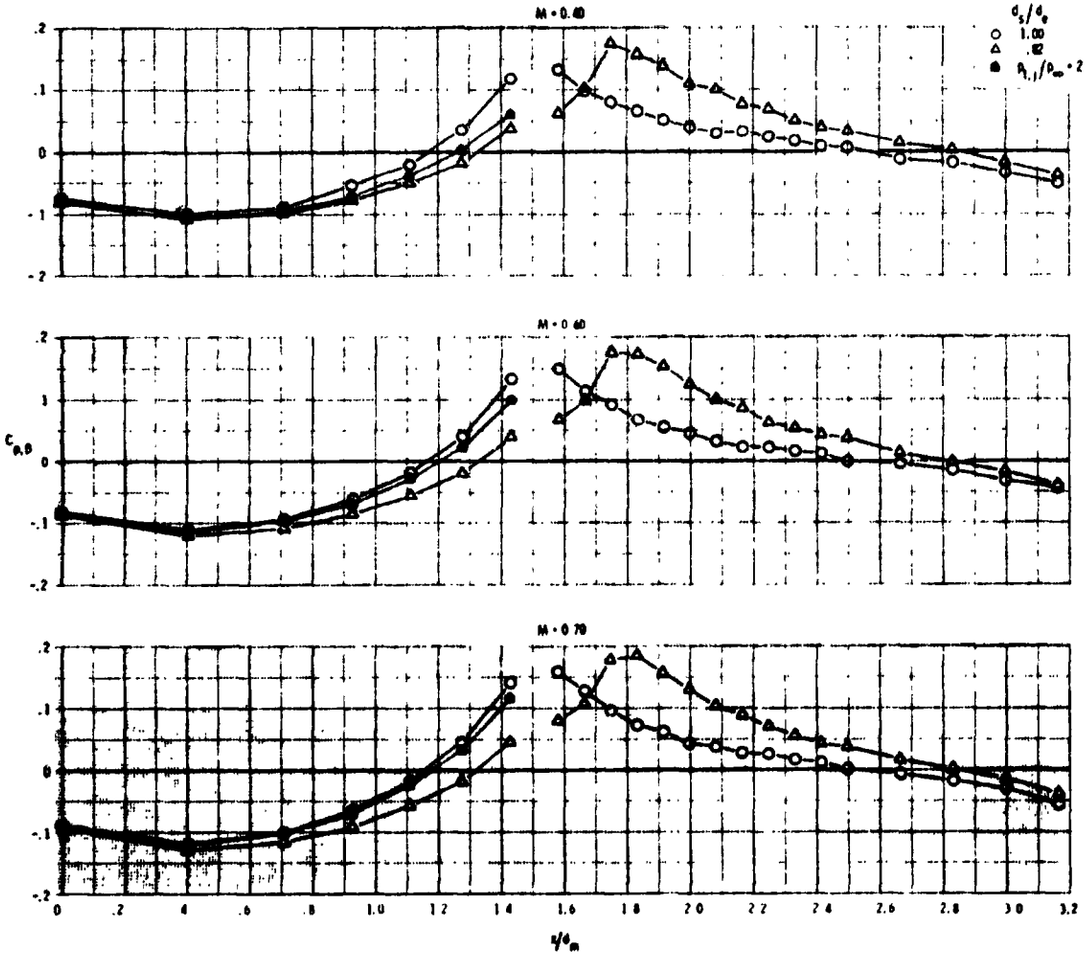

(a) M = 0.40, 0.60, and 0.70

Figure 10.- Comparison of pressure coefficient distributions obtained through the use of plume simulators with those obtained from jet operation at $p_{t,j}/p_\infty = 2$ for configuration 3 ($\ell/d_m = 1.50$, $d_e/d_m = 0.70$).

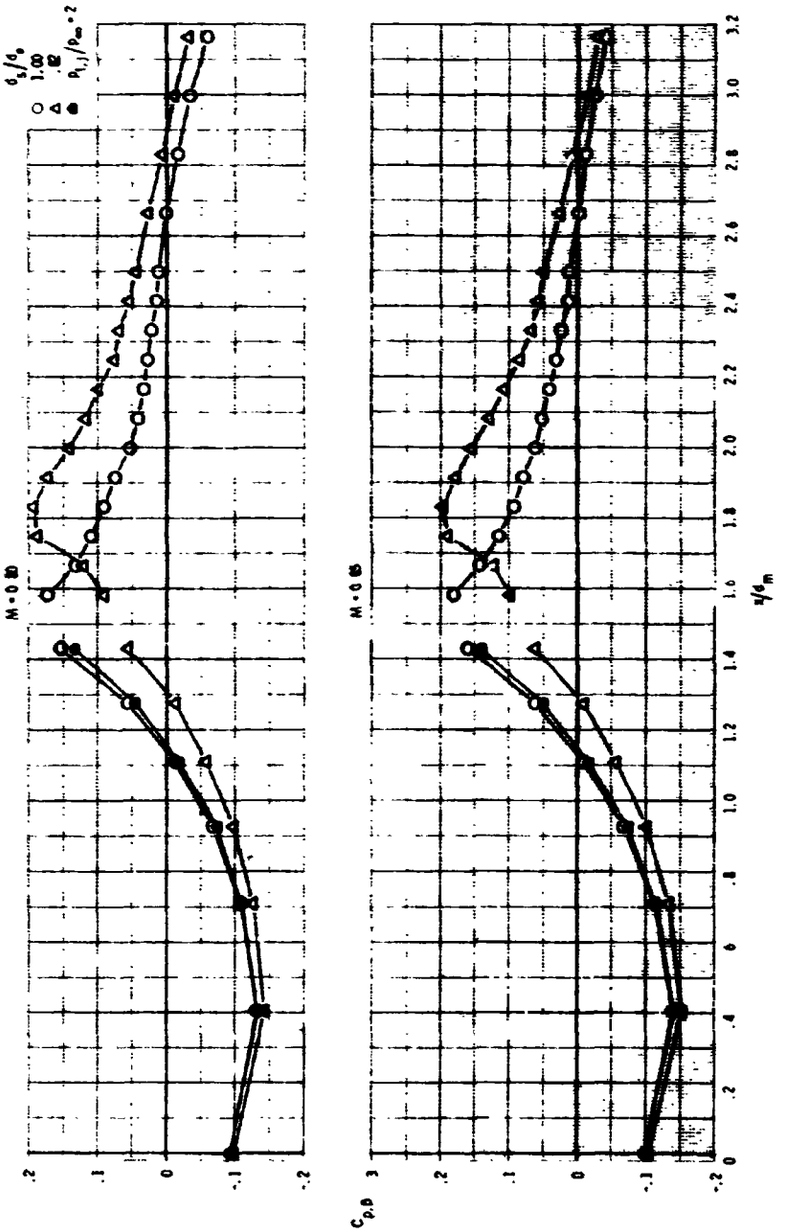

(b) M = 0.80 and 0.85

Figure 10.- Continued.

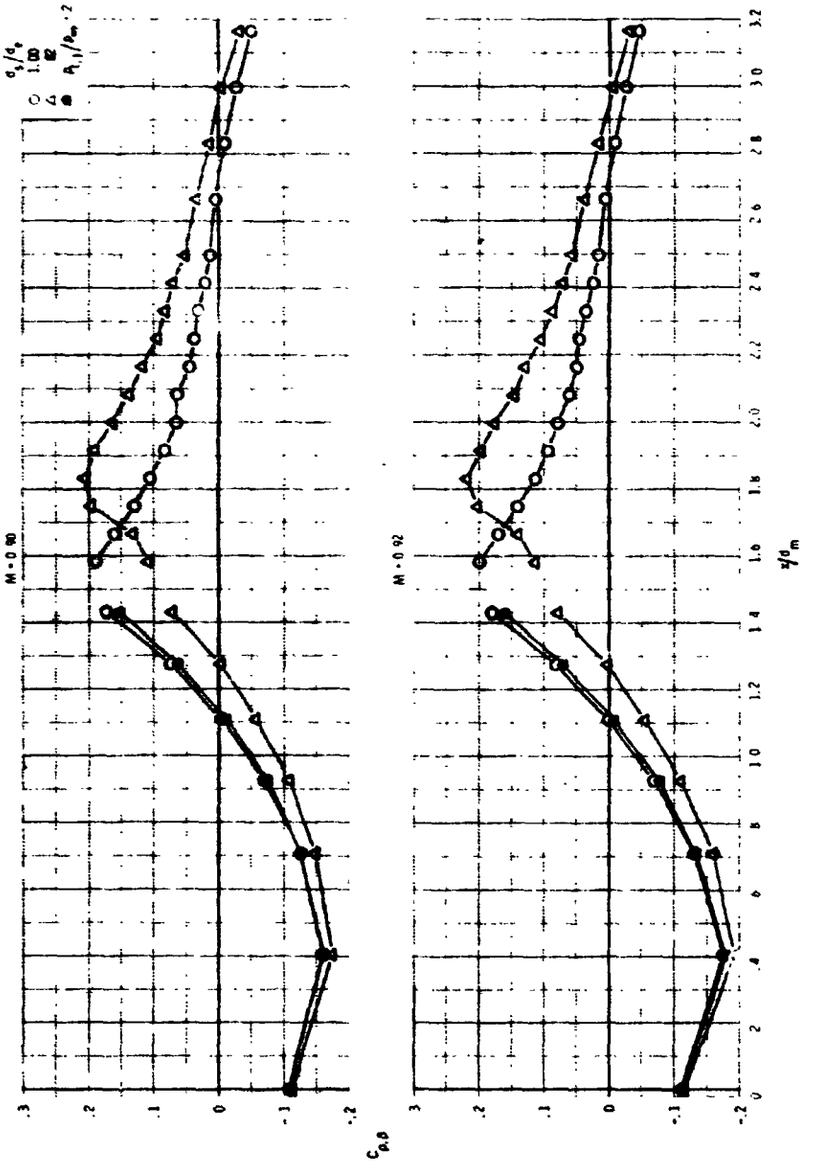

(c) M = 0.90 and 0.92

Figure 10.- Continued.

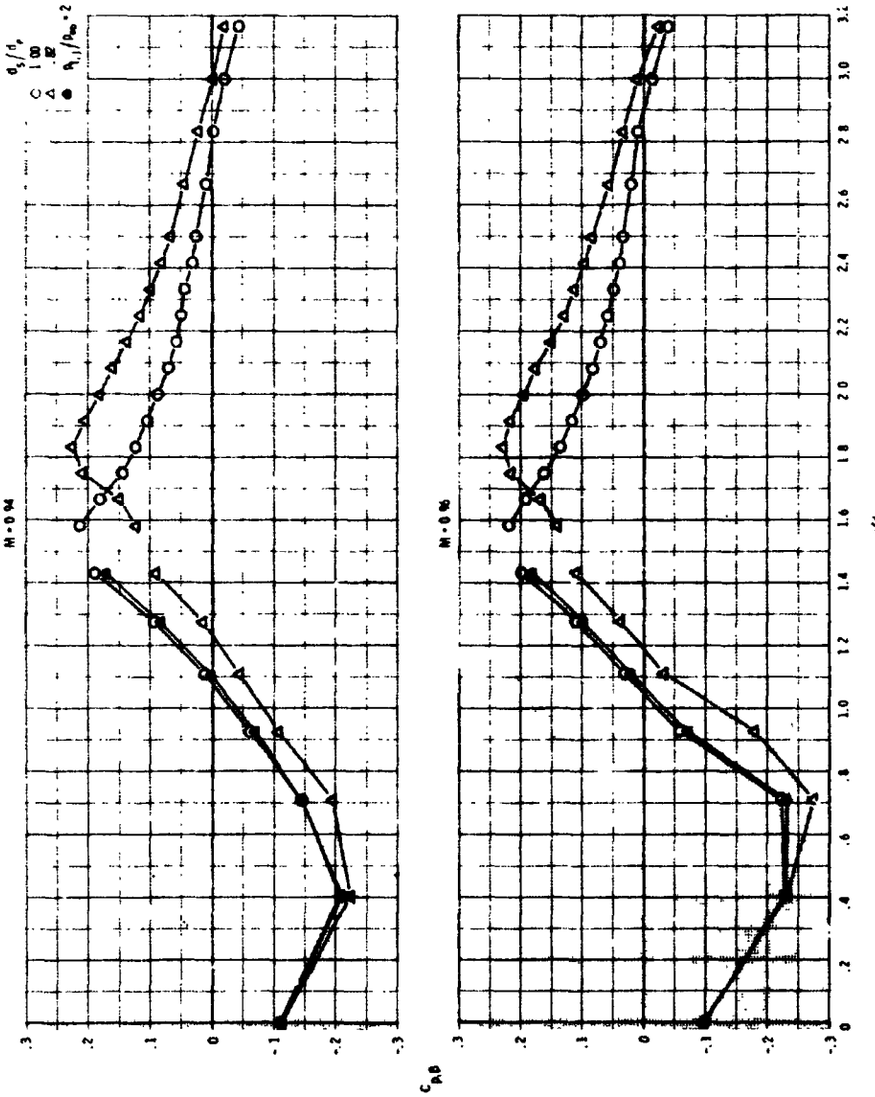

(d) M = 0.94 and 0.96

Figure 10.- Continued.

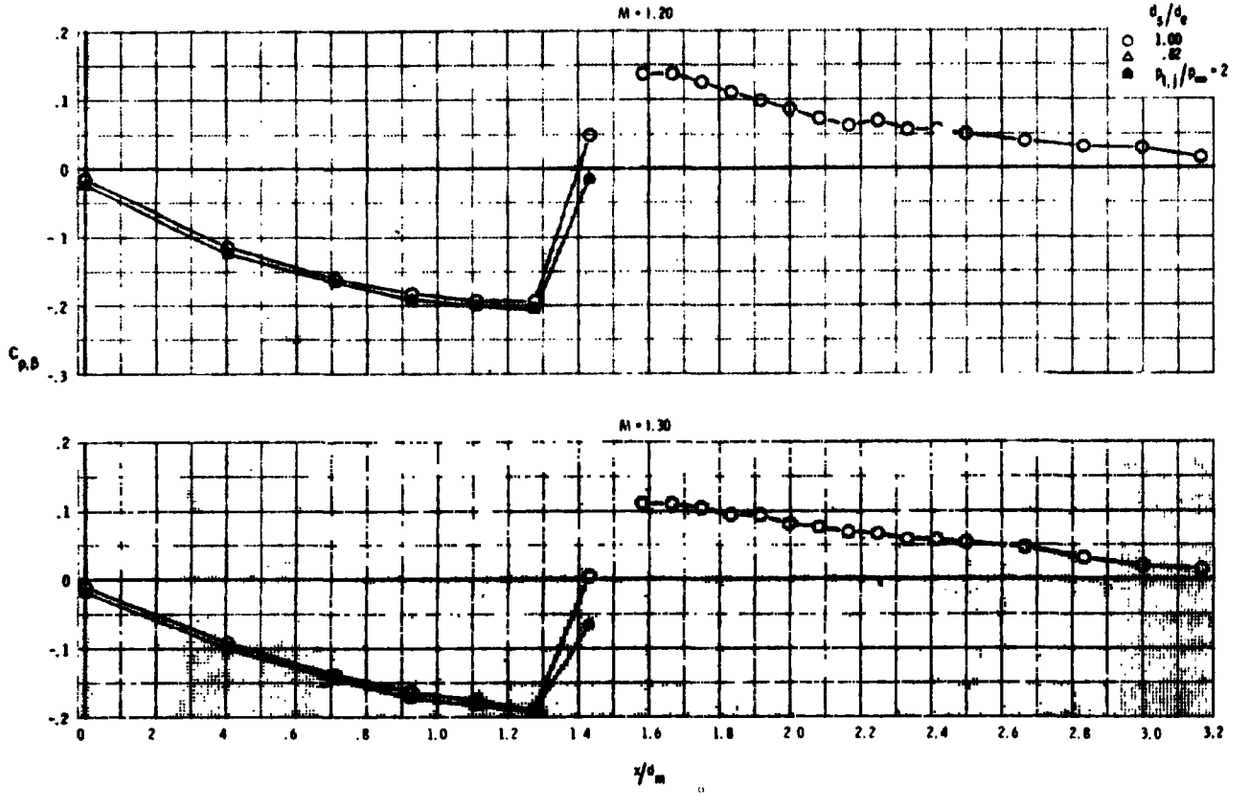

(e) M = 1.20 and 1.30

Figure 10.- Concluded.

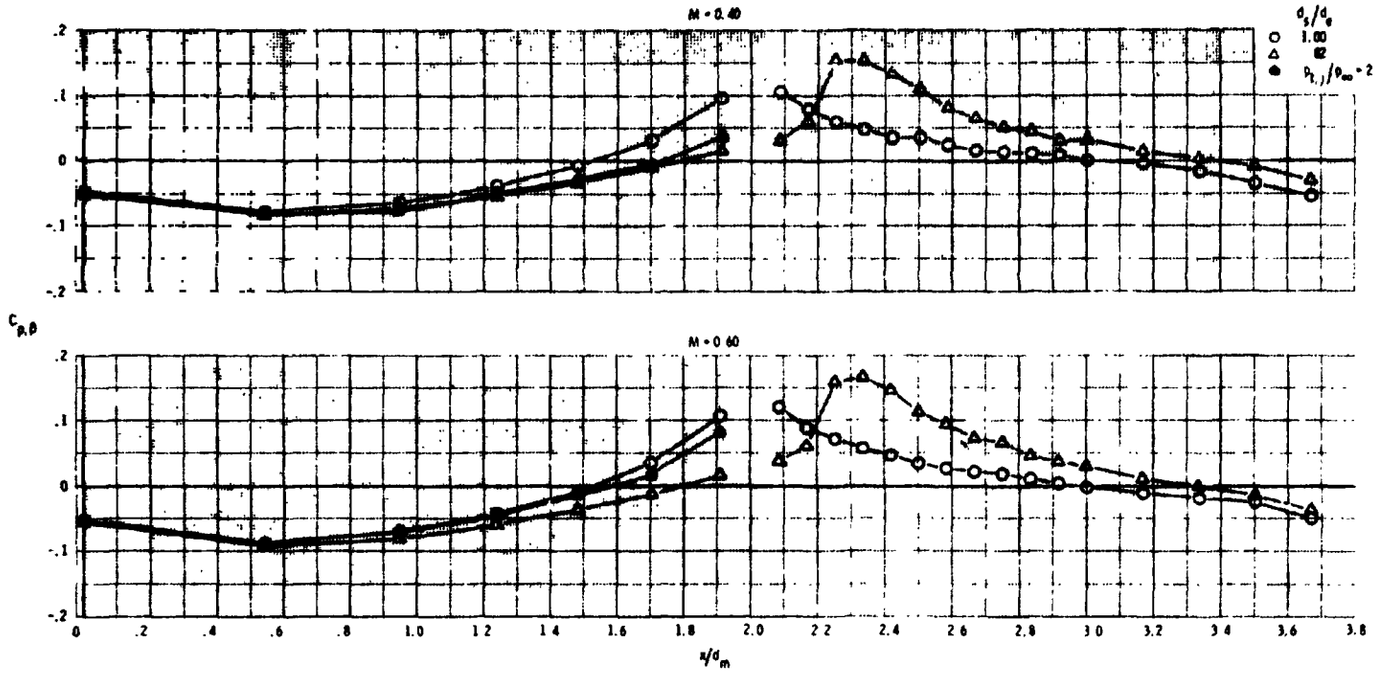

(a) M = 0,40 and 0,60

Figure 11.- Comparison of pressure coefficient distributions obtained through the use of plume simulators with those obtained from jet operation at $p_{t,j}/p_\infty = 2$ for configuration 4 ($\ell/d_m = 2.00$, $d_e/d_m = 0.70$).

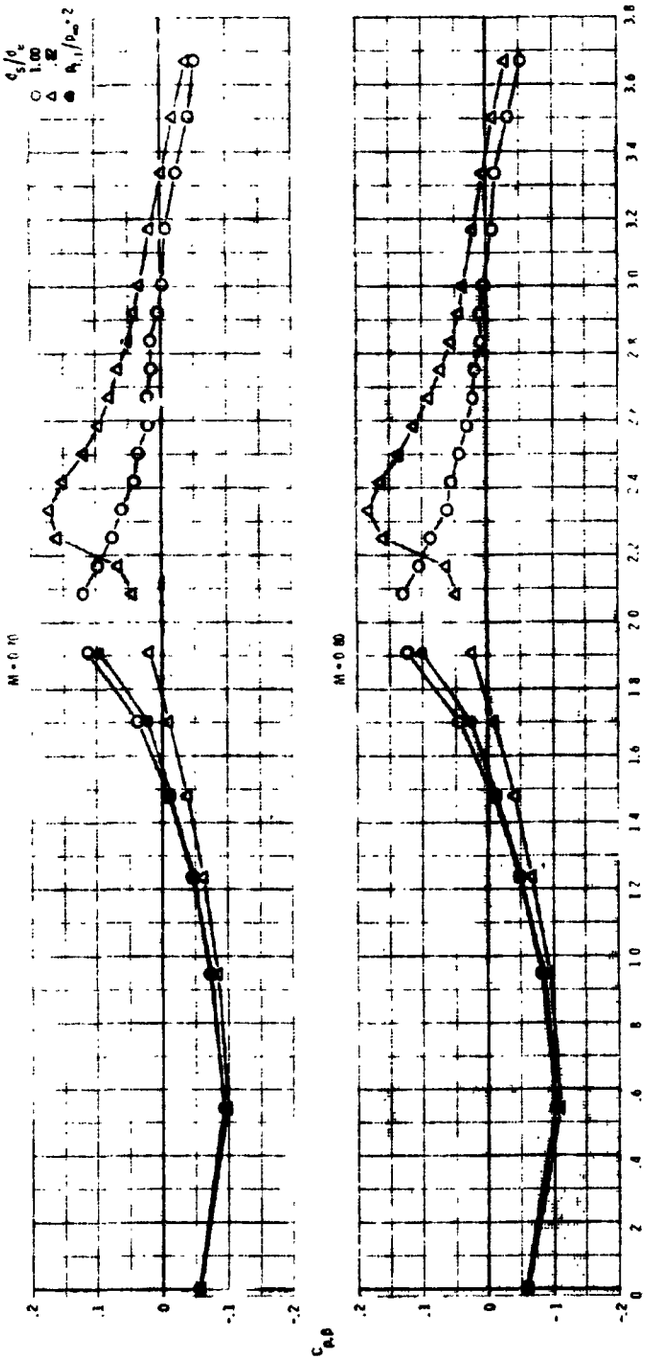

(b) M = 0.70 and 0.80

Figure 11.- Continued.

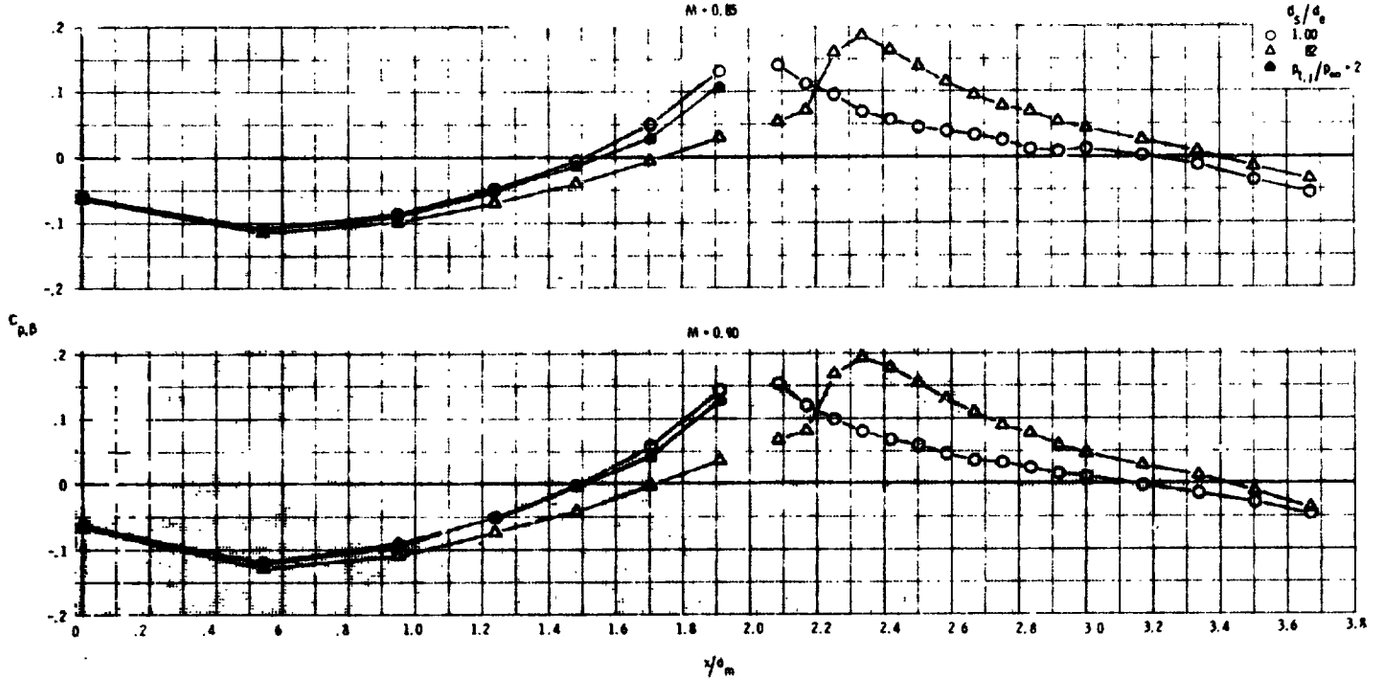

(c) M = 0.85 and 0.90

Figure 11.- Continued.

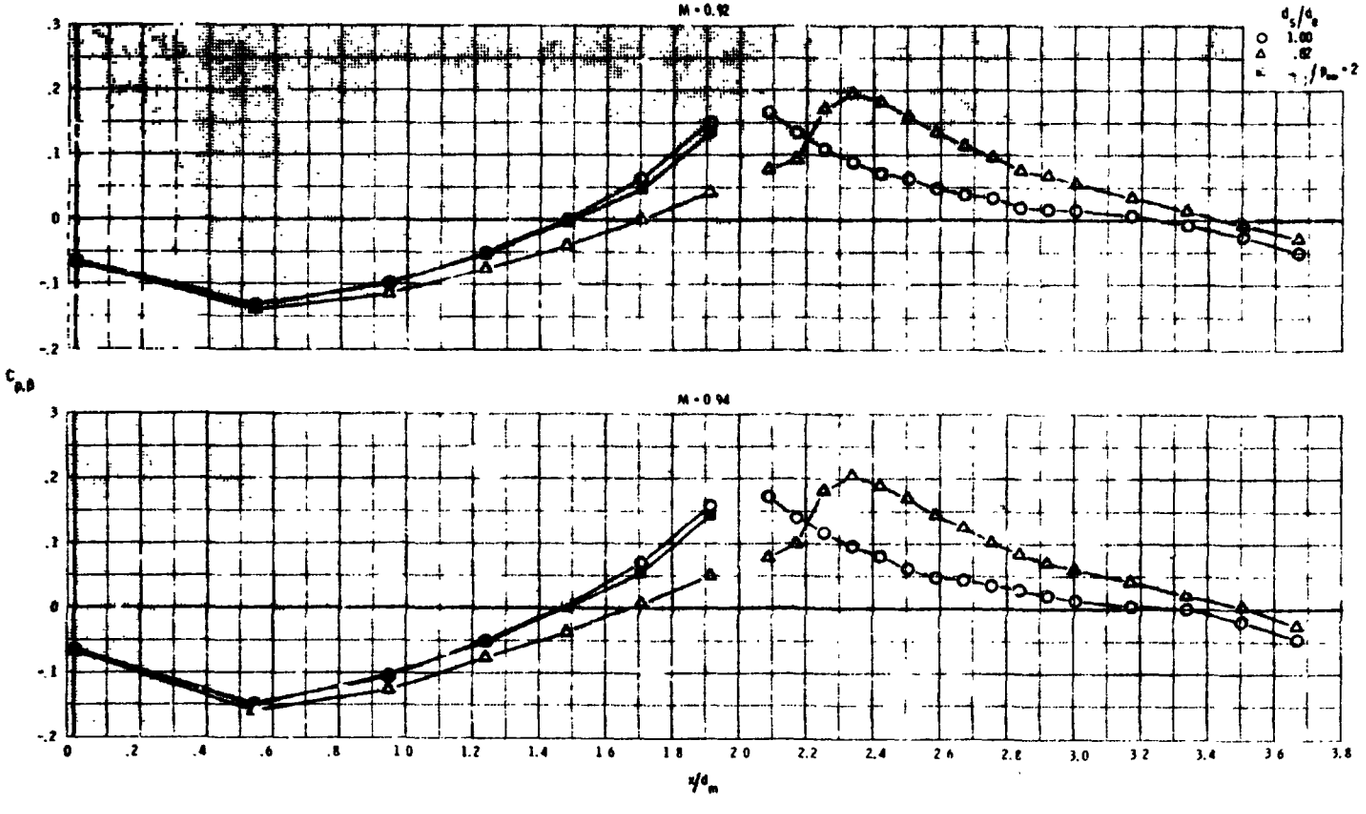

(a) M = 0.92 and 0.94

Figure 11.- Continued.

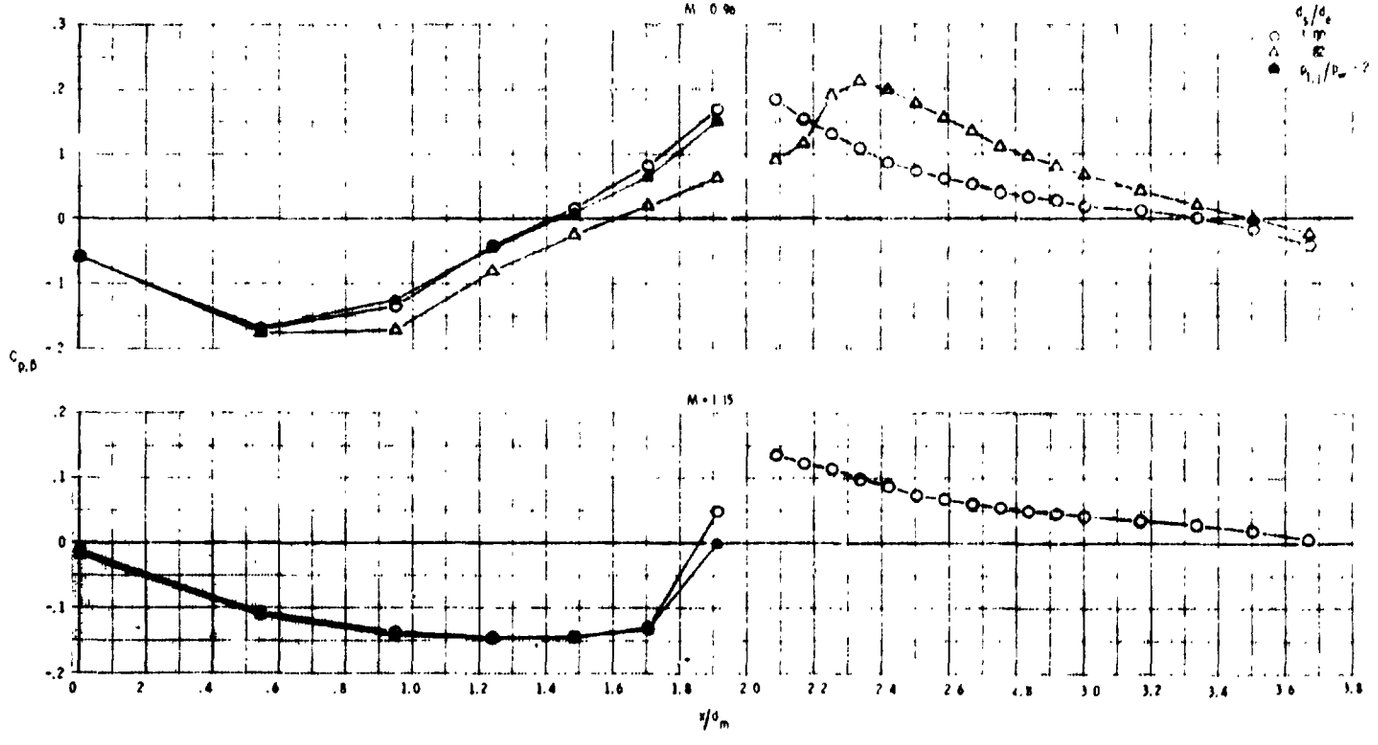

(e) M = 0.96 and 1.15

Figure 11.- Continued.

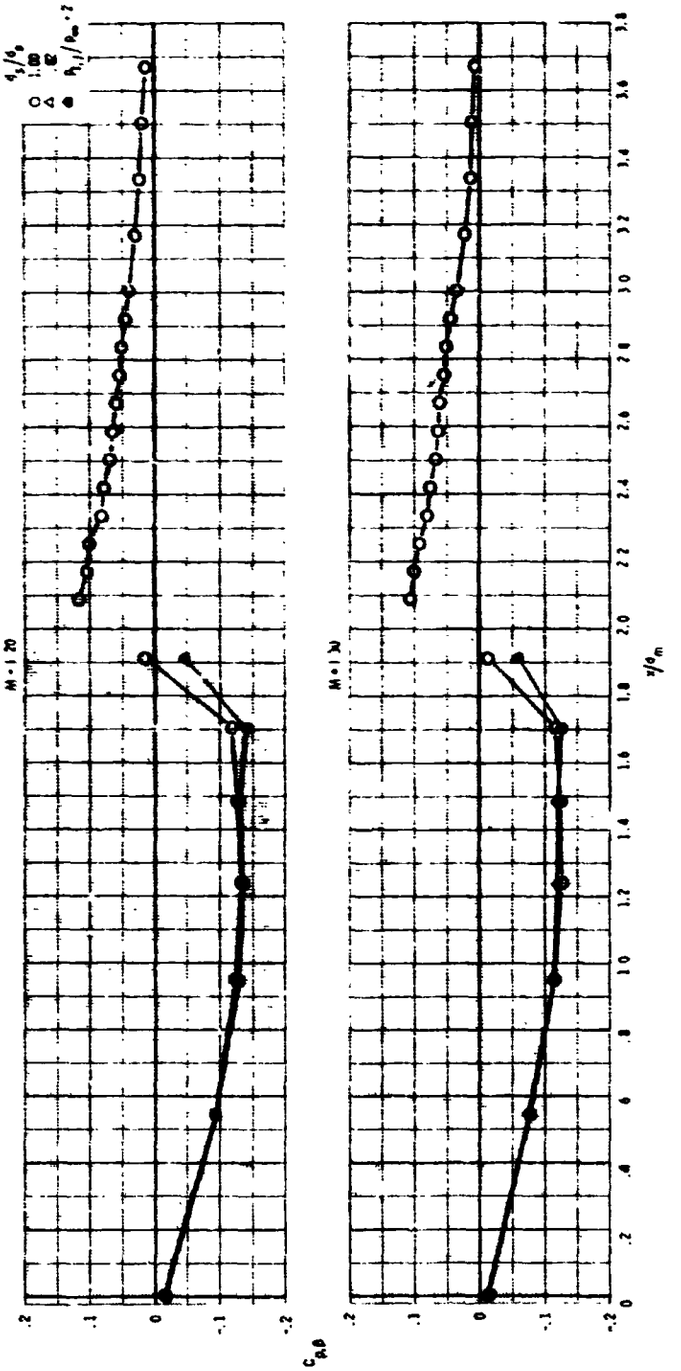

(f) M = 1.20 and 1.30

Figure 11.- Concluded.

to account for the contributions due to boundary layer development the method of reference 26 has been modified at the Langley 16-foot transonic tunnel by the addition of an iterative boundary layer solution which was adapted from reference 34 (modified Reshotko-Tucker solution). Although this particular solution was used because of the relative ease in adapting an existing computer program there are several other boundary layer solutions which could be adapted to serve the same purpose (eg. refs. 42 to 47). Reference 27 discusses a boundary layer solution which is used in conjunction with its inviscid solution, however thi. program is still under development and the boundary layer solution does not work correctly for most configurations at the present time.

Figures 12 to 15 present comparisons of the afterbody pressure coefficient distributions for the four configurations of this paper obtained both jet-on at a jet total-pressure ratio of two and with the $d_s/d_e = 1.00$ simulator at various Mach numbers with the pressure coefficient distributions as predicted by the theoretical methods. In all cases the solid body used to simulate the jet plume shape for the method of reference 26 was a circular cylinder with the diameter of the cylinder equal to the exit diameter of the nozzle (same as $d_s/d_e = 1.00$ simulator).

Figure 12 presents the pressure coefficient distribution comparisons for configuration 1 ($\ell/d_m = 1.77$, $d_e/d_m = 0.50$) at six subsonic Mach numbers from 0.40 to 0.90. At all Mach numbers except

M = 0.90 the method of reference 26 predicts the minimum pressure coefficient on the boattail very well and the general shape of the curve fairly well. Since this is an inviscid solution which neglects such things as the boundary layer "filleting" corners the predicted pressures near the boattail trailing edge are too high because a concave corner such as between the boattail and the assumed cylindrical plume results in the theory predicting a stagnation point. At M = 0.90 the theory under-predicts the peak negative pressure coefficient by a slight amount. This is probably due to the inadequacy of the Goethert similarity rule used in the solution at this transonic Mach number. The addition of the boundary layer solution to this method virtually eliminates the problem of the stagnation point at the trailing edge; however, it does result in the predicted boattail pressure coefficients being too high (It must be noted that the program would not run for configuration 1 at Mach numbers of 0.80, 0.85, and 0.90 and for configuration 2 at Mach numbers of 0.85 and 0.90 and, as a result, no boundary layer curves are shown for those conditions.).

The method of reference 27 produces varied results; at some Mach numbers the predicted pressure coefficients are lower than those obtained with the jet operating or with the plume simulators while at other Mach numbers it predicts pressure coefficients that are too high. The reason for this is that the program sets up a grid of streamlines and orthogonals at a given Mach number and refines it

until certain convergence criteria are met at which point it produces answers and proceeds to the next Mach number. At the next Mach number it starts with the already developed grid and does any further refinement necessary, produces answers, and starts the process over again. However, in most instances the refinement criteria are not sufficiently stringent and thus the same grid will satisfy the equations of motion for more than one Mach number and when this occurs the predicted pressure coefficient distributions will be essentially the same for both Mach numbers. It is at the Mach numbers where the grid has changed that the program predicts pressure coefficients lower than the data while an increase in Mach number above this but before the next grid refinement will result in a decrease in the measured pressure coefficients with the predicted coefficients remaining the same and thus changing the relationship of the two curves. In addition, this theory also predicts pressure coefficients that are too high in the region near the boattail trailing edge but they are not as high as those predicted by the method of reference 26.

Similar statements can be made for the comparisons for the other three configurations (figs. 13, 14, and 15). The theory of reference 26 does a reasonably good job of predicting the minimum pressure coefficient reached on the afterbodies but does a poor job at the trailing edge where it predicts a stagnation point. The addition of a boundary layer solution to this theory eliminates the problem with the trailing edge stagnation point but causes the whole pressure

coefficient distribution to be slightly high. Pressure coefficient distributions from the method of reference 27 are sometimes too low, sometimes too high, and have a slight problem at the boattail trailing edge but not as large as those obtained with the method of reference 26. In summary, these theoretical techniques do a reasonably good job of predicting the afterbody pressure coefficient distributions for these unseparated afterbodies but not as good a job as the $d_s/d_e = 1.00$ simulators. In addition, the integrated boattail pressure drag values which would be calculated from these theoretical pressure distributions would, in general, predict afterbody drags much lower than the jet-on, $p_{t,j}/p_\infty = 2$ drag for all configurations and therefore be unsatisfactory for drag estimation. Also, if separation occurs on an afterbody such as the configurations of references 24 and 25 not treated herein the theoretical pressure coefficient distribution predictions would be considerably more in error and the resultant afterbody drag values would be totally unrealistic.

Boattail drag.- Figures 16 to 19 show curves of boattail pressure drag coefficients as a function of jet total-pressure ratio ($p_{t,j}/p_\infty$) from references 24 and 25 with the pressure drag coefficients obtained using the simulators superimposed on them. As mentioned before, configuration 1 ($\ell/d_m = 1.77$, $d_e/d_m = 0.50$) was tested with four simulator diameters ($d_s/d_e = 1.00$, 0.98, 0.88, and 0.82) while the other three configurations were tested with only the $d_s/d_e = 1.00$ and 0.82 simulators. With the exception of configuration 2 ($\ell/d_m = 1.50$, $d_e/d_m = 0.60$) at $M = 0.40$ the drag coefficients obtained with the

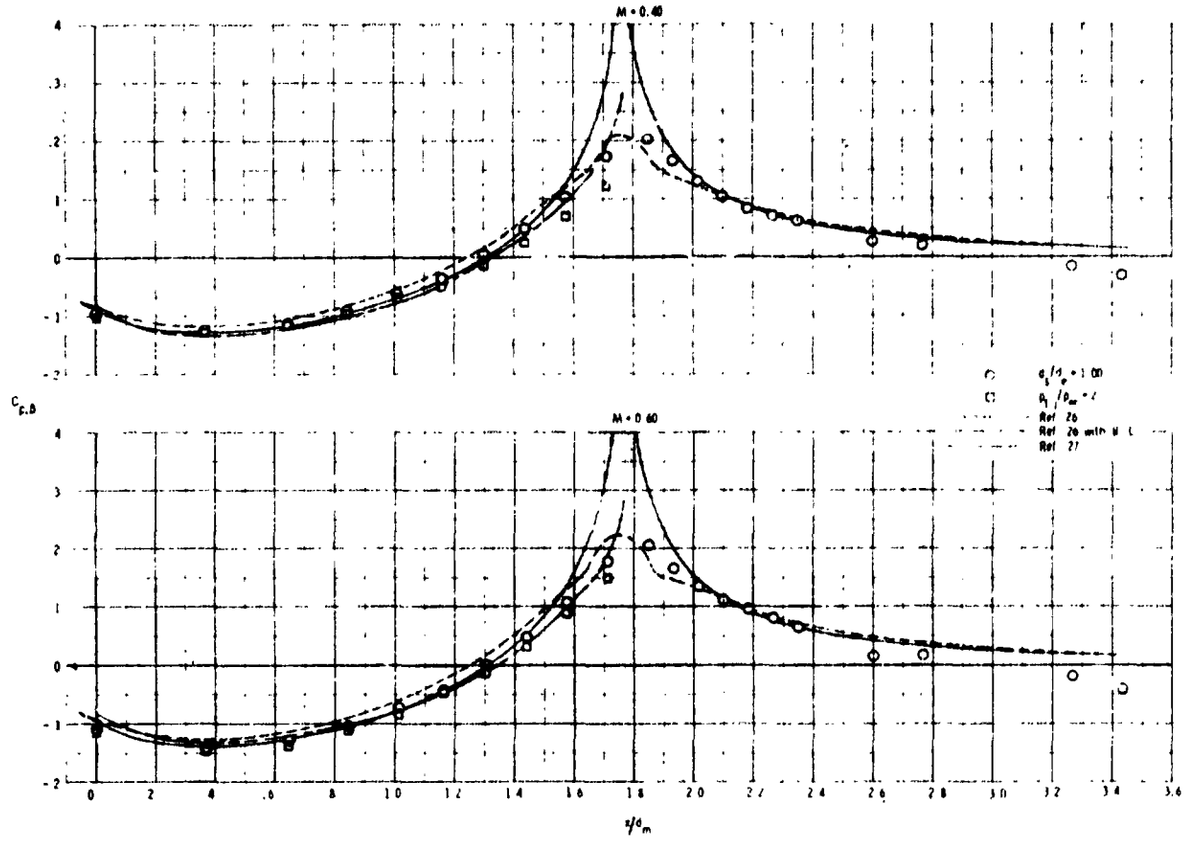

(a) M = 0.40 and 0.60

Figure 12.- Comparison of pressure coefficient distributions obtained by use of the theoretical techniques of references 26 and 27 with those obtained from jet operation at $p_{t,j}/p_\infty = 2$ and from use of the $d_s/d_e = 1.00$ simulator for configuration 1 ($\ell/d_m = 1.77$, $d_e/d_m = 0.50$).

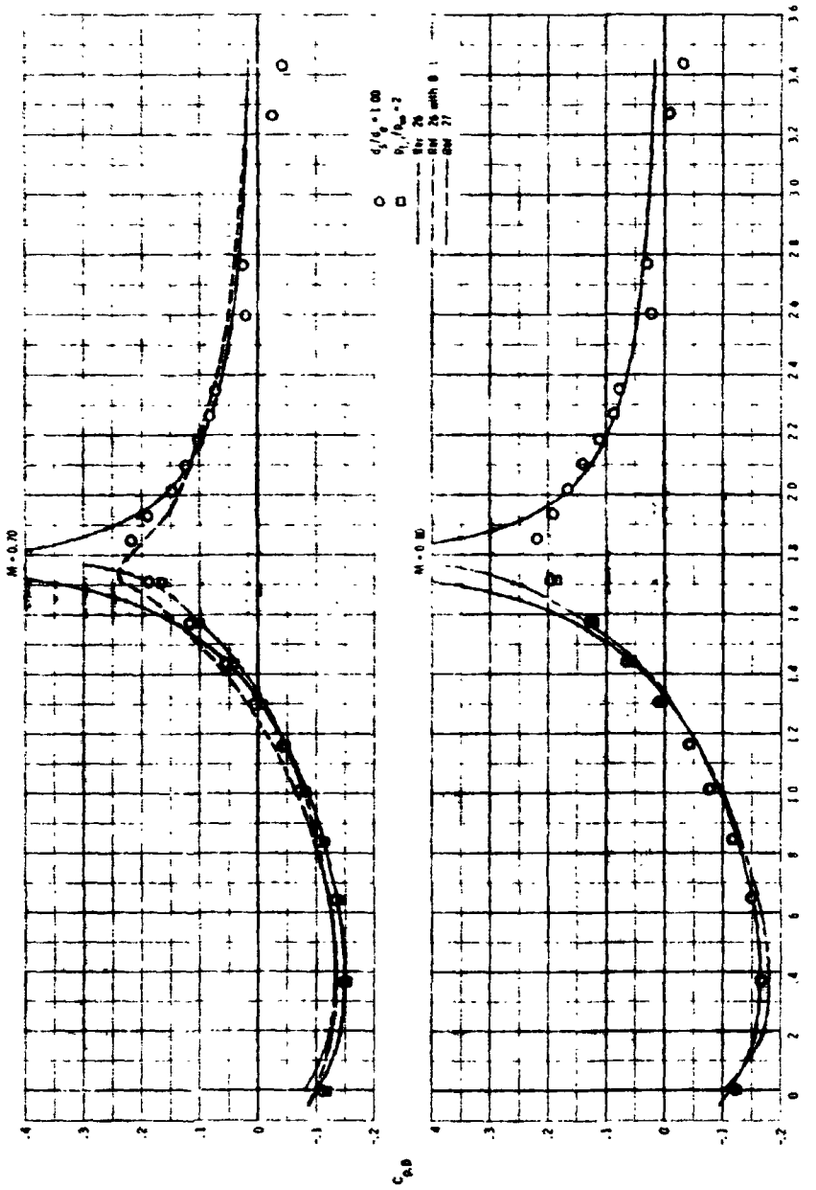

(b) M = 0.70 and 0.80

Figure 12.- Continued.

(c) M = 0.85 and 0.90

Figure 12.- Concluded.

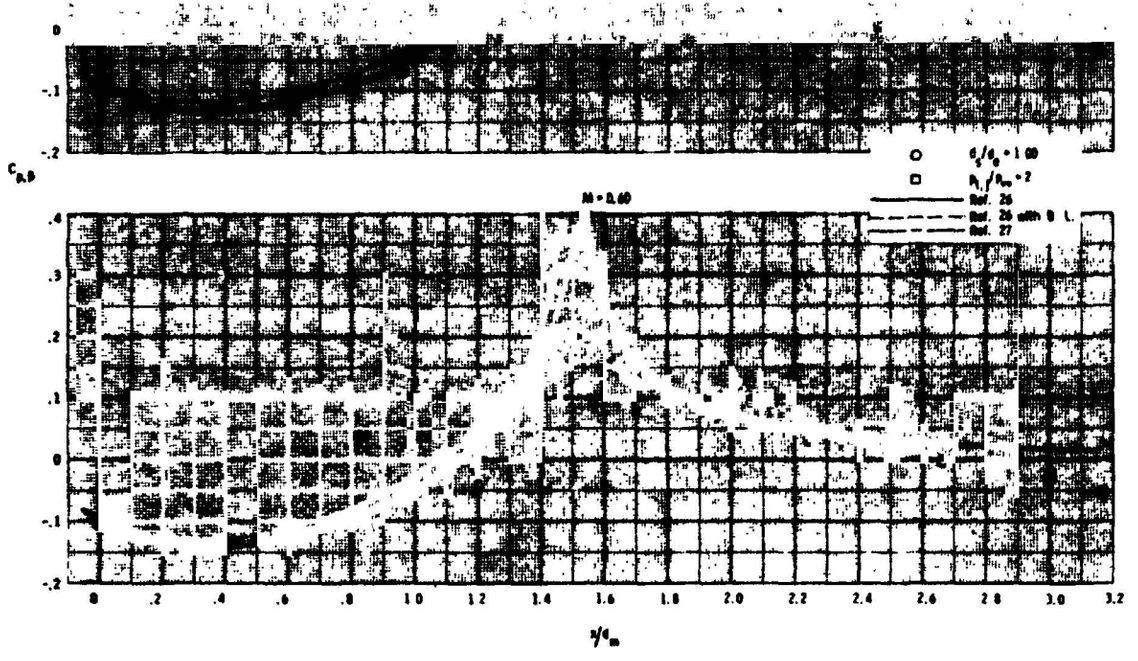

(a) M = 0.40 and 0.60

Figure 13.- Comparison of pressure coefficient distributions obtained by use of the theoretical techniques of references 26 and 27 with those obtained from jet operation at $p_{t,j}/p_\infty = 2$ and from use of the $d_s/d_e = 1.00$ simulator for configuration 2 ($\ell/d_m = 1.50$, $d_e/d_m = 0.60$).

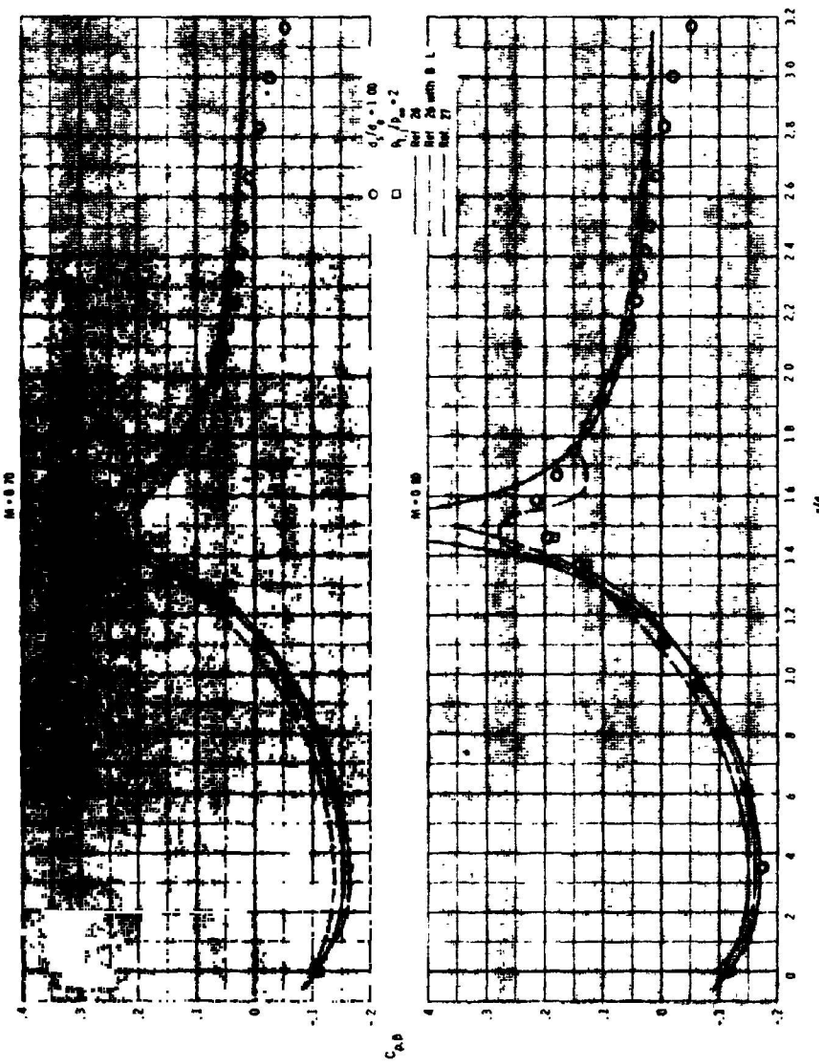

(b) M = 0.70 and 0.80

Figure 13.- Continued.

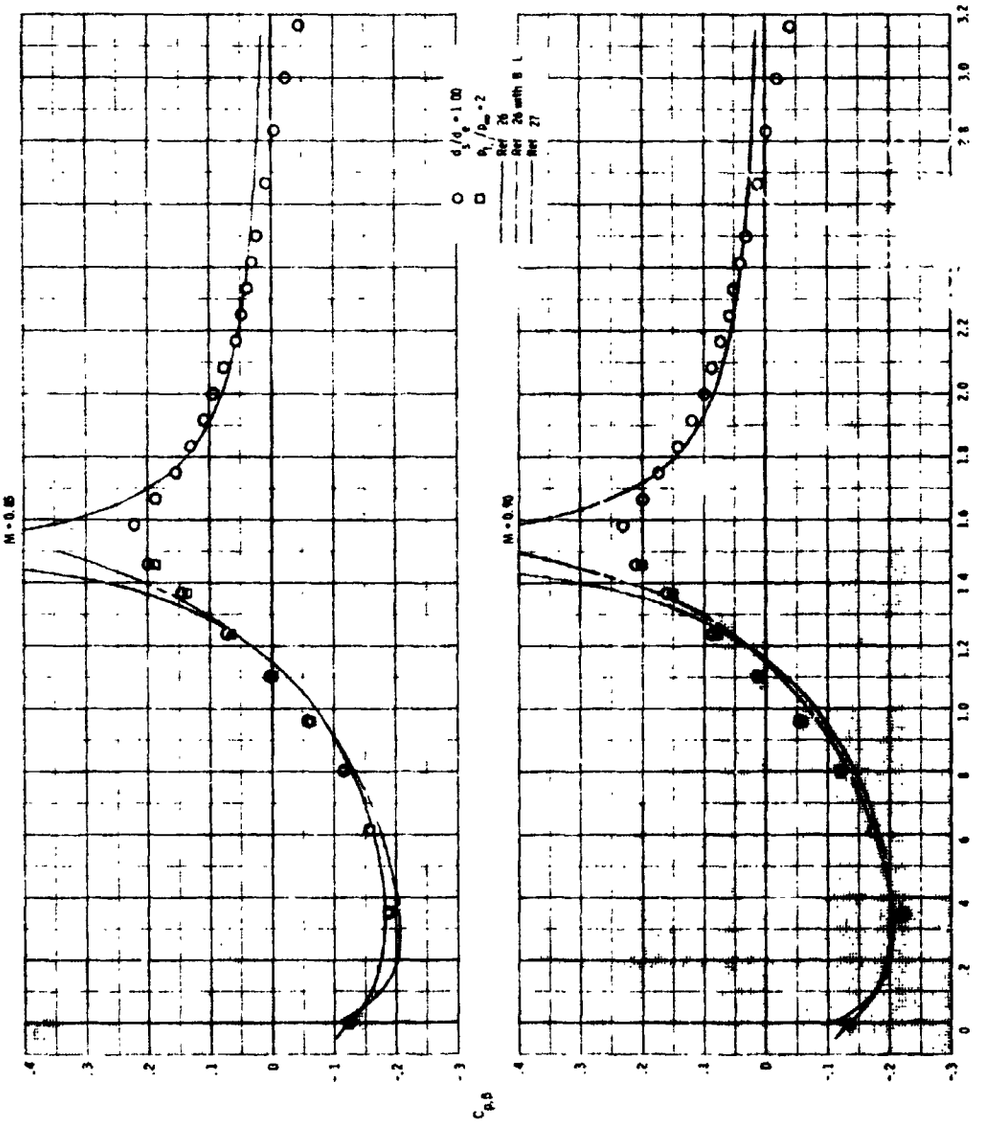

(c) M = 0.85 and 0.90

Figure 13.- Concluded.

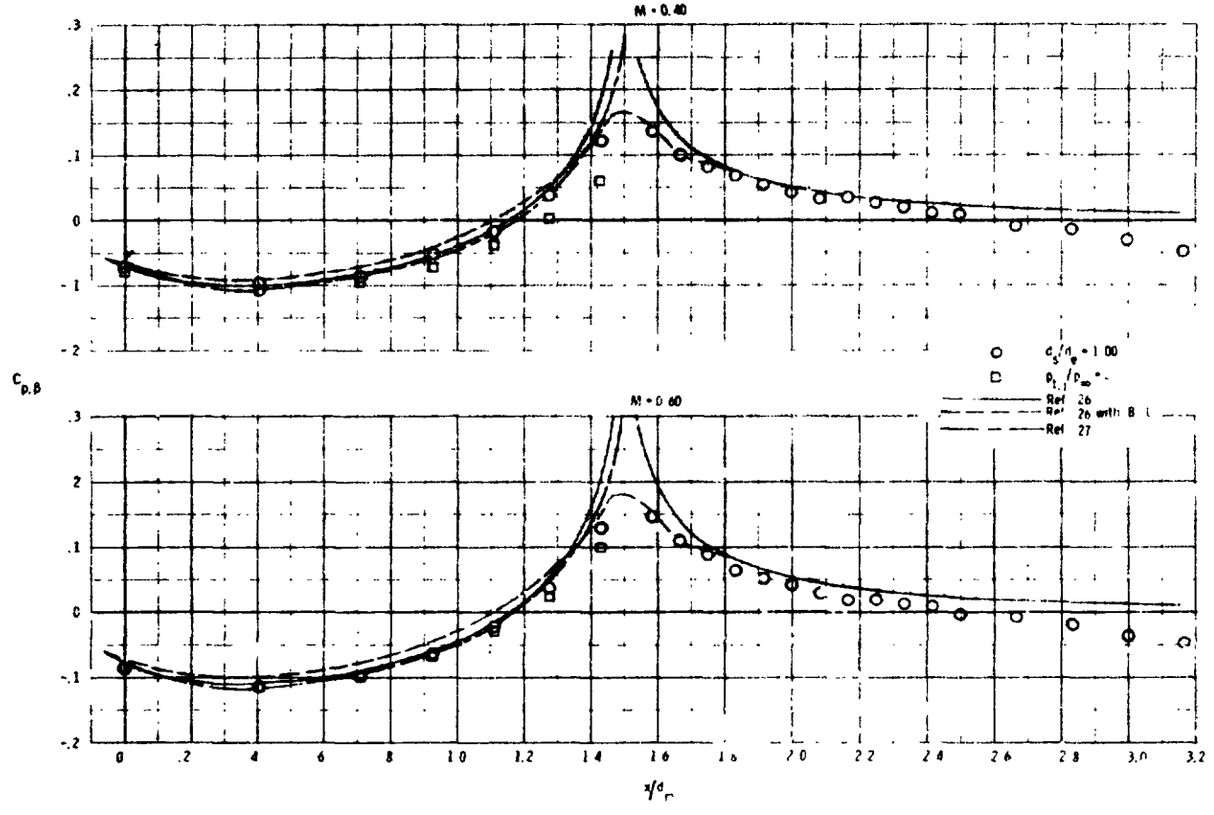

(a) M = 0.40 and 0.60

Figure 14.- Comparison of pressure coefficient distributions obtained by use of the theoretical techniques of references 26 and 27 with those obtained from jet operation at $p_{t,j}/p_\infty = 2$ and from use of the $d_s/d_e = 1.00$ simulator for configuration 3 ($\ell/d_m = 1.50$, $d_e/d_h = 0.70$).

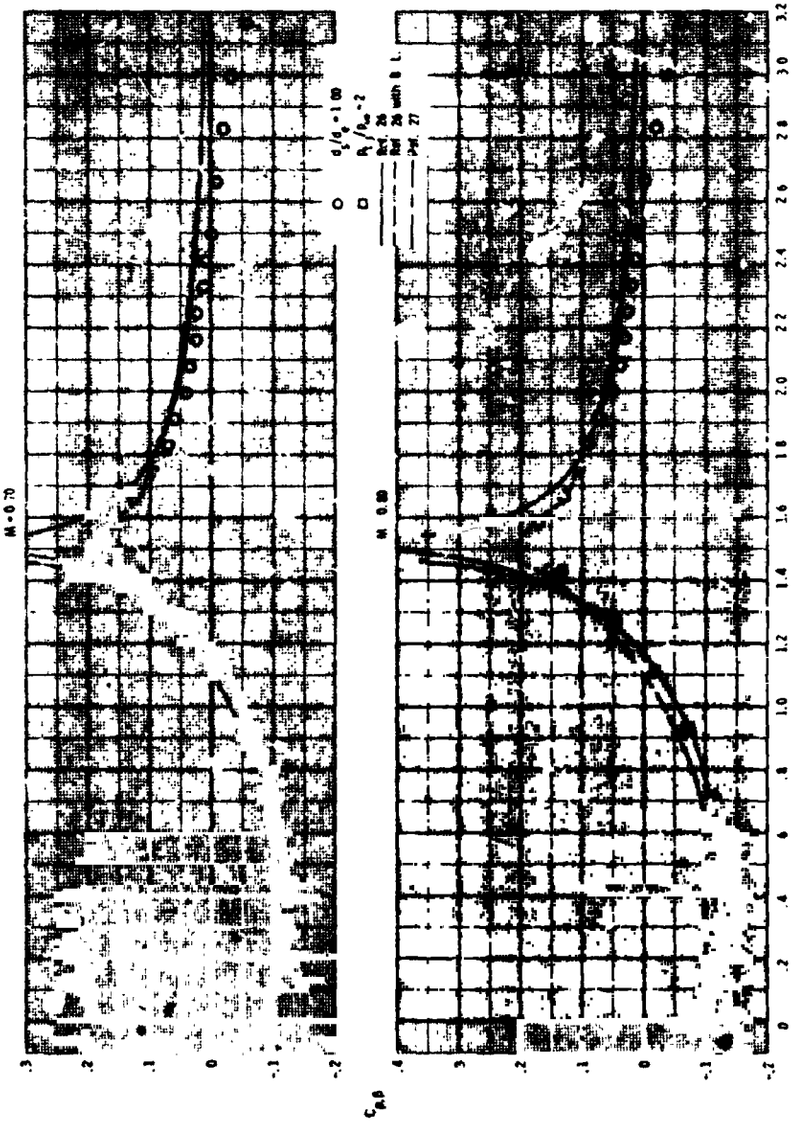

(b) M = 0.70 and 0.80

Figure 14.- Continued.

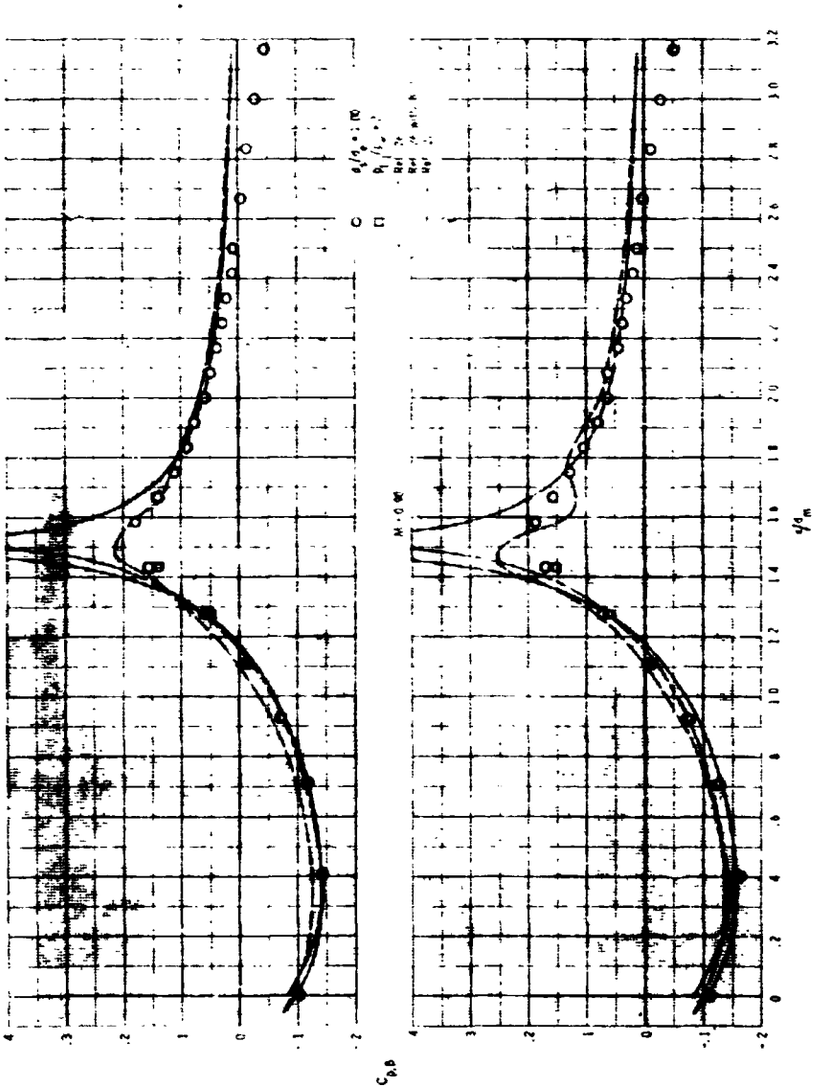

(c) M = 0.85 and 0.90

Figure 14.- Concluded.

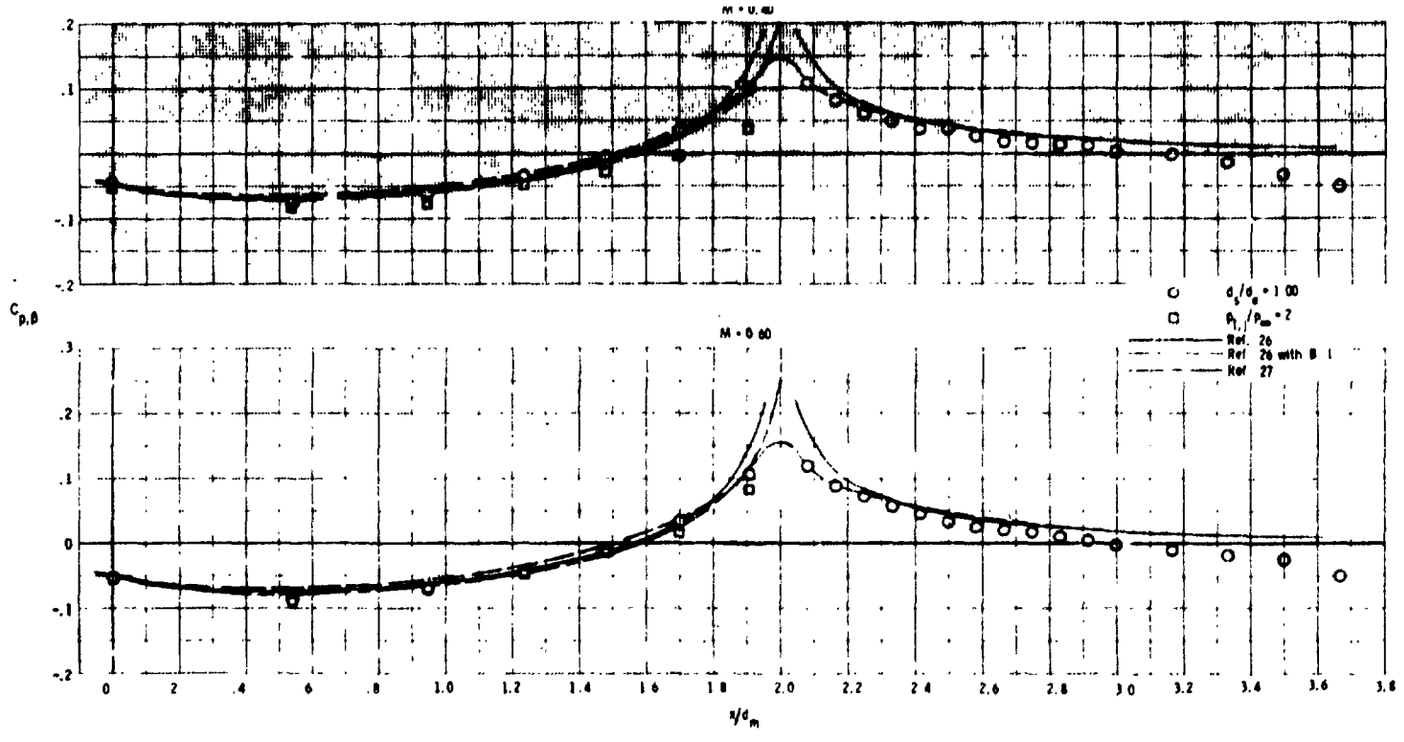

(a) M = 0.40 and 0.60

Figure 15.- Comparison of pressure coefficient distributions obtained by use of the theoretical techniques of references 26 and 27 with those obtained from jet operation at $P_{t,j}/P_\infty = 2$ and from use of the $d_s/d_e = 1.00$ simulator for configuration 4 ($\ell/d_m = 2.00$, $d_e/d_m = 0.70$).

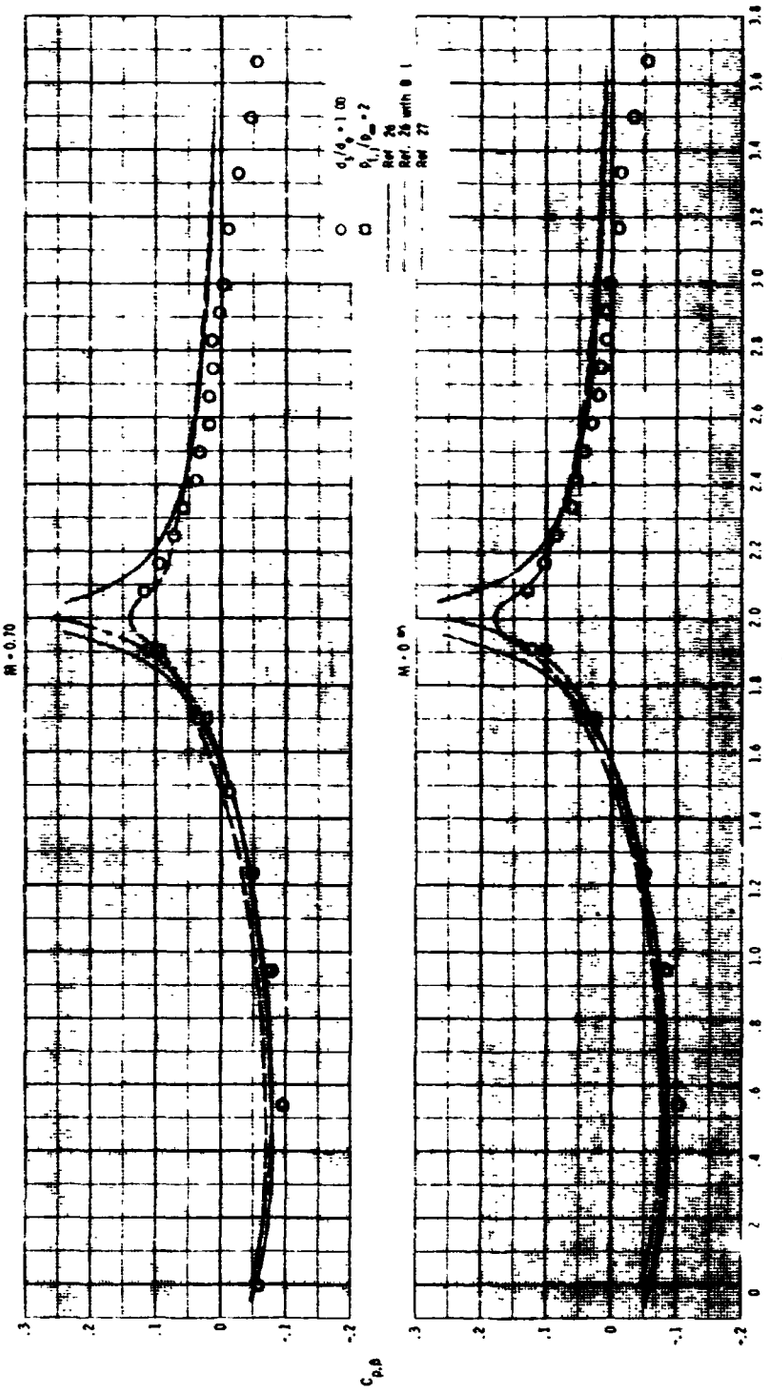

(b) M = 0,70 and 0,80

Figure 15.- Continued.

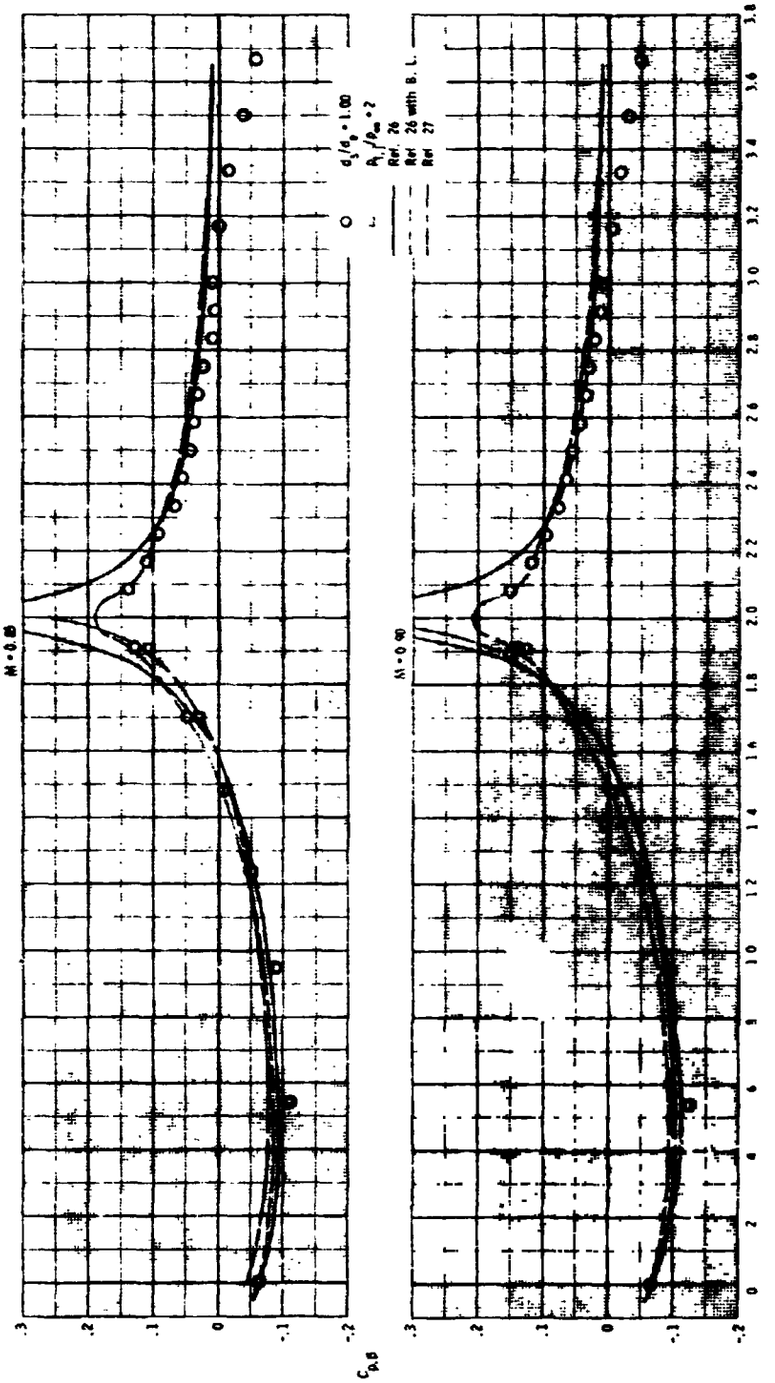

(c) M = 0.85 and 0.90

Figure 15.- Concluded.

d_s/d_e = 0.82 simulators were always higher than any jet-on drag coefficients obtained for the corresponding configurations at any Mach number. The drag coefficients obtained with the d_s/d_e = 0.88 simulator tested with configuration 1 were also higher than any jet-on drag coefficients with the exception of the Mach numbers of 0.40 and 0.60. Also for configuration 1, the boattail drag coefficients obtained with the d_s/d_e = 0.98 simulator generally crossed the $C_{D,\beta}$ vs. $p_{t,j}/p_\infty$ curve at a jet total-pressure ratio of between 1 and 2 at subsonic speeds and about a jet total-pressure ratio of 3 at supersonic speeds.

These results are generally as expected based on the pressure distributions. The smaller diameter simulators (d_s/d_e = 0.82 and 0.88) more closely match the drag coefficient levels at the low Mach numbers where the entrainment effects are large and these entrainment effects reduce the beneficial blockage effect of the full jet plume. The large diameter simulators (d_s/d_e = 1.00 and 0.98) more closely match the drag coefficients at the higher Mach numbers where the entrainment effects are not as great. However, use of the d_s/d_e = 1.00 simulators generally results in drag coefficient values corresponding to jet total-pressure ratios in the range of 2 to 3. Fortuitously, this is the typical operating range for subsonic transport aircraft and for fighter-type aircraft at subsonic cruise conditions as evidenced by the two typical curves of operating jet total-pressure ratio as a function of Mach number shown in figure 20. Therefore the drag coefficient data thus obtained by use of a model with the simulators

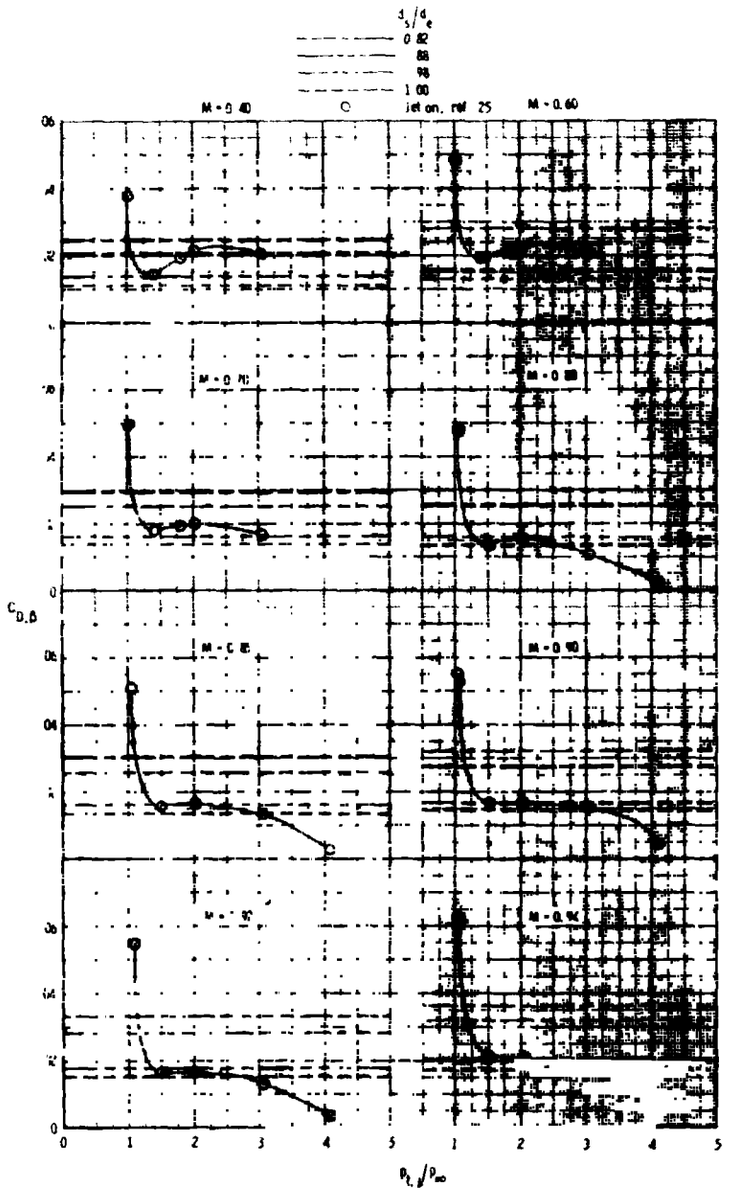

(a) M = 0.40 to 0.94

Figure 16.- Comparison of integrated boattail pressure drag coefficients obtained through use of the simulators with jet-on values for configuration 1 (ℓ/d_m = 1.77, d_e/d_m = 0.50).

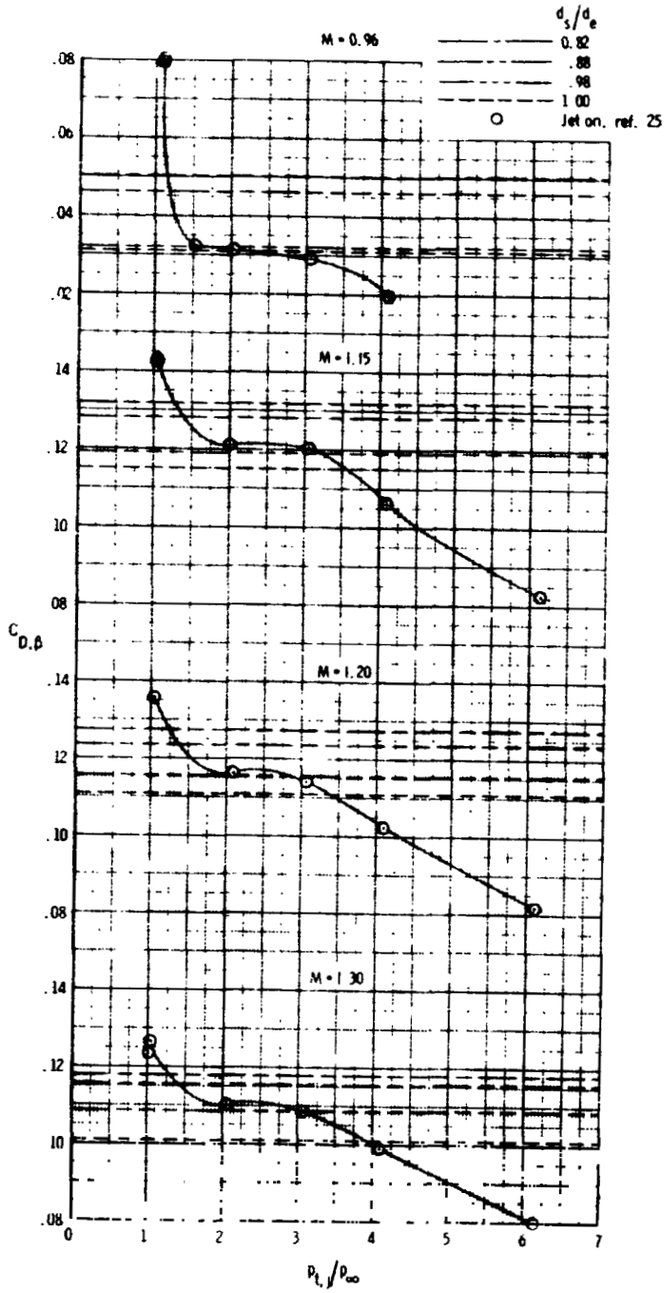

(b) M = 0.96 to 1.30

Figure 16.- Concluded.

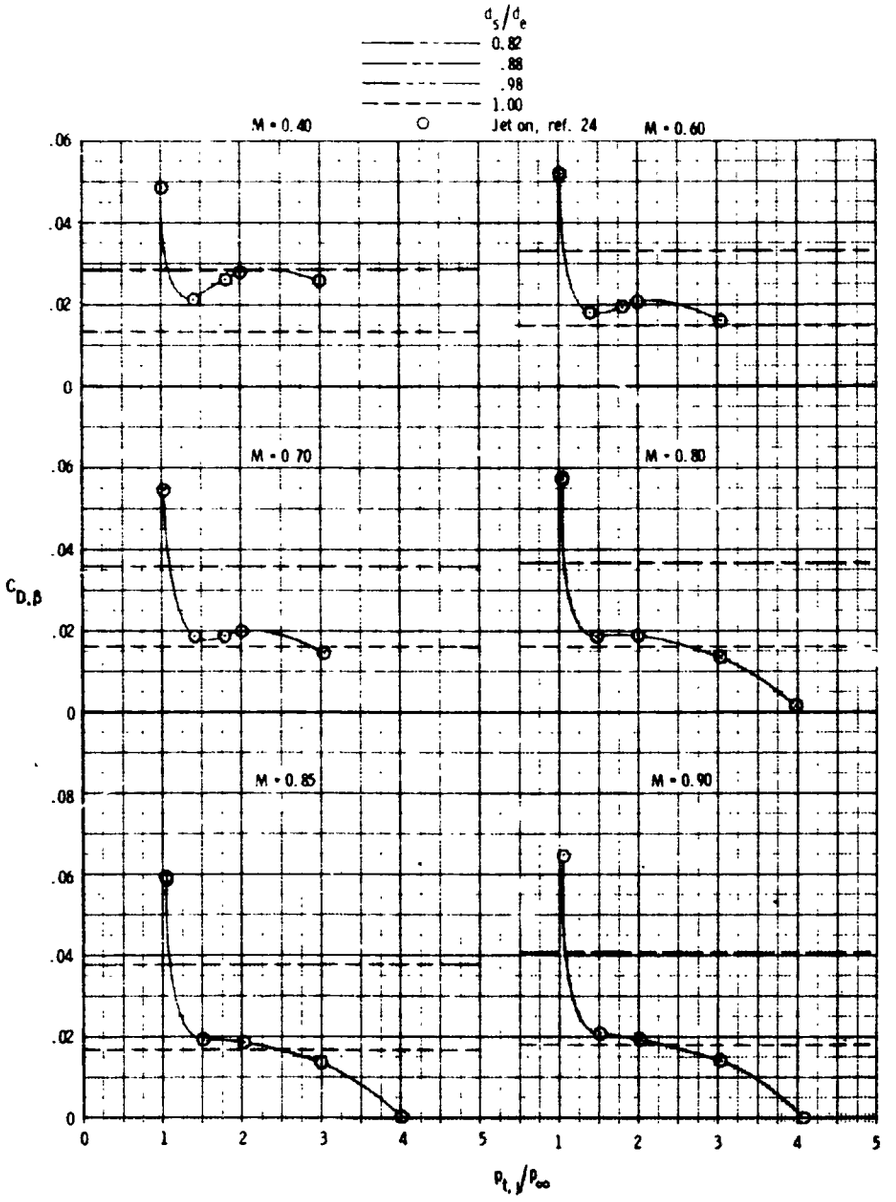

(a) M = 0.40 to 0.90

Figure 17.- Comparison of integrated boattail pressure drag coefficients obtained through use of the simulators with jet-on values for configuration 2 (ℓ/d_m = 1.50, d_e/d_m = 0.60).

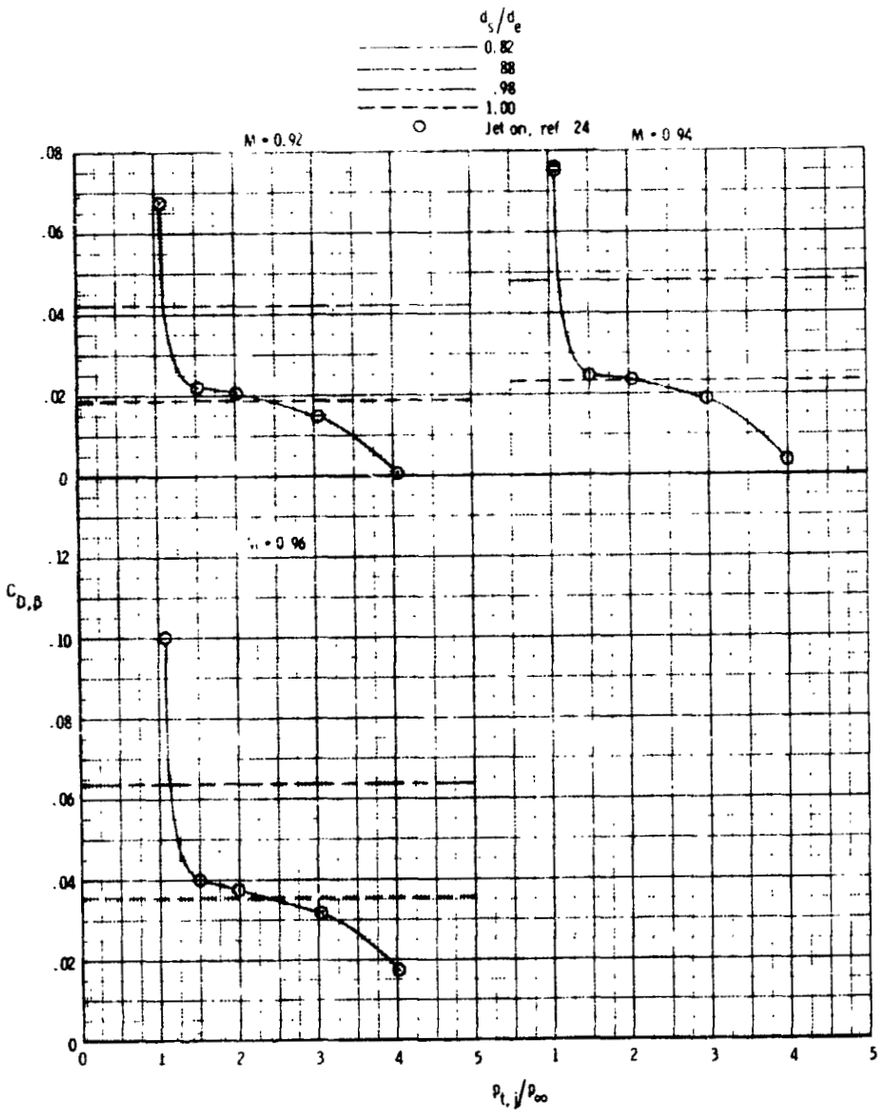

(b) M = 0.92 to 0.96

Figure 17.- Continued.

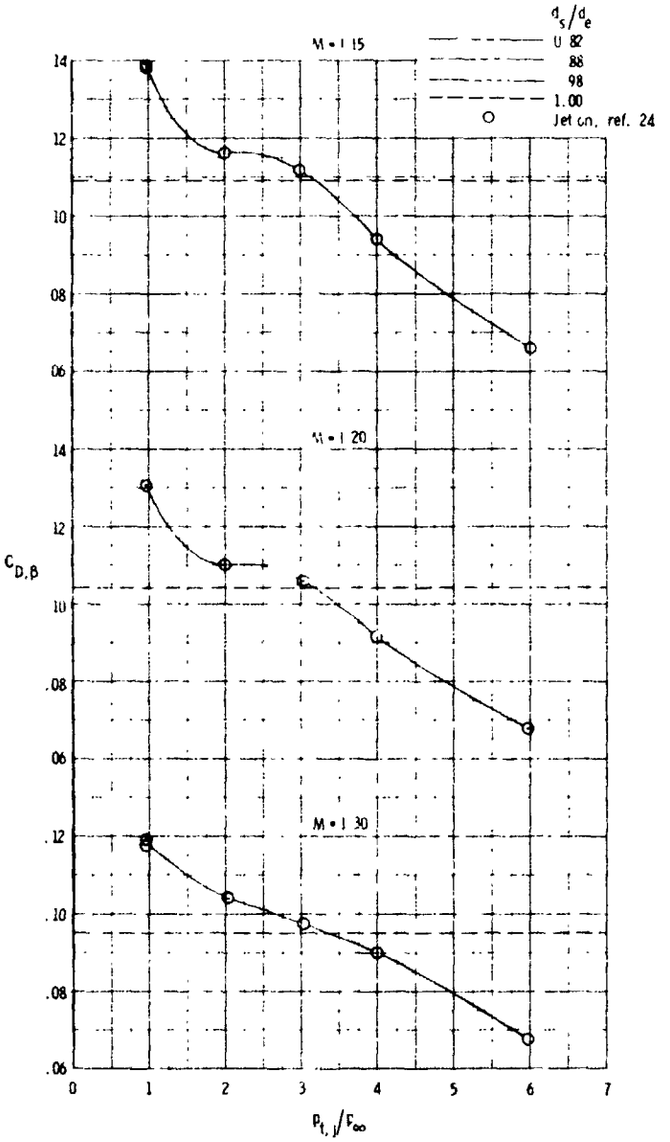

(c) M = 1.15 to 1.30

Figure 17.- Concluded.

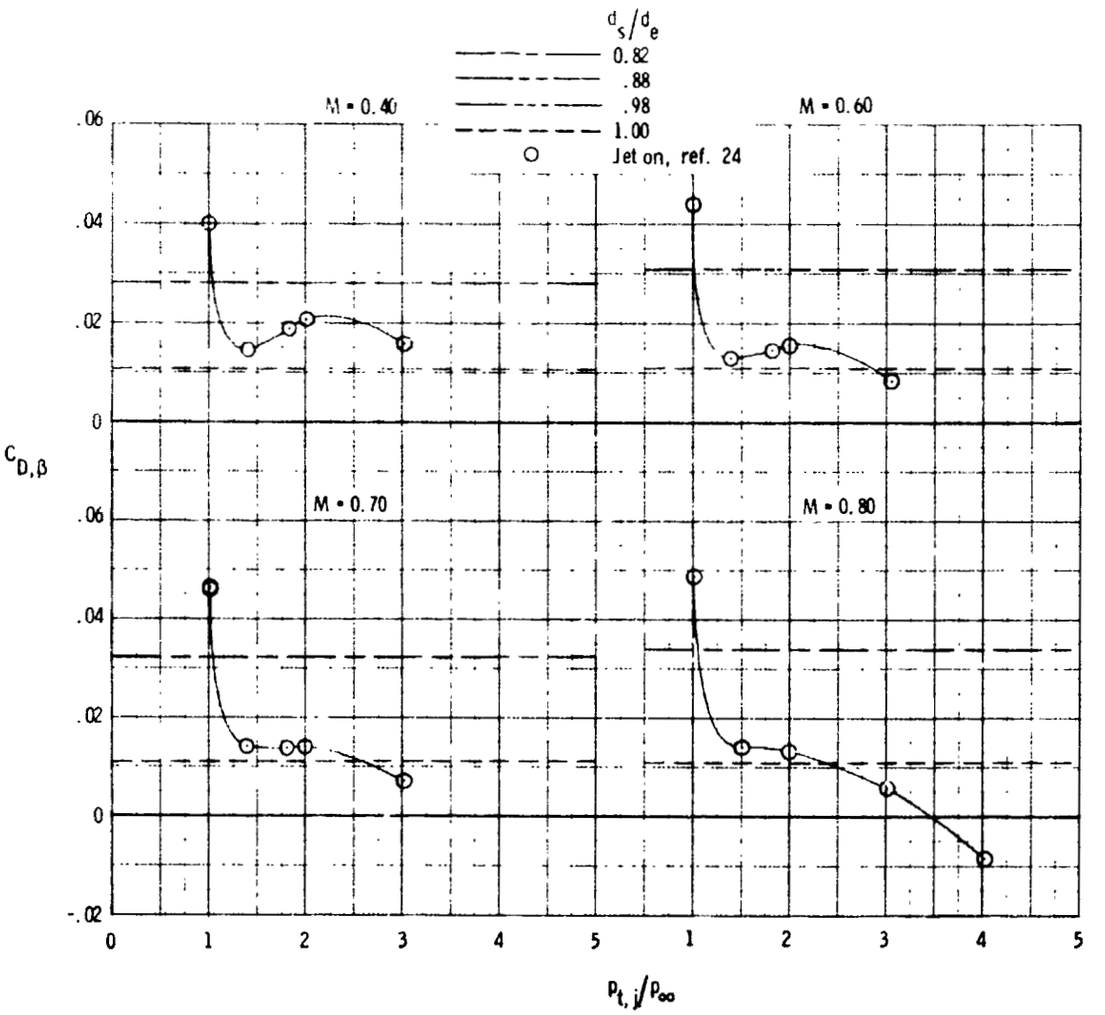

(a) M = 0.40 to 0.80

Figure 18.- Comparison of integrated boattail pressure drag coefficients obtained through use of the simulators with jet-on values for configuration 3 (ℓ/d_m = 1.50, d_e/d_m = 0.70).

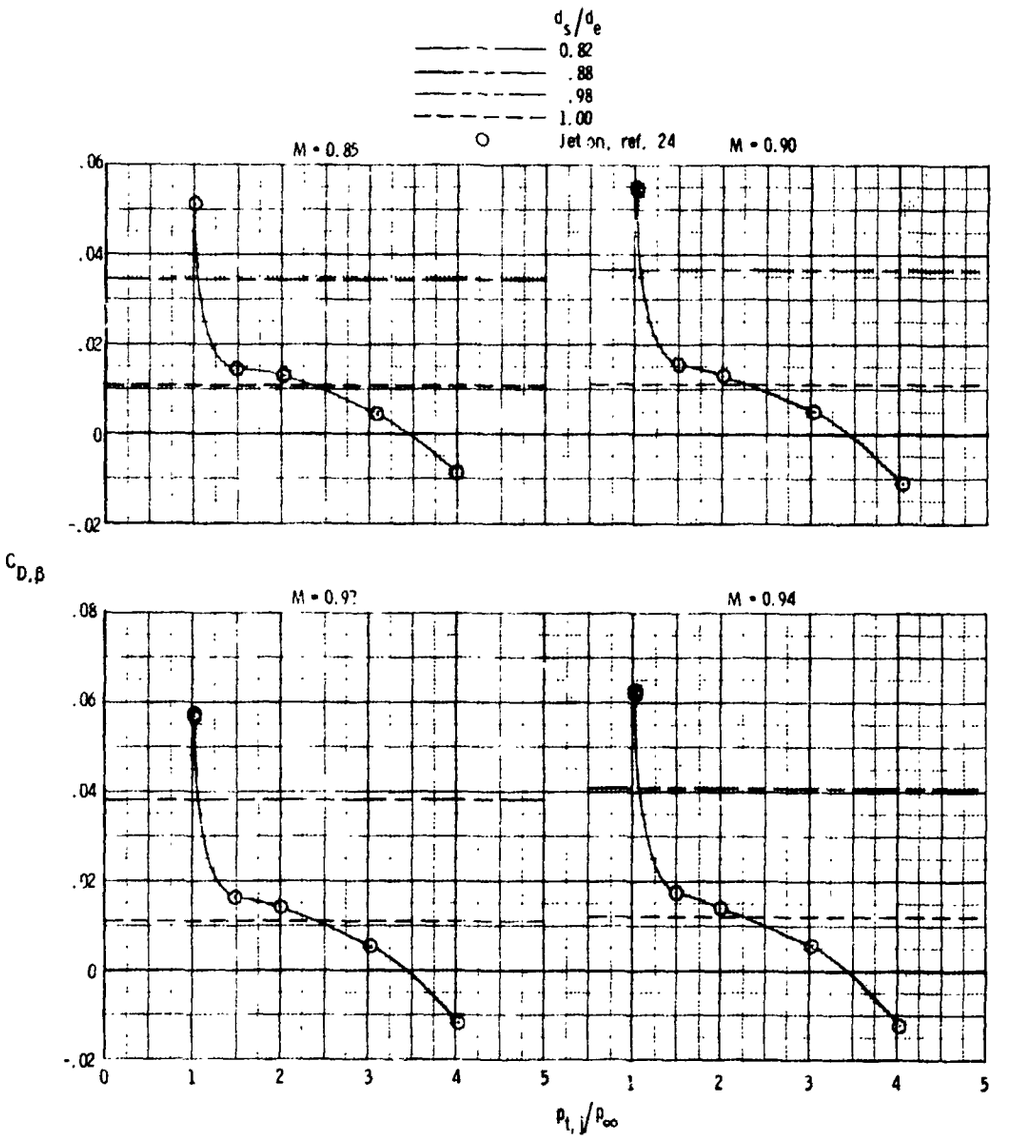

(b) M = 0.85 to 0.94

Figure 18.- Continued.

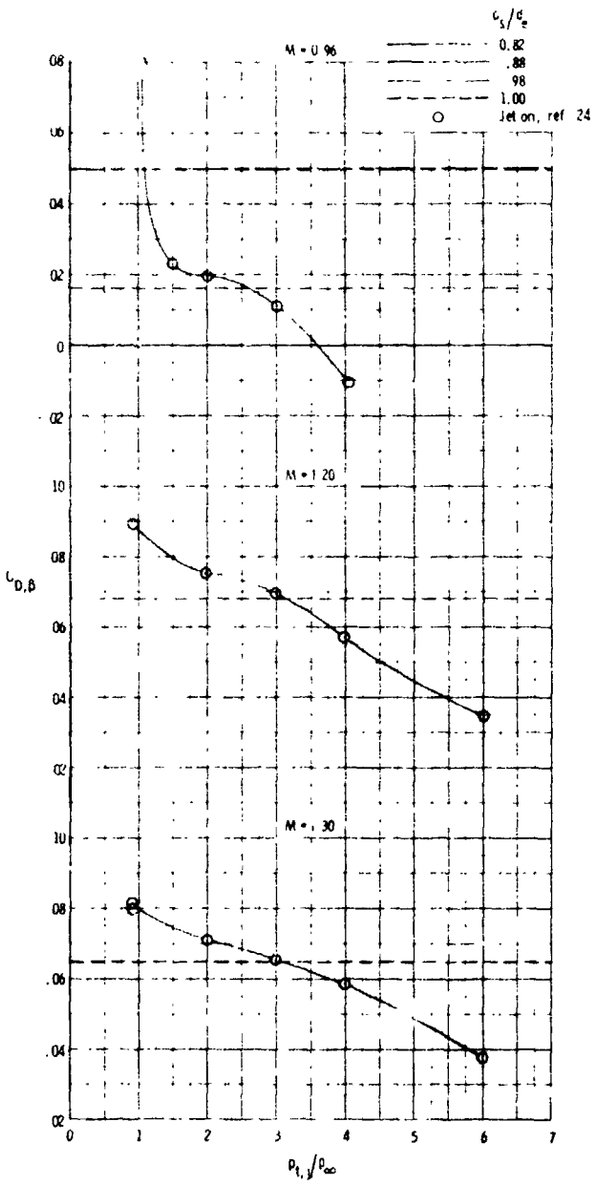

(c) M = 0.96 to 1.30

Figure 18.- Concluded.

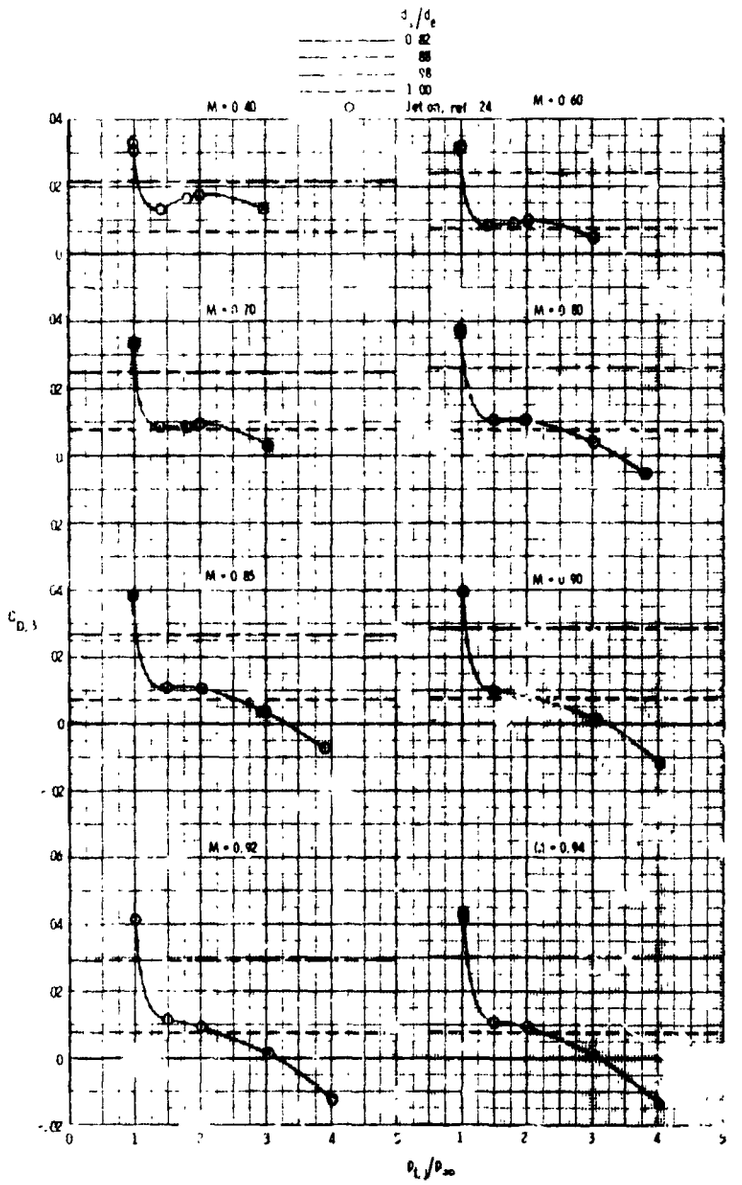

(a) ℓ/d_m = 0.40 to 0.94

Figure 19.- Comparison of integrated boattail pressure drag coefficients obtained through use of the simulators with jet-on values for configuration 4 (ℓ/d_m = 2.00, d_e/d_m = 0.70).

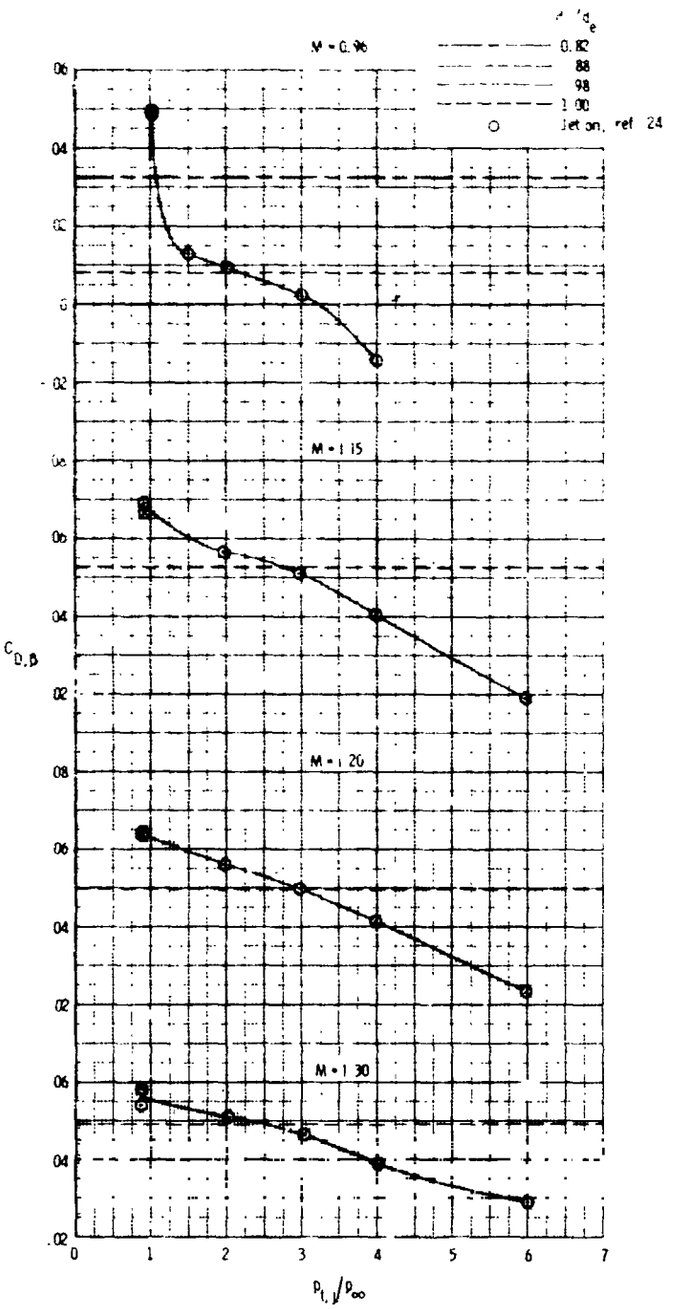

(b) M = 0.96 to 1.30

Figure 19.- Concluded.

would provide useful information for early design pertaining to the jet-on operation of the aircraft configuration especially when compared to having to rely on drag data obtained at jet-off conditions.

To further illustrate the capability of the simulators to provide reasonable approximations of the drag coefficients for an afterbody configuration with jet operation the boattail drag coefficients obtained with the simulators have been plotted as a function of Mach number and compared with jet-on $p_{t,j}/p_{\infty} = 2$ (design point - where the plume should be a cylinder with a diameter equal to the exit diameter) drag coefficient data from references 24 and 25 in figures 21 to 24. The comparisons for a given configuration are initially shown with the drag coefficient data for an individual afterbody-simulator configuration compared to the jet-on data and then the drag coefficient data for all the simulators tested with the particular afterbody configuration in question are shown together with the jet-on drag coefficient data for that configuration (where all the simulators are plotted together the jet-on data points are filled for ease in reading the figure). As was concluded from the previously presented data it is evident that the larger diameter ($d_s/d_e = 0.98$ and 1.00) simulators more closely match the jet-on drag coefficients for all four configurations for a greater range of Mach numbers and, in particular, for the more important transonic range of Mach numbers than do the smaller diameter simulators ($d_s/d_e = 0.82$ and 0.88). To be able to choose one simulator diameter for general use to reach a compromise between plume blockage and entrainment effects would require

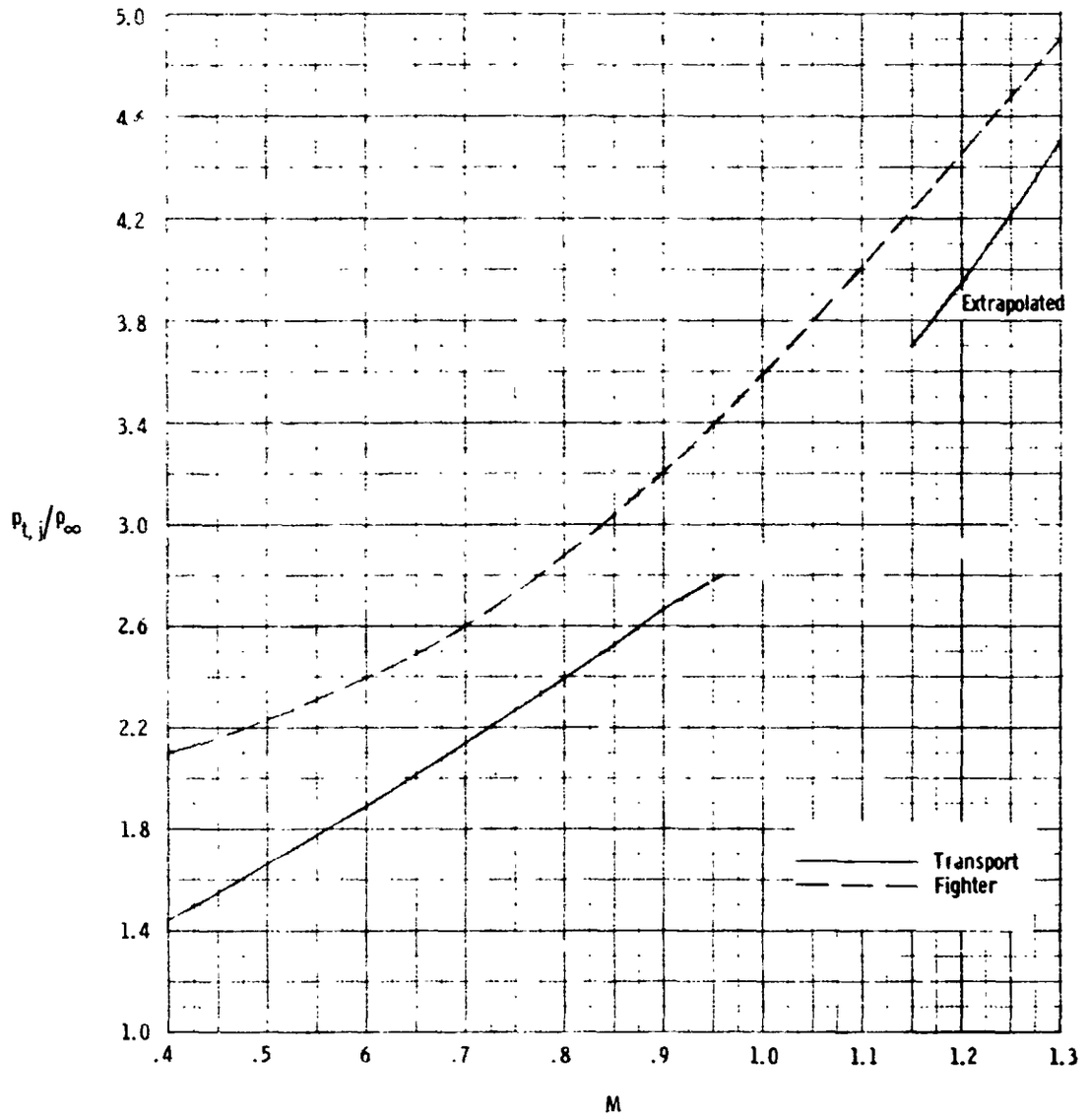

Figure 20.- Jet total-pressure ratio variation with Mach number for typical transport and fighter turbofan engines.

additional tests with both the $d_s/d_e = 1.00$ and 0.98 simulators and simulators of slightly smaller diameter (down to possibly $d_s/d_e = 0.95$) with a greater number of configurations. However, the present results do indicate that the simulators can be an effective tool to gain information about the jet-on drag characteristics of an afterbody configuration both quickly and relatively inexpensively.

Additionally, figure 25 shows cross-plots of the jet-on drag coefficient data from references 24 and 25 for the four configurations of this paper at the transport jet total-pressure ratio schedule of figure 20 compared to the drag coefficient data obtained using the various simulators with those configurations. Again, the larger diameter simulators ($d_s/d_e = 0.98$ and 1.00) more closely match the jet-on drag coefficients for all four configurations for a larger range of Mach numbers and for those Mach numbers in the critical high subsonic regime than do the smaller diameter ($d_s/d_e = 0.82$ and 0.88) simulators. This similarity to the $p_{t,j}/p_\infty = 2$ comparisons is due to the following: The jet total-pressure ratio schedule of figure 20 does not vary too far from a $p_{t,j}/p_\infty$ of 2 for the range of subsonic Mach numbers tested, and the jet-on drag coefficients for these afterbodies do not vary significantly from the $p_{t,j}/p_\infty = 2$ values of jet total-pressure ratios near 2.

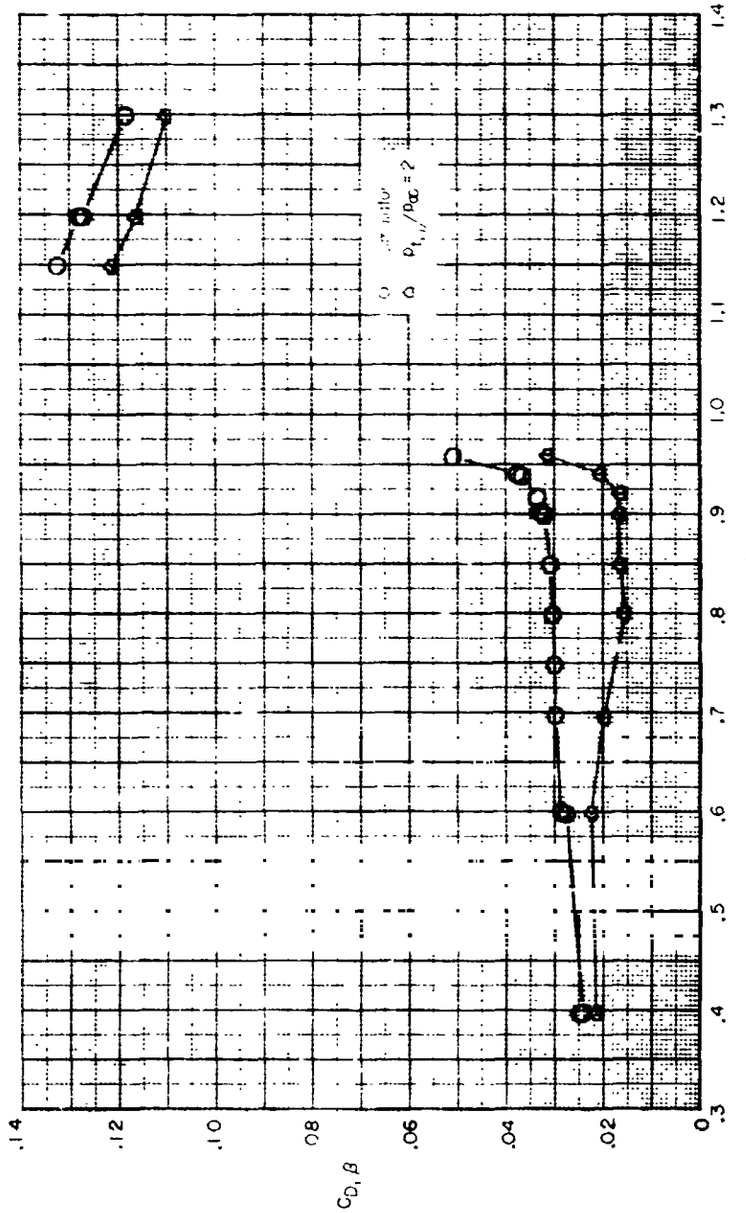

(a) $d_s/d_e = 0.82$

Figure 21.- Comparison of integrated boattail pressure drag coefficients obtained through use of the simulators with jet-on, $P_{t,j}/p_\infty = 2$ values as a function of Mach number for configuration 1 ($\ell/d_m = 1.77$, $d_e/d_m = 0.50$).

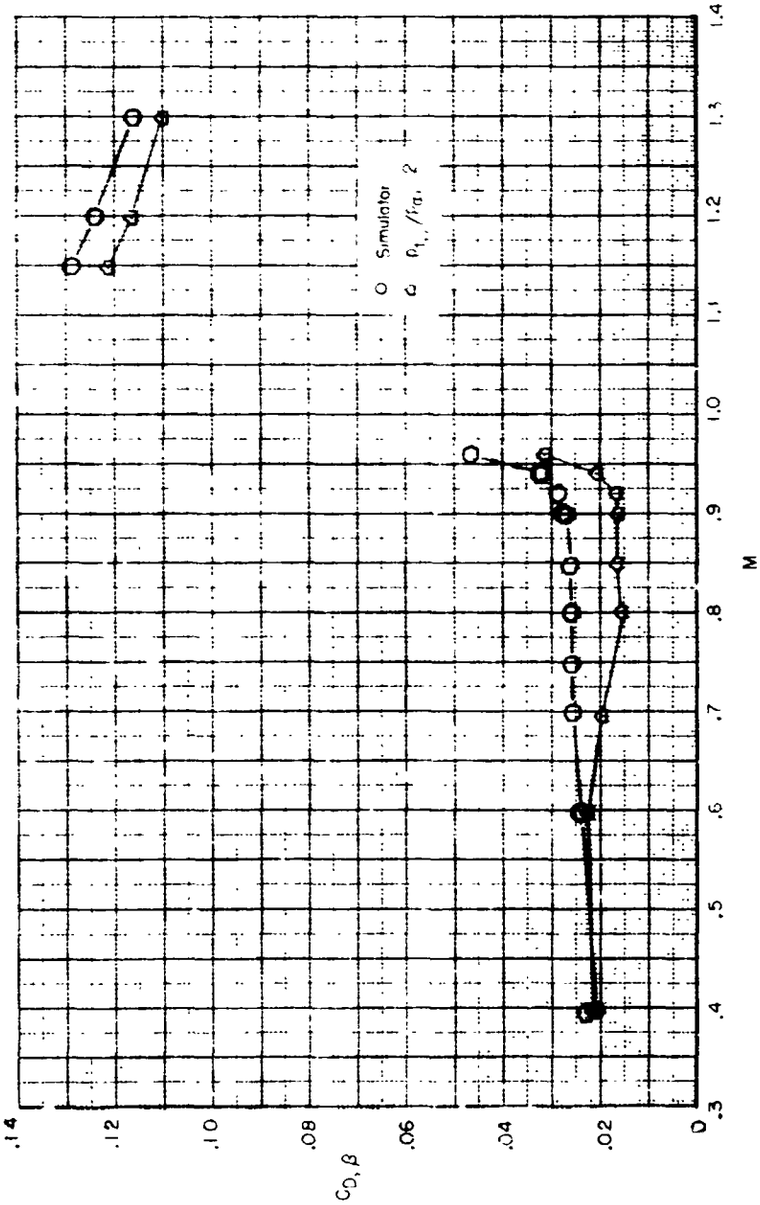

(c) $d_s/d_e = 0.88$

Figure 21.- Continued.

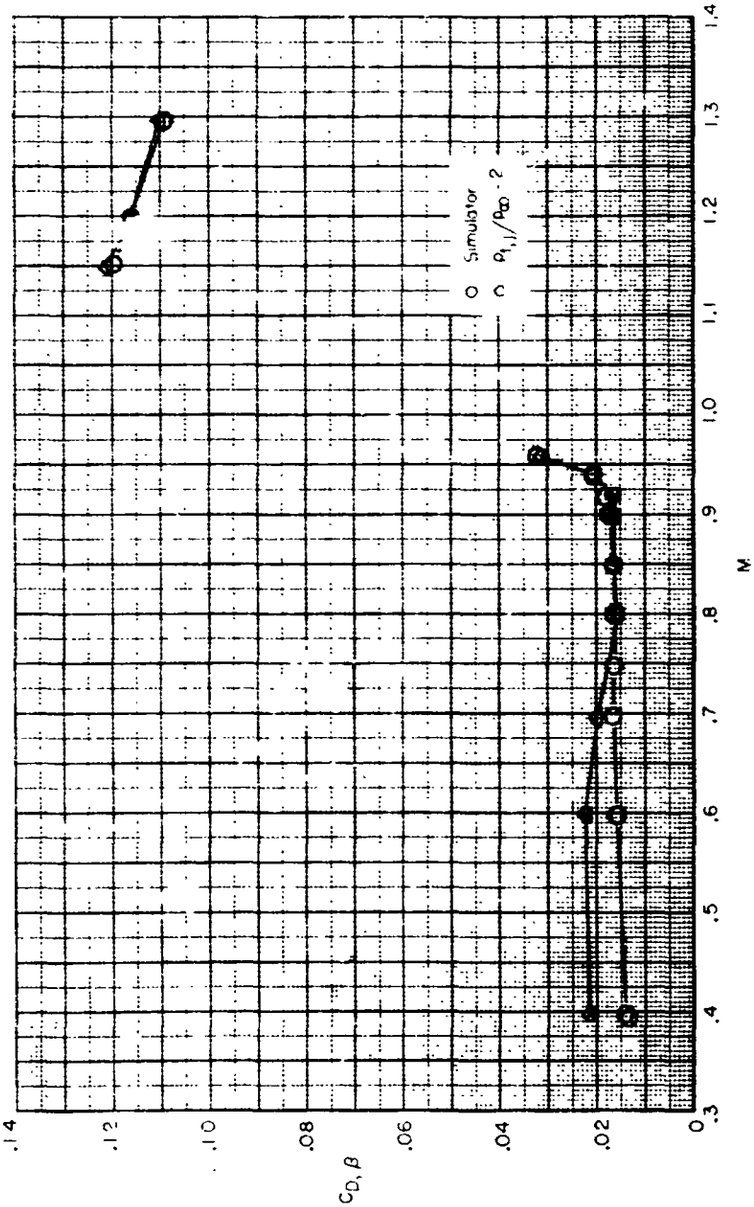

(c) $d_s/d_e = 0.9C$

Figure 21.- Continued.

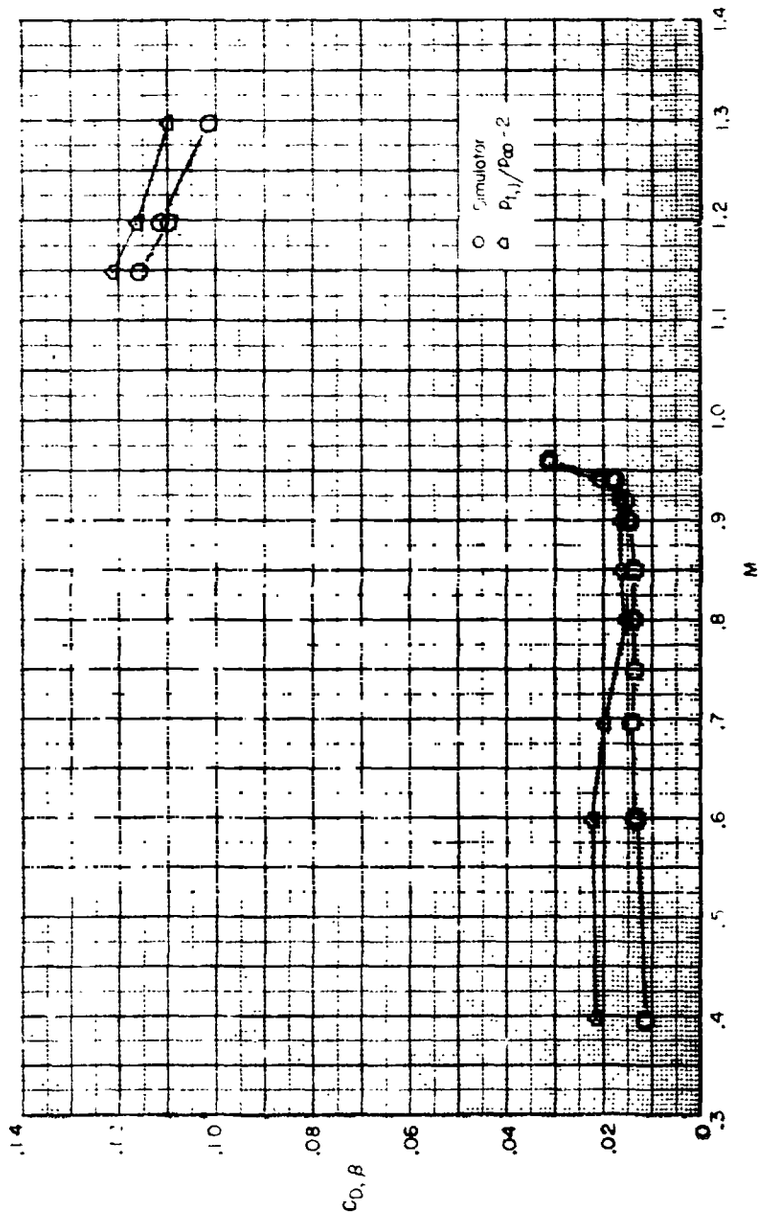

(d) d_s/d_e = 1.00

Figure 21.- Continued.

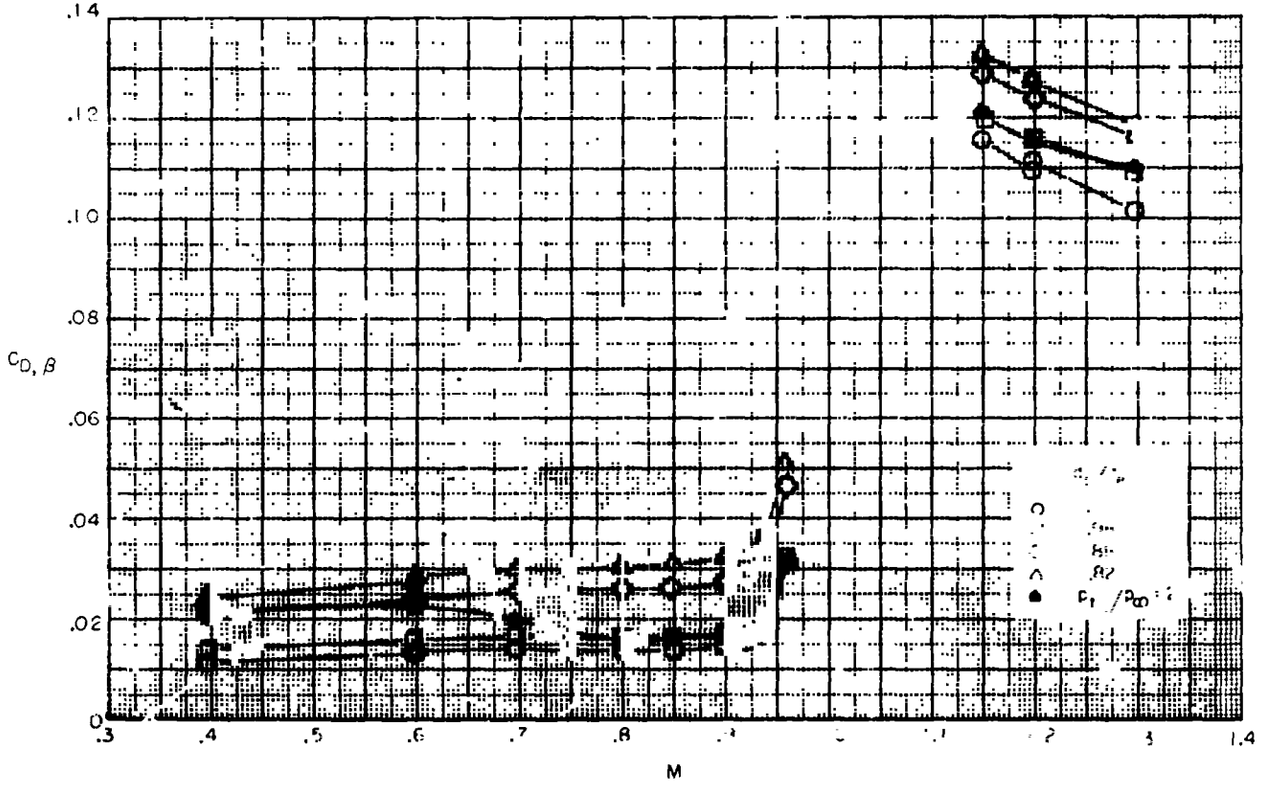

(e) All d_s/d_e

Figure 21.- Concluded.

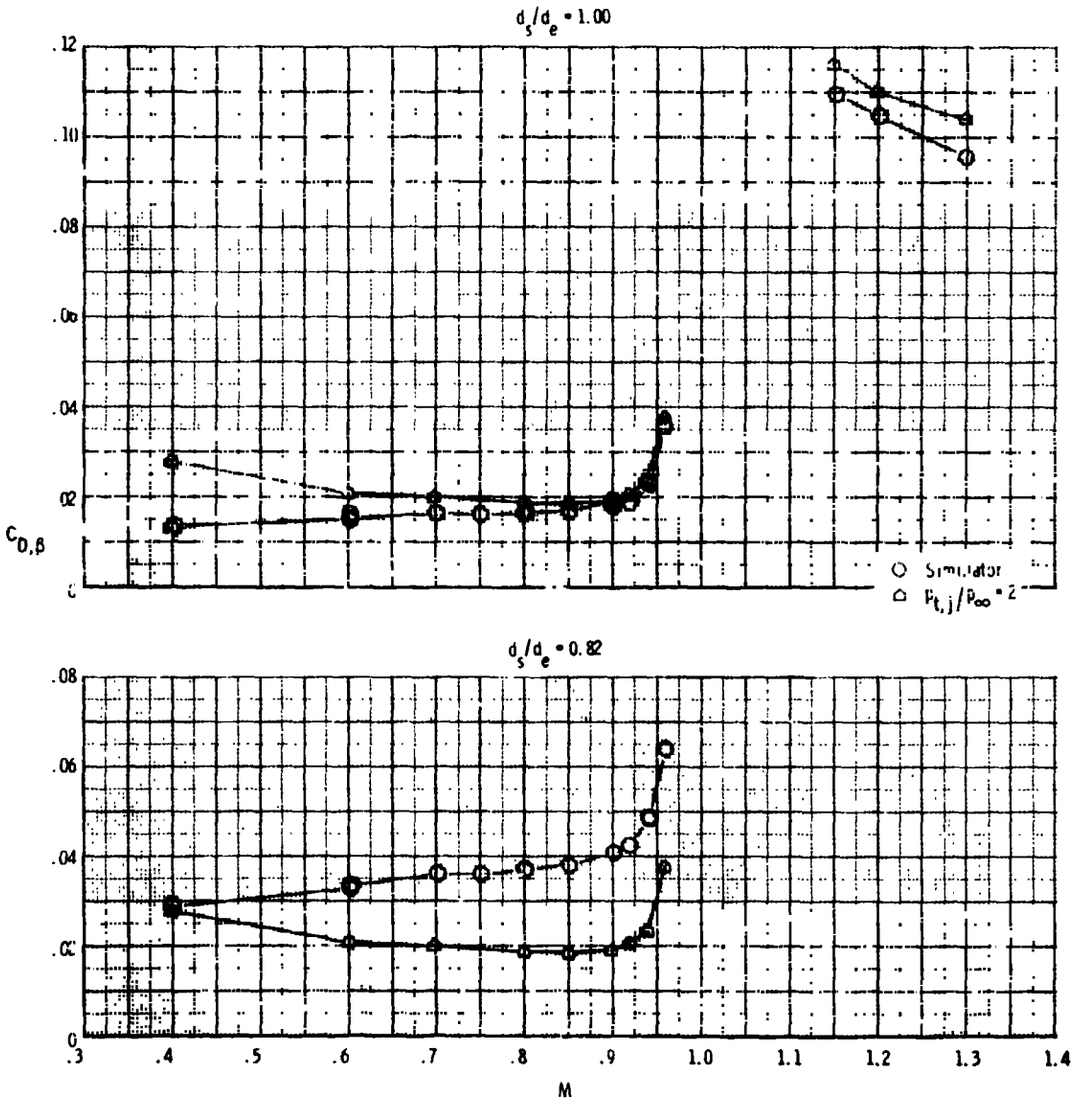

(a) d_s/d_e = 0.82 and 1.00

Figure 22.- Comparison of integrated boattail pressure drag coefficients obtained through use of the simulators with jet-on, $P_{t,j}/P_\infty$ = 2 values as a function of Mach number for configuration 2 (ℓ/d_m = 1.50, d_e/d_m = 0.60).

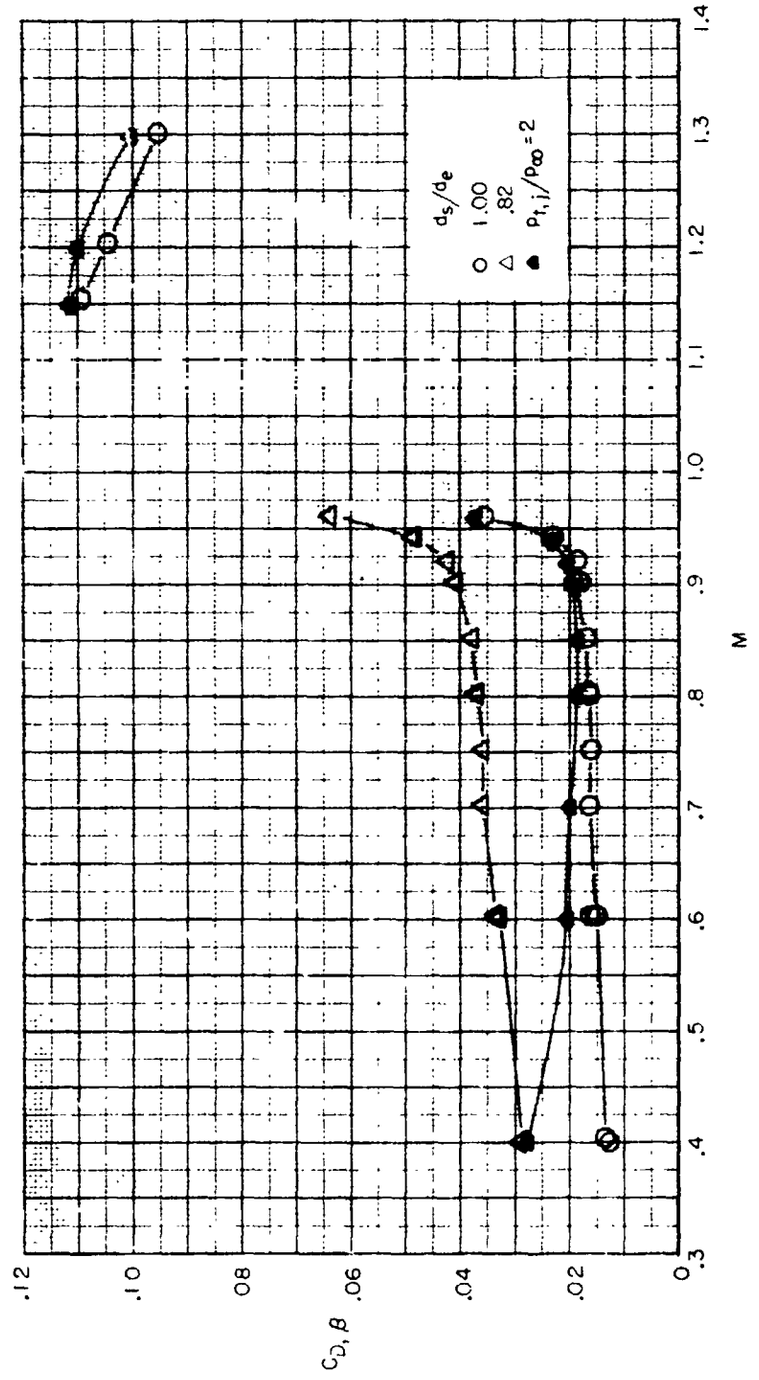

(b) All d_s/d_e

Figure 22.- Concluded.

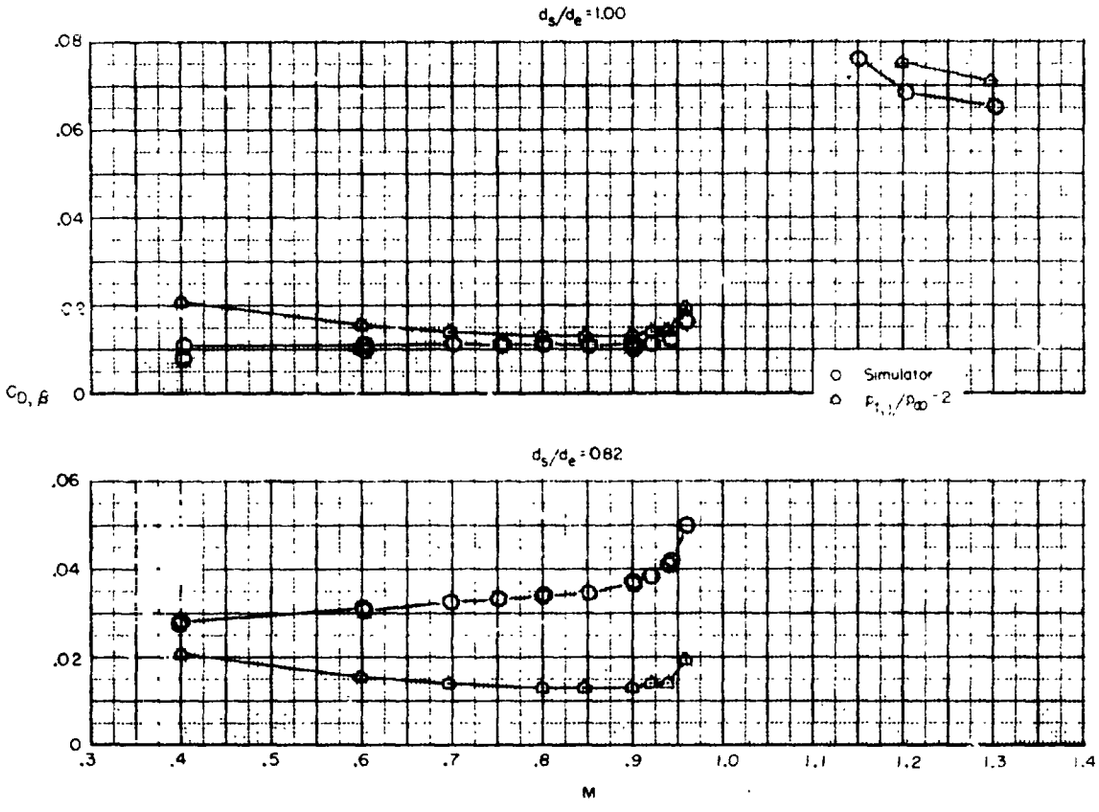

(a) d_s/d_e = 0.82 and 1.00

Figure 23.- Comparison of integrated boattail pressure drag coefficients obtained through use of the simulators with jet-on, $p_{t,j}/p_\infty$ = 2 values as a function of Mach number for configuration 3 (ℓ/d_m = 1.50, d_e/d_m = 0.70).

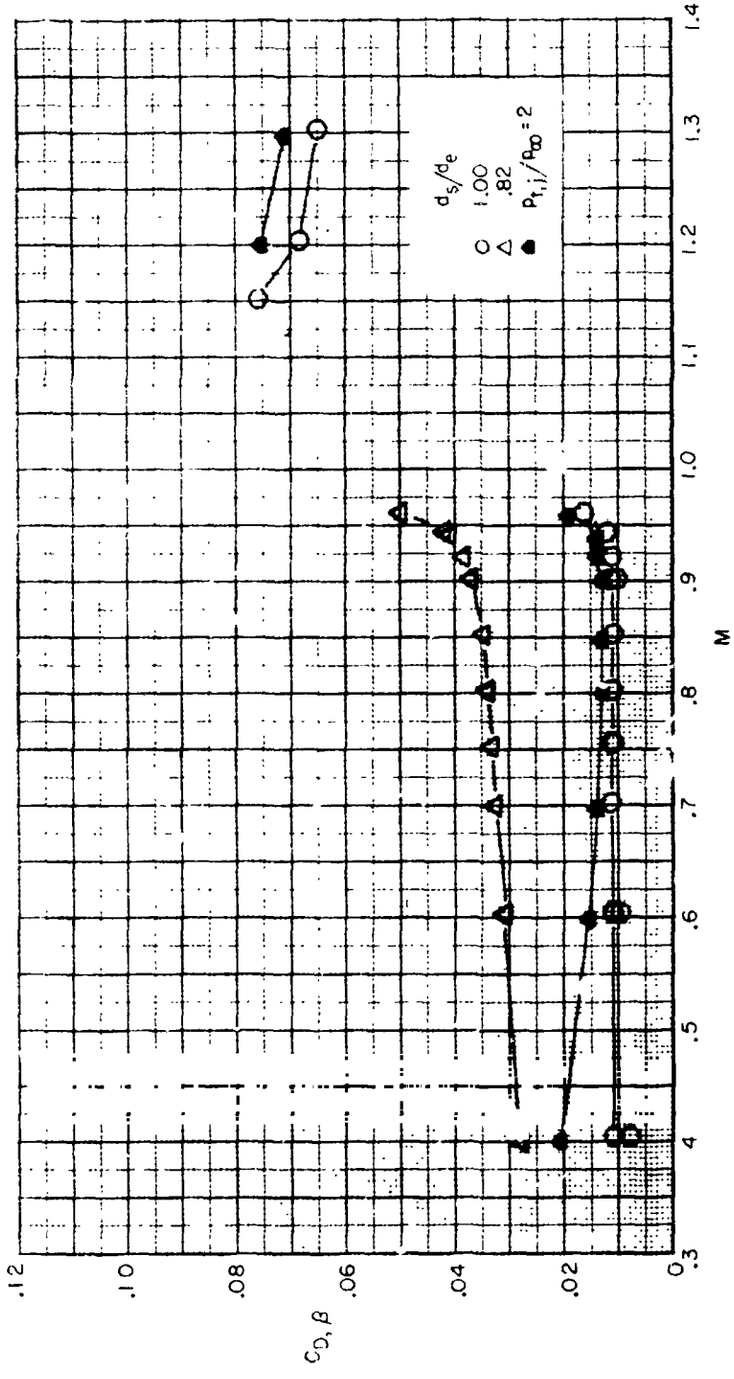

(b) All d_s/d_e

Figure 23.- Concluded.

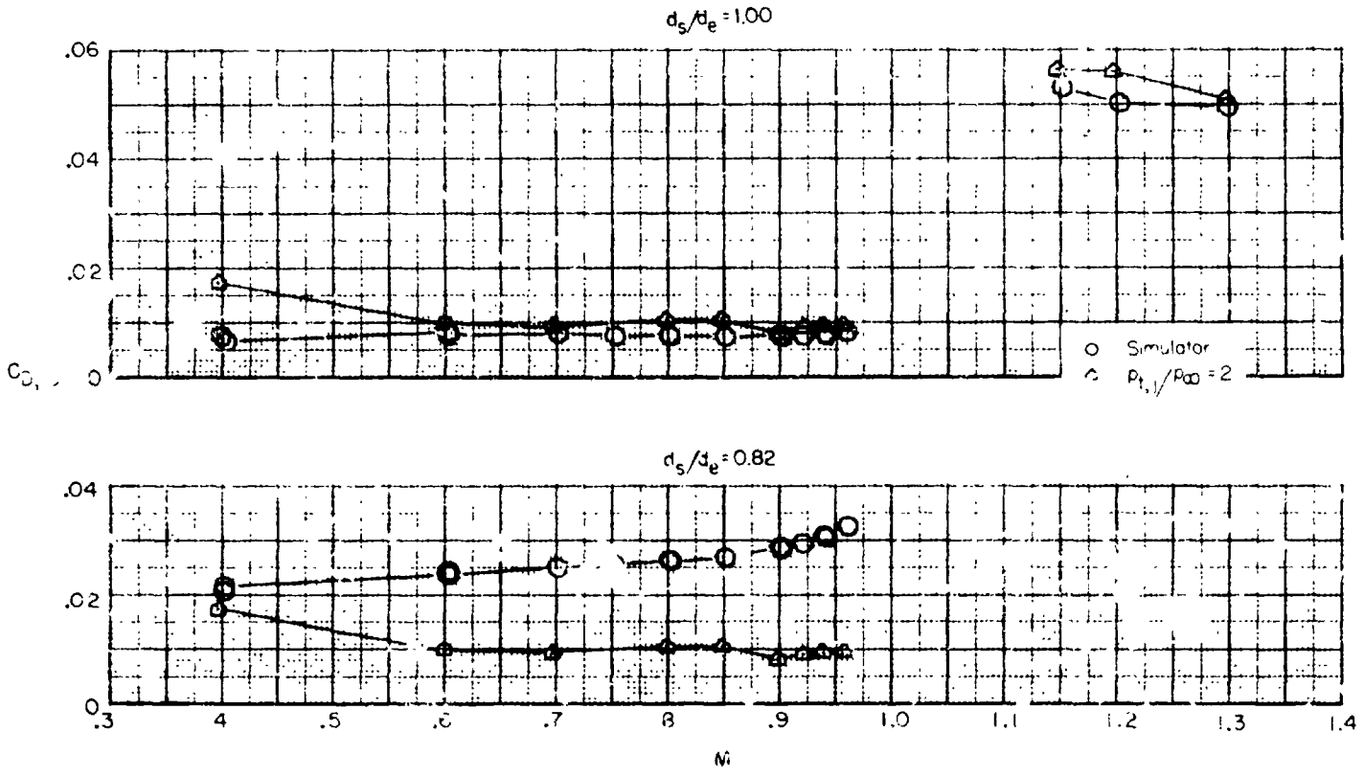

(a) d_s/d_e = 0.82 and 1.00

Figure 21.- Comparison of integrated boattail pressure drag coefficients obtained through use of the simulators with jet-on, $p_{t,j}/p_\infty = 2$ values as a function of Mach number for configuration 4 ($\ell/d_m = 2.00$. $d_c/d_m = 0.70$).

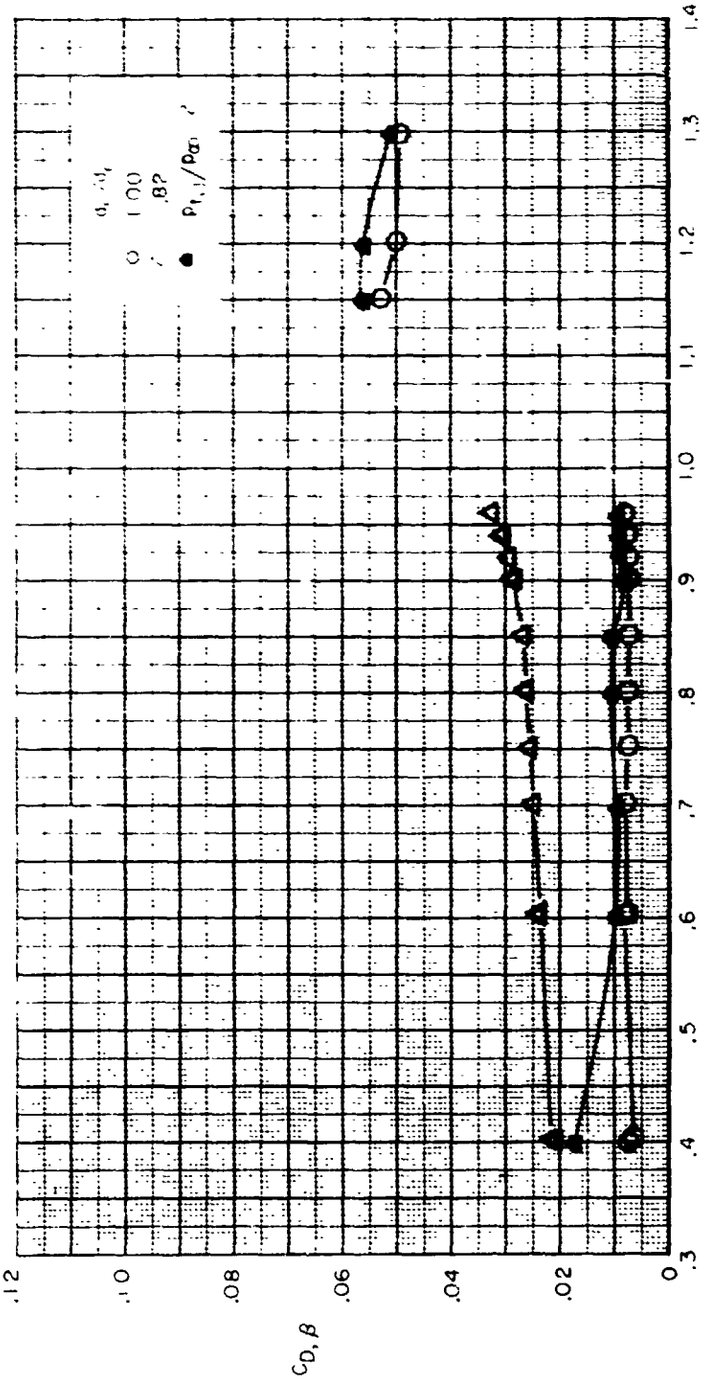

(b) All d_s/d_e

Figure 24.- Concluded.

C-2

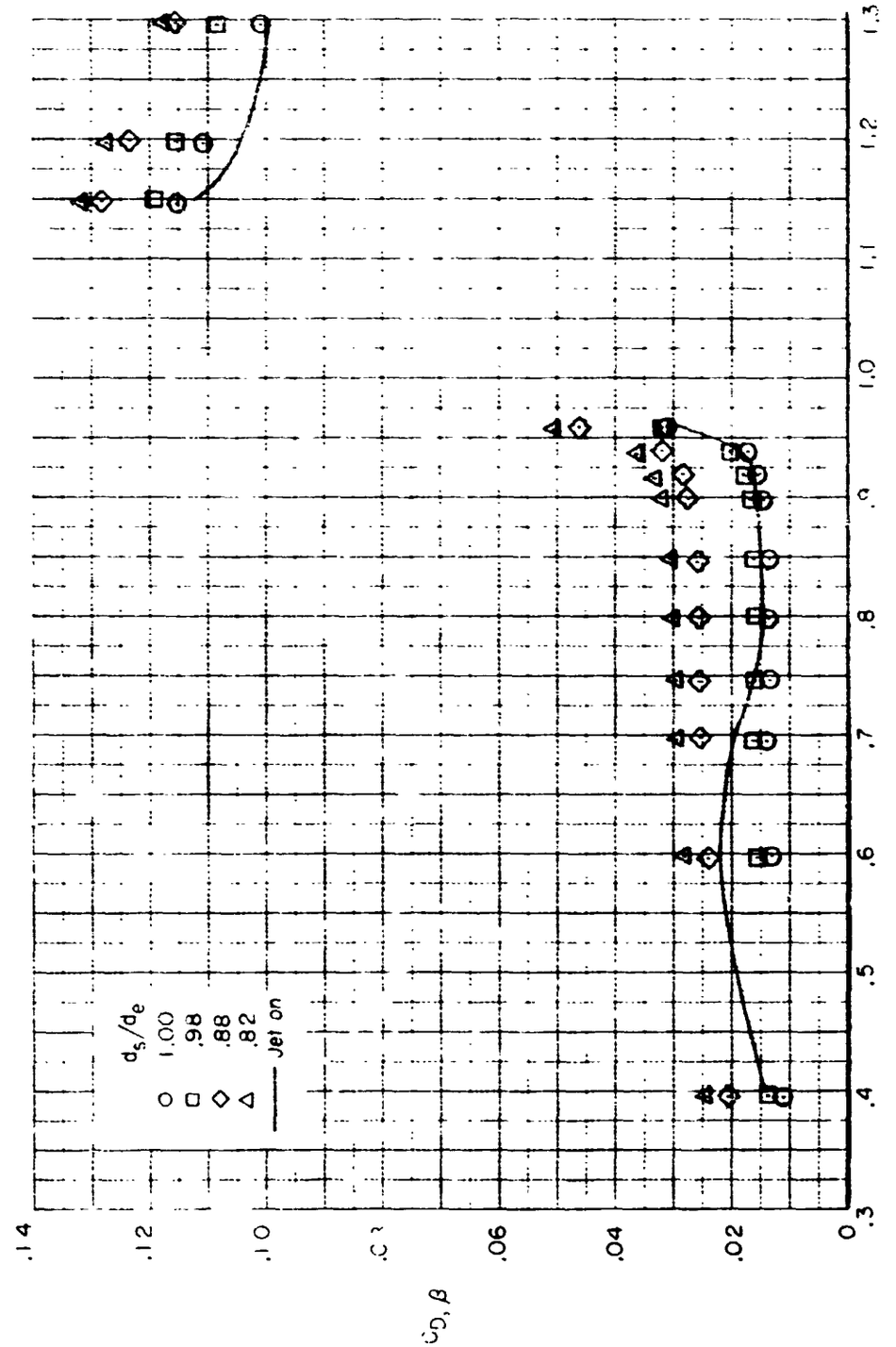

(a) Configuration 1 (ℓ/d_m = 1.77, d_e/d_m = 0.50)

Figure 25.- Comparison of integrated boattail pressure drag coefficients obtained through use of the simulators with jet-on values at the transport jet total-pressure schedule of figure 20.

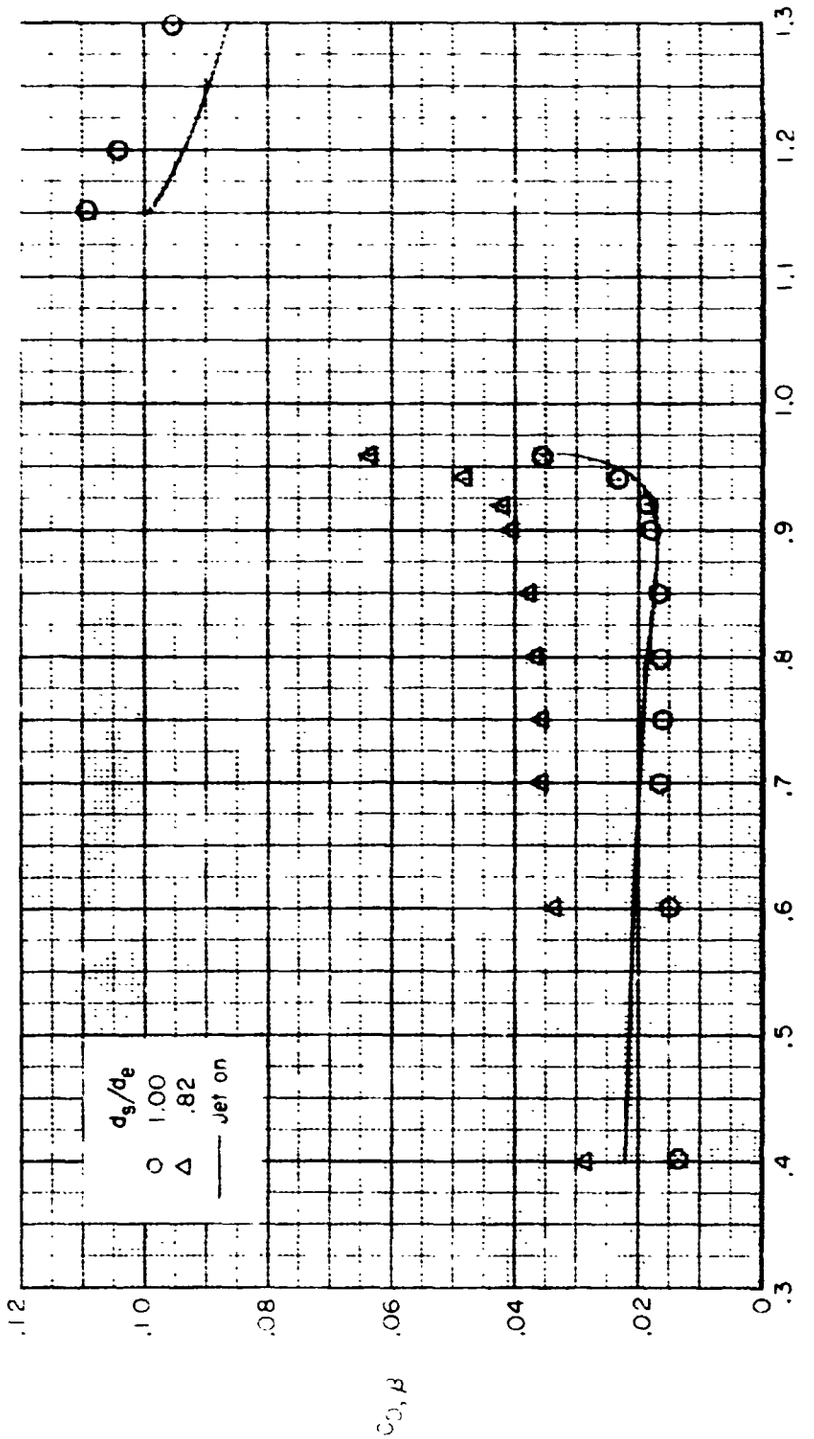

(b) Configuration 2 (ℓ/d_m = 1.50, d_e/d_m = 0.60)

Figure 25.- Continued.

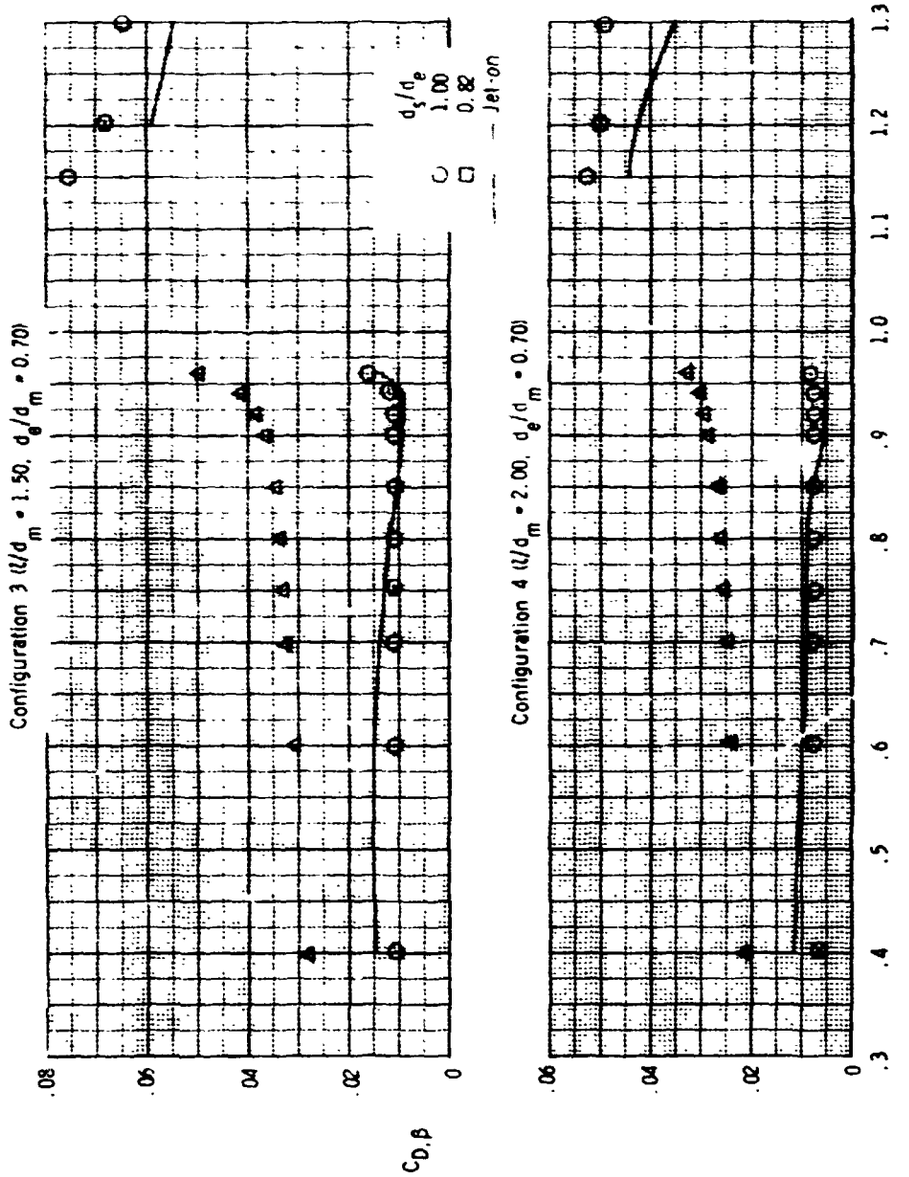

(c) Configurations 3 and 4

Figure 25.- Concluded.

CHAPTER IV

CONCLUDING REMARKS

An investigation at 0° angle of attack has been conducted in the Langley 16-foot transonic tunnel at Mach numbers from 0.40 to 1.30 to determine the effectiveness of utilizing solid circular cylinders to simulate the jet exhaust plume effects on a series of four isolated, nonseparating, circular arc afterbodies. The results of this investigation indicate three primary conclusions:

1. Use of the jet plume simulators resulted in boattail pressure coefficient distributions close to jet-on ($p_{t,j}/p_\infty = 2$) pressure coefficient distributions for all configurations at all Mach numbers. The smaller diameter simulators ($d_s/d_e = 0.82$ and 0.88) generally produced pressure coefficient distributions which more closely matched the jet-on distributions at low subsonic Mach numbers (eg. M = 0.40 and 0.60) where entrainment effects are large. The larger diameter simulators ($d_s/d_e = 0.98$ and 1.00) generally more closely matched the jet-on pressure coefficient distributions at the higher subsonic Mach numbers (eg. M = 0.80 to 0.96) and transonic Mach numbers where the blockage effect predominates. However, use of one of the larger diameter simulators at all Mach numbers would generally result in pressure coefficient distributions with the correct shape and minimum pressure coefficient satisfactory for preliminary design work.

2. Comparisons of the integrated pressure drag values obtained through use of the simulators with those jet-on values from the references follow the same trends as the pressure coefficient distribution comparisons. At the lower Mach numbers the small diameter simulators (d_s/d_e = 0.82 and 0.88) match drag coefficients more closely while at the higher Mach numbers the larger diameter simulators (d_s/d_e = 0.98 and 1.00) are somewhat better. Again, use of the large diameter simulators for all Mach numbers would probably result in integrated drag coefficients which would be of value in the early design stages of an aircraft configuration. Choice of a simulator/exit diameter ratio to most accurately simulate the dual plume effects of blockage and entrainment for general use would require further testing with a number of simulators and additional afterbodies.

3. Both of the theoretical techniques evaluated as a part of this investigation gave reasonably good approximations to the correct pressure coefficient distributions when compared with the jet-on distributions from the references although both predict a stagnation point at the boattail trailing edge. The method of reference 26 would probably be preferred for its consistency in predicting the peak negative pressure coefficients reached on each boattail for most Mach numbers. It must be noted that, although the pressure coefficient distributions were reasonable, the resultant pressure drag coefficients were unsatisfactory.

REFERENCES

1. Shrewsbury, George D.: Effect of Boattail Juncture Shape on Pressure Drag Coefficients of Isolated Afterbodies. NASA TM X-1517, 1968.

2. Shrewsbury, George D.: Effect of a Simulated Wing on the Pressure-Drag Coefficients of Various 15° Boattails at Mach Numbers From 0.56 to 1.30. NASA TM X-1662, 1968.

3. Blaha, Bernard J.; and Mikkelson, Daniel C.: Wind Tunnel Investigation of Airframe Installation Effects on Underwing Engine Nacelles at Mach Numbers From 0.56 to 1.46. NASA TM X-1683, 1968.

4. Blaha, Bernard J.; and Bresnahan, Donald L.: Wind Tunnel Installation Effects on Isolated Afterbodies at Mach Numbers From 0.56 to 1.5. NASA TM X-52581, 1969.

5. Harrington, Douglas E.: Jet Effects on Boattail Pressure Drag of Isolated Ejector Nozzles at Mach Numbers From 0.60 to 1.47. NASA TM X-1785, 1969.

6. Wilcox, Fred A.; Samanich, Nick E.; and Blaha, Bernard J.: Flight and Wind Tunnel Investigation of Installation Effects on Supersonic Cruise Exhaust Nozzles at Transonic Speeds. AIAA Paper No. 69-427, 1969.

7. Blaha, Bernard J.: Effect of Underwing Engine Nacelle Shape and Location on Boattail Drag and Wing Pressures at Mach Numbers From 0.56 to 1.46. NASA TM X-1979, 1970.

8. Mikkelson, Daniel C.; and Blaha, Bernard J.: Flight and Wind Tunnel Investigation of Installation Effects on Underwing Supersonic Cruise Exhaust Nozzles at Transonic Speeds. NASA TM X-52827, 1970.

9. Bergman, Dave: Implementing the Design of Airplane Engine Exhaust Systems. AIAA Paper No. 72-1112, 1969.

10. Chamberlin, Roger; and Blaha, Bernard J.: Flight and Wind Tunnel Investigation of the Effects of Reynolds Number on Installed Boattail Drag at Subsonic Speeds. NASA TM X-68162, 1973.

11. Glasgow, Edsel R.; Santman, Don M.; Miller, Leonard D.; et al: Integrated Airframe-Nozzle Performance for Designing Twin-Engine Fighters. AFFDL-TR-73-71, 1973.

12. Bergman, Dave; "Unique Characteristics of Exhaust-Plume Interference," Journal of Aircraft, Vol. 10, No. 8, Aug. 1973, pp. 508-510.

13. Grund, E.; Presz, W., Jr.; and Konarski, M.: Predicting Airframe/Exhaust Nozzle Interactions at Transonic Mach Numbers. AIAA Paper No. 71-720, 1971.

14. Hill, Philip G.; and Peterson, Carl R.: Mechanics and Thermodynamics of Propulsion. Addison-Wesley Publishing Co., 1965.

15. Hesse, Walter J.; and Mumford, Nicholas. V. S., Jr.: Jet Propulsion for Aerospace Applications. Second ed., Pitman Publishing Corporation, 1964.

16. Englert, Gerald W.: Operational Method of Determining Initial Contour of and Pressure Field About a Supersonic Jet. NASA TN D-279, 1960.

17. Nagamatsu, H.T.; Sheer, R. E., Jr.; and Gill, M. S.: Flow and Acoustic Characteristics of Subsonic and Supersonic Jets from Convergent Nozzle. NASA CR-1693, 1970.

18. Putnam, Lawrence E.; and Capone, Francis J.: Experimental Determination of Equivalent Solid Bodies to Represent Jets Exhausting Into a Mach 2.20 External Stream. NASA TN D-5553, 1969.

19. Burt, James R., Jr.: An Experimental Investigation of Several Rocket Plume Simulators on the Pressure Distribution of a Body of Revolution at Free Stream Mach Numbers of 0.9 to 1.2. Redstone Arsenal Report RD-TR-70-23, 1970.

20. Burt, James R., Jr.: An Investigation of the Effectiveness of Several Devices in Simulating a Rocket Plume at Free Stream Mach Numbers of 0.9 to 1.2. Redstone Arsenal Report RD-TR-71-22, 1971.

21. Vick, Allen R.; Andrews, Earl H., Jr.; Dennard, John S.; and Craidon, Charlotte B.: Comparisons of Experimental Free-Jet Boundaries With Theoretical Results Obtained With the Method of Characteristics. NASA TN D-2377, 1964.

22. Korst, H. H.: Approximate Determination of Jet Contours Near the Exit of Axially Symmetrical Nozzles as a Basis for Plume Modeling. Redstone Arsenal Report RD-72-14, 1972.

23. Smoot, L. D.; Simonsen, J. M.; and Williams, G.A.: Exhaust Plume Prediction Model for a Low-Altitude, Supersonic Missile. AIAA Paper No. 72-1170, 1972.

24. Reubush, David E.: Effects of Fineness and Closure Ratios on Boattail Drag of Circular-Arc Afterbody Models With Jet Exhaust at Mach Number up to 1.3. NASA TN D-7163, 1973.

25. Reubush, David E.; and Runckel, Jack F.: Effect of Fineness Ratio on the Boattail Drag of Circular-Arc Afterbodies Having Closure Ratios of 0.50 With Jet Exhaust at Mach Numbers up to 1.30. NASA TN D-7192, 1973.

26. Hess, J. L.; and Smith, A. M. O.: Calculation of Potential Flow About Arbitrary Bodies. Progress in Aeronautical Sciences, Vol. 8, D. Kuchemann, ed., Pergamon Press, Ltd., c. 1967, pp. 1-138.

27. Keith, J. S.; Ferguson, D. R.; Merkle, C. L.; Heck, P. H.; and Lahti, D. J.: Analytical Method for Predicting the Pressure Distribution About a Nacelle at Transonic Speeds. NASA CR-2217, 1973.

28. Fink, Martin R.: Transonic Theory For Flow Past Slender Fuselages and Afterbodies. AIAA Paper No. 70-556, 1970.

29. Grossman, B.; and Moretti, G.: Time-Dependent Computation of Transonic Flows. AIAA Paper No. 70-1322, 1970.

30. Stahara, Stephen S.; and Spreiter, John R.: Calculative Techniques for Transonic Flows About Certain Classes of Wing-Body Combinations. NASA CR-2103, 1972.

31. Woodward, F. A.: An Improved Method for the Aerodynamic Analysis of Wing-Body-Tail Configurations in Subsonic and Supersonic Flow. NASA CR-2228, 1973.

32. Grossman, Bernard; and Moretti, Gino: Development of Analytical Methods of Predicting the Pressure Distribution About a Nacelle at Transonic Speeds - Exact Solution. NASA CR-112271, 1973.

33. Armstrong, R. S.; and Miller, S. R.: Subsonic Aerodynamic Performance of Nozzle Installations in Supersonic Airplanes. AIAA Paper No. 67-452, 1967.

34. Anon: Users Manual For the External Drag and Internal Nozzle Performance Deck (Deck XI). Pratt and Whitney Aircraft Report: PWA-3465 Supplement F, Part 1, 1968.

35. Glasgow, E. R.; Divita, J. S.; Everting, P. C.; and Laughrey, J.A.: Analytical and Experimental Evaluation of Performance Prediction Methods Applicable to Exhaust Nozzles. AIAA Paper No. 71-719, 1971.

36. Ward, Vernon G.; Whitcomb, Charles F.; and Pearson, Merwin D.: Air-Flow and Power Characteristics of the Langley 16-Foot Transonic Tunnel With Slotted Test Section. NACA RM L52E01, 1952.

37. Schaefer, William T., Jr.: Characteristics of Major Active Wind Tunnels at the Langley Research Center. NASA TM X-1130, 1965.

38 Corson, Blake W., Jr.; Runckel, Jack F.; and Igoe, William B.: The 16-Foot Transonic Wind Tunnel Calibration with Test Section Air Removal. NASA TR R-423, 1974.

39. Anon.: Flow Measurement by Means of Thin Plate Orifices, Flow Nozzles, and Venturi Tubes. Supplement on Instruments and Apparatus, pt. 5, ch. 4, Power Test Codes, ASME, 1959, pp. 5-91.

40. Braslow, Albert L.; and Knox, Eugene C.: Simplified Method for Determination of Critical Height of Distributed Roughness Particles for Boundary-Layer Transition at Mach Numbers From 0 to 5. NACA TN 4363, 1958.

41. Braslow, Albert L.; Hicks, Raymond M.; and Harris, Roy V., Jr.: Use of Grit-Type Boundary-Layer Transition Trips on Wind-Tunnel Models. NASA TN D-3579, 1966.

42. Englert, Gerald W.: Estimation of Compressible Boundary-Layer Growth Over Insulated Surfaces With Pressure Gradient. NACA TN-4022, 1957.

43. Rotta, J. C.: Recent Developments in Calculation Methods for Turbulent Boundary Layers With Pressure Gradients and Heat Transfer. J. Appl. Mech., June 1966, pp. 429-437.

44. Cebeci, T.; and Smith, A. M. O.: A Finite-Difference Method for Calculating Compressible Laminar and Turbulent Boundary Layers. J. Basic Engineering, Sept. 1970, pp. 523-535.

45. Economos, Constantino; and Boccio, John: An Investigation of High Speed Turbulent Boundary Layer With Heat Transfer and Arbitrary Pressure Gradient. NASA CR-1679, 1970.

46. Kuhn, Gary D.: Calculation of Compressible Nonadiabatic Boundary Layers in Laminar, Transitional and Turbulent Flow by the Method of Integral Relations. NASA CR-1797, 1971.

47. Economos, C.; and Boccio, J.: Calculation of Turbulent Boundary Layers With Heat Transfer and Pressure Gradient Utilizing a Compressibility Transformation. NASA CR-1923, 1971.